A new molecular mechanism to promote protean agonism at a G protein-coupled receptor

Dissertation

zur

Erlangung des Doktorgrades (Dr. rer. nat.)

der

Mathematisch-Naturwissenschaftlichen Fakultät

der

Rheinischen Friedrich-Wilhelms-Universität Bonn

vorgelegt von

Anna De Min

aus

Belluno
(Italien)

Bonn 2016

Angefertigt mit Genehmigung der Mathematisch-Naturwissenschaftlichen Fakultät der Rheinischen Friedrich-Wilhelms-Universität Bonn

1. Gutachter: Prof. Dr. Klaus Mohr

2. Gutachter: Prof. Dr. Ivar von Kügelgen

Tag der Promotion: 24.03.2017

Erscheinungsjahr: 2017

Die vorliegende Arbeit wurde in der Zeit von April 2013 bis September 2016 im Bereich Pharmakologie und Toxikologie des Pharmazeutischen Institutes der Rheinischen Friedrich-Wilhelms-Universität Bonn unter der Leitung von Herrn Prof. Dr. K. Mohr angefertigt.

A papà, mamma e Nicole

Table of contents

1 INTRODUCTION

1.1 G protein-coupled receptors (GPCRs)

The G protein-coupled receptor superfamily is one of the largest protein families, accounting for about 3% of the human genome. This family of membrane proteins is constituted by more than 800 genes and it is characterized by two fundamental elements, i.e. the presence of seven membrane-spanning helixes and the coupling to signaling proteins known as G proteins (Fredriksson et al., 2003). These receptors are also referred to as seven transmembrane helix (7TM) receptors, definition that is even more suitable than *GPCRs*, considering that not all 7TM receptors signal through G proteins (Pierce et al., 2002). The aforementioned receptors display several common features, i.e. an N-terminal extracellular domain, a C-terminal intracellular domain, three extracellular loops and three intracellular loops (Figure 1.1).

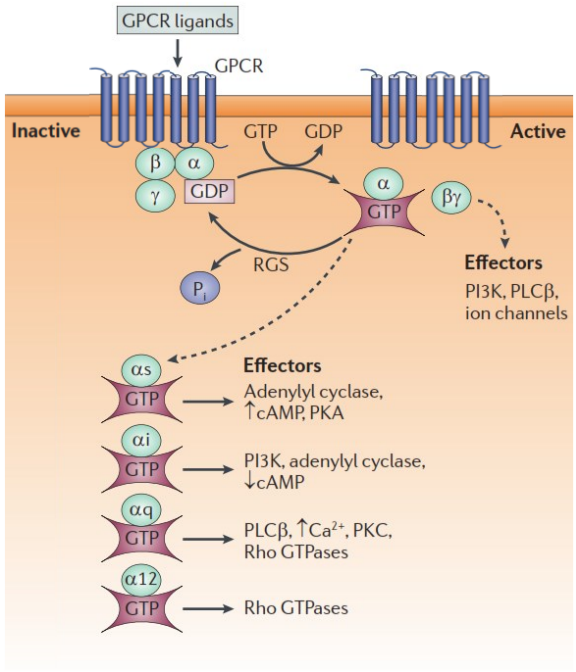

Figure 1.1: Common molecular architecture of GPCRs consisting of seven transmembrane domains. GPCR activation triggers signalling mediated by their membrane-bound partners, the heterotrimeric G proteins, which regulate a broad range of biological processes. cAMP, cyclic AMP; PI3K, phosphoinositide 3-kinase; PKA and PKC, protein kinase A and C; PLCβ, phospholipase Cβ; Rho, RAS homology; RGS, regulator of G protein signalling. Modified after Lappano and Maggiolini (2011).

GPCRs recognize a variety of diverse extracellular stimuli (e.g., photons, ions, biogenic amines, peptides, lipids and proteins, among others) and transduce their signals into the intracellular

environment *via* conformational rearrangements that cause the exposition of binding sites for cytosolic interactants, which then propagate the signaling within the cell (Pierce et al., 2002; Lefkowitz, 2004). Despite sharing a common structure, these receptors are characterized by a relatively low sequence identity (less than 20%) (Fredriksson et al., 2003). Vertebrate GPCRs are commonly divided into five main families, based on their sequence and structure similarities. Family A, that is the rhodopsin-like receptor group, comprises the largest number of receptors (701, of which 241 are non-olfactory), whose ligands are peptides, proteins, lipid-like substances, fatty acid derivatives, small organic compounds, photons and nucleotides. Family B is constituted by the human secretin-like receptors and includes 15 members. They bind rather large peptides that share high amino acid identity and usually act in a paracrine manner. Family C is known as the glutamate receptor family, which comprises 15 members, including metabotropic glutamate, $GABA_B$, and calcium-sensing receptors. A fourth family is represented by the adhesion receptors, and it is composed of 24 members, which present one or several functional domains with adhesion-like motifs in the N terminus. Finally, there is a fifth family, the frizzled/Taste2 family, which comprises 24 receptors. Among them, the TAS2 receptors mediate the human bitter taste, while the frizzled receptors bind secreted Wnt proteins, as well as other ligands, and play a critical role in the regulation of cell polarity (Fredriksson et al., 2003; Lagerström and Schiöth, 2008).

1.1.2 GPCRs activation

Regardless of the structural diversity of the ligands and ligand binding sites within the family of GPCRs, these receptors act through a similar molecular mechanism: the binding of extracellular ligands to GPCRs causes a conformational change in the receptor that promotes the coupling with distinct classes of guanine nucleotide-binding proteins (G proteins). These G proteins are heterotrimeric proteins consisting of an α-subunit bound to a βγ complex and are anchored to the cytoplasmic surface of the plasma membrane. There are several types of G proteins, classified in four broad classes: G_s, $G_{i/o}$, $G_{q/11}$ and $G_{12/13}$ (Figure 1.1), with coupling preference being determined by the individual receptor species (Simon et al., 1991; Milligan and Kostenis, 2006).

Interaction of the ligand-activated receptor with the G protein stimulates the exchange of GTP for GDP in the α-subunit, resulting in the dissociation of the G protein from the receptor and the dissociation of the G protein α-subunit from the βγ complex. The G-protein subunits, α-GTP and free βγ, are then able to interact with distinct effector enzymes and ion channels, stimulating

different physiological responses. Since all α-subunits possess intrinsic GTPase activity, α-GTP is ultimately hydrolyzed to α-GDP, which is able to bind free βγ complexes with high affinity. This reaction returns the system to the original resting state (Wess, 1998). Despite this being the common model of G protein activation, it was discovered that G protein subunits of the $G_{i/o}$ subtype undergo a molecular rearrangement rather than dissociation during activation (Bünemann et al., 2003; Frank et al., 2005). Regarding G proteins of the G_s family, it was instead confirmed that they actually dissociate from the βγ complex (Janetopoulos et al., 2001).

Many mechanisms are known to fine-tune and regulate GPCR signaling. One of the most intensively studied is the "desensitization", which is achieved through receptor phosphorylation mediated either *via* second messenger kinases (protein kinase A (PKA) or protein kinase C (PKC)), or *via* G protein-coupled receptor kinases (GRKs). Phosphorylation carried out by PKA or PKC is known to cause a direct uncoupling of the receptor from the G protein, while GRK-mediated regulation involves the contribution of a small family of cytosolic proteins known as β-arrestins (Pierce et al., 2002). In this two-step process, agonist-occupied GPCRs become substrates for GRK-mediated phosphorylation and, in turn, the phosphorylated receptors recruit the cytosolic adaptors of the β-arrestin type. Further G-protein activation is blocked by β-arrestin-binding, which sterically impedes access to the receptor binding domains, causing desensitization of 7TMR-G protein signaling (Benovic et al., 1987). Additionally, β-arrestins can act as scaffold for enzymes such as phosphodiesterase or kinases, which degrade second messengers generated by G protein-coupling (Perry et al., 2002; Nelson et al., 2007), and they are also involved in receptor internalization via clathrin-coated vesicles (Moore et al., 2007). Furthermore, it was discovered that in many cases β-arrestins function as receptor-activated scaffolds to coordinate upstream and downstream components of particular signal transduction pathways, indicating that these proteins take part in the agonist-induced signaling events, and not only in the switch-off of the signaling cascade (Shenoy and Lefkowitz, 2011).

1.2 Influence of sodium on GPCRs

In the recent past, X-ray crystallography on GPCRs allowed the resolution of an increasing number of receptor structures, permitting an accurate mapping of amino acidic residue orientation and of the location of ligand binding sites. Lately, the improvement of this technique led to high resolution structures in which also the position of water molecules and ions could be identified. In

particular, the presence of a sodium ion bound to an allosteric site in the transmembrane region was recognized at several class A GPCRs in their inactive state (Katritch et al., 2014), i.e. the adenosine A_{2A} receptor, the protease-activated receptor 1, the adrenergic β_1 receptor and the delta opioid receptor, and was shown to maintain the receptor in a quiescent state (Wu et al., 2012; Zhang et al., 2012; Fenalti et al., 2014; Miller-Gallacher et al., 2014). The fact that sodium ions have a negative influence on the activation of GPCRs was not unexpected. Indeed, the first report describing sodium ions as negative allosteric modulators dates back to 1973, when Pert and Snyder (1973) divulged that 100 mM NaCl, i.e. a relevant physiologic concentration, increased antagonist affinity and decreased agonist binding at opioid receptors. Numerous following reports described the effects of sodium ions, mainly in the form of NaCl, as modulators of GPCRs signaling and binding. The results of these studies are not conclusive and a uniform effect of Na^+ on GPCRs has not been identified so far. Indeed, investigations on the effect of this cation on ligands showed that in most of the cases the affinity of agonists is reduced upon an increase in Na^+ in the buffer (Pert and Snyder, 1973; U'Prichard and Snyder, 1978; Rosenberger et al., 1980; Neve, 1991; Malmberg and Mohell, 1995). When NaCl was tested against antagonist's affinities, it was rather noted that their affinity was either increased (Pert and Snyder, 1973; Malmberg and Mohell, 1995), left unaltered (U'Prichard and Snyder, 1978), or diminished (Rosenberger et al., 1980). Additionally, NaCl was shown to have differential effects at the same receptor (α_2AR) when several agonists were tested, and was found to either increase or decrease their affinity at 40 mM NaCl compared to 0 mM NaCl (Pihlavisto et al., 1998), further demonstrating that generalizations on the entity and orientation of Na^+ influence on ligand affinity are not feasible.

1.3 Classification of GPCRs ligands

The two biological properties of a GPCR ligand that can be quantified and are used to pharmacologically characterize a drug, are affinity and efficacy. The first one is a measure of the avidity of the ligand for the binding site of the receptor and it can simply be measured and quantified by the calculation of the parameter K_A, i.e. the dissociation constant of ligand binding at the receptor protein (Shonberg et al., 2014). Efficacy is a parameter that was proved to be more difficult to quantify, for instance, in case of cellular signal amplification and in particular after emerging evidences that a receptor can couple to multiple signaling pathways and may have a preference for a specific downstream effect, a phenomenon known as biased signaling (see 1.4)

(Urban et al., 2007; Kenakin, 2011). Classically, according to the two-state model of receptor activation (Leff, 1995), an agonist is considered the molecule that shifts the equilibrium of the receptors, which exist in active and inactive forms, towards the active state, stimulating the corresponding effect; an antagonist, instead, is thought to bind the active and inactive state with the same affinity, having a "silent" effect (Kenakin, 2002). With the observation that receptors can display constitutive activity, i.e. they can stimulate downstream signaling even in the absence of an agonist (Samama et al., 1993; Milligan, 2003), many antagonists were reclassified as inverse agonists, i.e. drugs that bind preferentially to the inactive state, inhibiting constitutive receptor activity. Another class of ligands is that of partial agonists. In fact, not all agonists display a fully agonistic efficacy, e.g. that reported for the endogenous ligand, but they may display submaximal efficacies even at full receptor occupancy. Conversely, there is also a recently identified class of ligands, the so-called superagonists, which are ligands endowed with a greater efficacy than the endogenous agonist (Schrage et al., 2013; Schrage et al., 2015). Superagonists have been reported for several GPCRs, e.g. muscarinic M_2 and M_4 receptors, ghrelin receptor and somatostatin sst_4 receptors among others (Engström et al., 2005; Holst et al., 2005; Bennett et al., 2009; Schrage et al., 2013).

1.3.1 Protean agonism

A particularly fascinating, albeit seldom described, category of GPCR ligands are protean agonists, i.e. compounds which display agonism in quiescent receptor systems without any spontaneous receptor activity and inverse agonism in constitutively active systems (Kenakin, 1995a). In other words, protean agonists change the direction of their effect according to the degree of spontaneous activity of the GPCR to which the compound binds. One explanation for this intriguing phenomenon is thought to reside in the efficacy of the ligand bound-receptor complex. Theoretically, if a ligand-receptor complex has an intrinsic efficacy that is lower than that of the spontaneously active receptor, but still higher than the efficacy of the quiescent receptor, this will result in (i) negative agonism in a system mainly composed by constitutively active receptors, since receptor activation would be diminished, or (ii) partial agonism, if most of the receptors are in the quiescent state (Kenakin, 1995a, 1997) (Fig. 1.2).

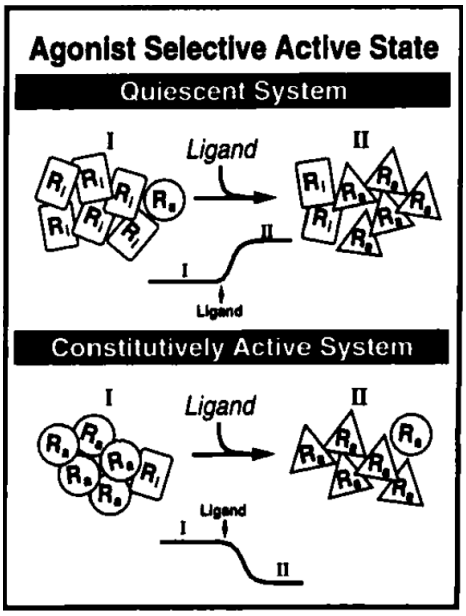

Figure 1.2: Proposed mechanism of action of protean agonists. The ligand produces a pseudo-active state (R_a, triangle) that promotes a response with a lower efficacy than the naturally active state (R_a, circle). In a quiescent system, the increase in R_a triangle produces an increased agonist response. However, in a spontaneously active system, the agonist converts the constitutively active state receptor to a less efficacious species, reversing constitutive agonism. Source: Kenakin (1997).

Up to now, although virtually conceivable for all GPCRs, protean agonists have only been identified for a small number of receptors, for instance cannabinoid receptor 2 (CB_2) (Yao et al., 2006; Mancini et al., 2009; Xu et al., 2010; Bolognini et al., 2012), histamine receptor 3 (H_3) (Gbahou et al., 2003a), alpha-2A adrenergic receptor (α_{2A}AR) (Jansson et al., 1998; Pauwels et al., 2002), serotonin receptor 1B (5-HT_{1B}) (Newman-Tancredi et al., 2003), bradykinin receptor 2 (B_2) (Fathy et al., 1999; Marie et al., 1999) and beta-2 adrenergic receptor (β_2AR) (Chidiac et al., 1994; Chidiac et al., 1996). Nevertheless, protean agonists are highly valuable tools as they might be most useful for the identification of ligand-specific active states of GPCRs: these compounds select a particular receptor conformation that is different from both the spontaneously formed and the full-agonist induced conformation (Kenakin, 2011). Furthermore, protean agonists may represent a promising new compound class in targeted drug therapy for those cases in which receptor mutations cause constitutive activity. Under these conditions, protean agonists can re-establish the original tone of receptor activation (Jansson et al., 1998; Mancini et al., 2009). Moreover, the identification of protean agonists is of significant importance, because they may be mistaken for inverse or partial agonists in *in vitro* assays (in which constitutive receptor activity might be an unwanted phenomenon in commonly applied receptor overexpressing systems) (Chidiac et al., 1994), but act as agonists *in vivo* (Yao et al., 2006; Mancini et al., 2009; Xu et al., 2010). The rather few examples

of GPCR protean agonists are, at least in part, due to the lack of experimental systems with a reliable and reproducible amount of spontaneous GPCR activity. Moreover, specific design strategies to generate protean ligands are missing.

1.4 Orthosteric and allosteric binding sites

GPCRs possess an orthosteric site, which is the binding site of the endogenous agonist. Beyond the endogenous ligands, also classic competitive antagonists, inverse agonists and exogenous agonists can target the orthosteric site. Historically, GPCR-based drug discovery had focused on the development of more selective and/or potent ligands that act at the orthosteric site of the receptor of interest. This approach has the advantage of endowing selectivity and specificity in activity to the investigated drugs. On the other hand, the major drawback was shown to be a lack in subtype selectivity, considering that some GPCR families display high sequence conservation within the orthosteric binding domain across receptor subtypes (May and Christopoulos, 2003; Wess et al., 2007). A new possibility to develop subtype-selective ligands emerged with the discovery of the presence of allosteric sites on several GPCRs, e.g. muscarinic, adenosine, adrenergic, dopamine and serotonin receptors (Lüllmann et al., 1969; Stockton et al., 1983; Conn et al., 2009). An allosteric site is defined as a modulatory binding site, topographically distinct from the orthosteric site; allosteric ligands, also known as allosteric modulators, are able to fine-tune receptor activity through conformational changes in the receptor protein. These modifications are transmitted from the allosteric site to the orthosteric site and/or directly to effector coupling sites, while still allowing, in many instances, the concomitant binding of orthosteric ligands. The simultaneous binding of the receptor by an orthosteric and an allosteric ligand is referred to as "ternary complex formation" (Christopoulos, 2002).

Since the discovery of the phenomenon of allosterism, several models have been developed to describe this mechanism; the first was proposed by Monod, Wyman and Changeux (MWC model), who suggested that a protein exists in a spontaneous equilibrium between active and inactive states in the absence of ligand, and that the binding of either an orthosteric ligand or an allosteric modulator to the respective binding sites would stabilize one state at the expense of another; the apparent effect that the presence of one ligand has on the other ligand was referred to as the allosteric interaction (Monod et al., 1965).

Afterwards, the "allosteric ternary complex model" (ATCM) was developed (Stockton et al., 1983; Ehlert, 1988), which assumes cross-interactions between topographically distinct sites. It describes

the simplest allosteric effect, i.e. a reciprocal modulation of ligand affinity, in terms of the respective dissociation constants (K_A, K_B) that an orthosteric ligand, A, and an allosteric modulator, B, have for their binding sites on the unoccupied receptor. This model introduces a new parameter, termed the "cooperativity factor", α, which quantifies the magnitude by which the affinity of one ligand is changed by the other ligand (and *vice versa*) when both are bound to the receptor to form the ternary complex, and the extent to which the dissociation constant of each ligand is modified in the presence of the other. Values of α greater than 1 indicate an allosteric reduction of affinity for the receptor (negative cooperativity); values of α between 0 and 1 denote an allosteric enhancement in affinity (positive cooperativity); an α value equal to 1 represents no net effect on binding affinity at equilibrium (neutral cooperativity). The limitation of this model is that it does not consider the isomerization of a GPCR between the active and inactive state (Hall, 2000).

The ATCM model was therefore extended in the "allosteric two-state model" (ATSM) (Hall, 2000), which explicitly incorporates the isomerization of a receptor between active (R*) and inactive (R) states, and introduces additional coupling constants to describe the selective stabilization of these states by orthosteric and allosteric ligands.

Since orthosteric and allosteric ligands display reciprocity of effect if present together, the phenomenon of allosterism exhibits several peculiar properties; first, the effect is saturable, which means that there is a limit in the allosteric effect at high concentration of modulator, so that the efficacy of the highest concentration of modulator on orthosteric ligand potency approaches a limit above which no further allosteric modulation is observed (Hall, 2000; Christopoulos, 2002; Chan et al., 2008). A second characteristic is the "probe dependence": the extent and direction of an allosteric interaction can vary with the nature of the orthosteric ligand used as a probe of receptor function, because different orthosteric ligands induce different receptor conformations that alter the structure of the allosteric binding site (Watson et al., 2005; Leach et al., 2010). And third, allosteric modulators can exert differential effects on affinity and efficacy of orthosteric ligands (Price et al., 2005); they can act on these two parameters in opposite ways, for example showing a positive cooperativity at the level of ligand binding and a negative cooperativity at the level of orthosteric ligand function.

Another important advantage of allosterism is the possibility of obtaining selective activation of specific cellular signaling pathways at the expense of others. This phenomenon was first proposed on theoretical grounds based on experimental findings that were inconsistent with the concept of

a single receptor active state, and was referred to as “stimulus trafficking” (Kenakin, 1995b). This theory, now known as “biased agonism” or “functional selectivity” (Urban et al., 2007; Violin and Lefkowitz, 2007), was confirmed by many experimental data that show that different agonists do not uniformly activate all pathways in cells to which receptors are coupled (Kenakin, 2003; Urban et al., 2007). This selective receptor activation is a consequence of the existence of numerous receptor conformations capable of signaling (Kjelsberg et al., 1992); a modulator may then selectively bind to one of these conformers, thereby increasing the proportion of this conformer in the total protein population and producing the observed effect (“conformational selection”), or it can convert the protein into a conformation that it would not spontaneously adopt in its unligated state (“conformational induction”) (Teague, 2003). These different conformations may show altered position of amino acids in numerous locations, allowing or preventing the binding of the receptor to an effector protein (Kenakin, 2007). The importance of biased agonism resides in the fact that allosteric modulators could then be exploited not only to achieve receptor specificity, but also signaling selectivity.

1.5 Muscarinic acetylcholine receptors

Acetylcholine is a neurotransmitter present in both the peripheral nervous system (PNS) and central nervous system (CNS), that exerts its action through two different types of receptors: the nicotinic acetylcholine receptors (nAChRs, also known as "ionotropic" acetylcholine receptors), which are particularly responsive to nicotine, and the muscarinic acetylcholine receptors (mAChRs, also known as "metabotropic" acetylcholine receptors), which are particularly responsive to muscarine (Hulme et al., 1990).

The mAChRs belong to the family A of GPCRs; there are five different subtypes that have been discovered through pharmacological and genetic studies, classed M_1-M_5, with different patterns of distribution and functions (Bonner et al., 1987; Bonner et al., 1988). All the mAChRs are expressed in many regions of the CNS (in both neurons and glial cells) and in various peripheral tissues. The M_1, M_4 and M_5 receptors are predominantly expressed in the CNS, whereas the M_2 and M_3 receptor subtypes are widely distributed in both CNS and peripheral tissues. It is also known that most tissues and cell types express at least two or more mAChR subtypes (Wess et al., 2007).

A broad number of behavioral, cognitive, sensory, motor and autonomic processes are regulated by central mAChRs, and changes in the expression levels and activity of these receptors are

implicated in the pathophysiology of many CNS diseases, including Parkinson's and Alzheimer's disease, depression, schizophrenia and drug addiction. The functions of peripheral mAChRs include ACh-mediated decrease in heart rate (M_2) and increase in smooth-muscle contractility and in glandular secretion (M_3), actions mediated by mAChRs on effector tissues that are innervated by parasympathetic nerves. A broader overview of the processes mediated by the different subtypes of mAChRs is presented in Table 1.1.

$G_{i/o}$-coupled receptors:	**$G_{q/11}$-coupled receptors:**
M_2: vagal heart actions, facilitation of smooth muscle contraction, inhibitory auto- and heteroreceptor, tremor, antinociception, contribution to cognitive functions	M_1: locomotor activity, contribution to cognitive functions
	M_3: smooth muscle contraction, salivation, food intake
M_4: antinociception, inhibitory auto- and heteroreceptor, central motor and behavioral functions	M_5: contribution to ACh-mediated endothelium dependent vasodilatation, to central motor function and drug addiction

Table 1.1: Physiological processes mediated by muscarinic subtypes in CNS and PNS. Adapted from Wess (2004).

The M_1–M_5 receptors can be subdivided into two major functional classes according to their G protein-coupling preference: the odd-numbered receptors preferentially couple to G proteins of the $G_{q/11}$ family, activating phospholipase C beta (PLCβ) and mobilizing calcium ions from intracellular stores (e.g. the endoplasmatic reticulum), whereas the even-numbered receptors preferentially activate $G_{i/o}$-type G proteins, inhibiting adenylyl cyclase and reducing the intracellular concentration of cAMP (Wess et al., 2007; Langmead et al., 2008).

Even though each receptor subtype has a specific coupling preference, it was proven that all five mAChR subtypes couple promiscuously to multiple G proteins, usually in a cell background dependent manner. Moreover, they are linked to additional intracellular pathways, including activation of mitogen activated protein kinases, Rho GTPases, nitric oxide synthases, multiple phospholipases, and the modulation of a variety of potassium, calcium and chloride ion channels (Lanzafame et al., 2003).

1.5.1 M_2 receptor

The M_2 muscarinic acetylcholine receptor (M_2 receptor) is largely distributed in both CNS and peripheral tissues, and it is essential for the physiological control of cardiovascular function. It is indeed efficiently coupled to G proteins of the $G_{i/o}$ class, which mediate the inhibition of adenylyl cyclase, resulting in a decrease of cAMP accumulation and attenuation of cAMP-dependent signaling (Ashkenazi et al., 1987). Following M_2 activation, the released βγ subunits interact with a specific subtype of G protein-coupled inwardly-rectifying potassium channels (GIRKs) named I_{KACh}, set in the heart. This ion channel, once activated, opens and becomes permeable to potassium ions, resulting in hyperpolarization of the cell (Reuveny et al., 1994). The M_2 receptor represents the prevailing subtype of muscarinic receptor in the heart (Krejcí and Tucek, 2002); the principal effects of its stimulation are hyperpolarization and a slowed spontaneous depolarization, resulting in reduced sinus nodal rate in the sinoatrial node, a shortened action potential duration, a decreased contractile force in the atrium, a decreased conduction velocity in the atrioventricular node and finally a slight decrease in force of the ventricle (Dhein et al., 2001).

The M_2 receptor is considered a "model receptor" for the study of allosterism since allosteric regulation of GPCRs was first observed for this receptor (Doughty and Wylie, 1951; Della Bella et al., 1961; Lüllmann et al., 1969; Brown and Crout, 1970; Rathbun and Hamilton, 1970), and it has been one of the most extensively characterized allosteric model systems. It is known that the M_2 receptor presents at least two allosteric sites; the best characterized one is referred to as the "common" allosteric site, and is present in all five muscarinic receptors, but it displays different affinities for allosteric modulators depending on the receptor subtype. Generally, M_2 is the receptor that has the highest affinity for many "common-site" modulators, such as gallamine (Ellis et al., 1993; Gnagey and Ellis, 1996), alkane-bis-ammonium type compounds (Buller et al., 2002) and alcuronium (Jakubík et al., 1995), while M_5 is the one that has the lowest affinity for these compounds. The residues which are important for allosteric modulators selectivity and affinity were identified through site-directed mutagenesis studies, the use of receptor chimeras (Ellis et al., 1993; Gnagey and Ellis, 1996; Buller et al., 2002; Huang et al., 2005; Prilla et al., 2006), and from the recently published crystal structure of the active M_2 bound to an allosteric modulator (Figure 1.3) (Kruse et al., 2013). The position of the "common" allosteric site was identified as being located at the opening of the orthosteric binding pocket, in the extracellular loop region of the receptor.

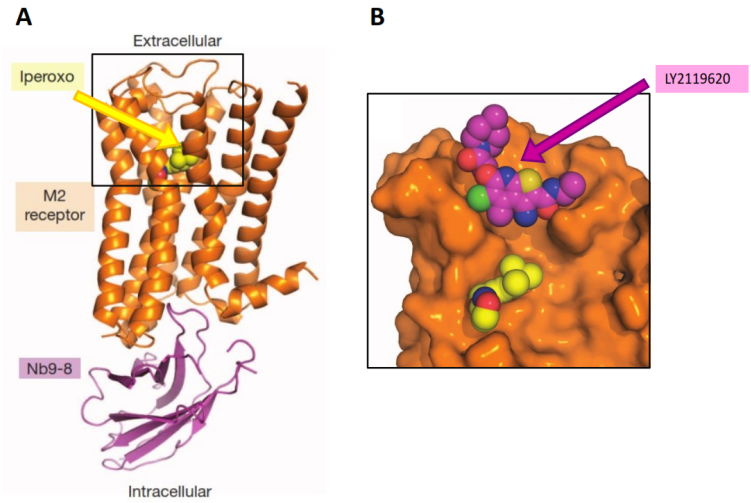

Figure 1.3: A) Overall structure of the active-state M_2 receptor in complex with the orthosteric agonist iperoxo and the active-state stabilizing nanobody Nb9-8. B) Cross-section through the membrane plane of the region comprising allosteric and orthosteric binding sites. The allosteric ligand LY2119620 binds to the extracellular vestibule just above the orthosteric agonist. Modified after Kruse et al. (2013).

A cluster of acidic amino acids, the EDGE sequence (residues 172-175), located in the third extracellular loop, was found to be critical for gallamine affinity, and it is also considered to play an important role in the interaction between the allosteric and orthosteric binding sites (Leppik et al., 1994). Three amino acids were identified as lining the core region of the allosteric site, Tyr^{177}, Thr^{423} and Trp^{422}, and they were shown to have a key role for the binding of allosteric agents (Buller et al., 2002; Voigtländer et al., 2003; Prilla et al., 2006). Analysis of the active crystal structure of M_2 further supported these mutagenic studies, highlighting that Trp^{422} engages an aromatic stacking interaction with the allosteric modulator LY2119620, crystallized in complex with iperoxo to the receptor (Kruse et al., 2013).

1.6 Dualsteric ligands and dynamic ligand binding

In order to obtain molecules that are able to bind both the orthosteric and allosteric sites of the muscarinic receptors, and that, as a consequence, could provide subtype-specific binding, heterobivalent allosteric/orthosteric compounds were synthesized. The first work reporting the rational engineering of these new type of molecules, named bitopic or dualsteric compounds, was that of Disingrini et al. (2006); the orthosteric building blocks of the nonselective orthosteric muscarinic agonists oxotremorine, oxotremorine-M and related agonists were combined with parts of the allosteric modulators W84 and naphmethonium, two subtype-selective allosteric

antagonists for the M_2 receptor. These compounds showed improved subtype selectivity but no gain in affinity compared with their parental molecules.

Theoretically, a heterobivalent ligand can be distributed across a given receptor population in more than one orientation: it can engage both orthosteric and allosteric sites in a dualsteric mode (*dualsteric binding pose*), or it can adopt a different pose that recognizes the allosteric site exclusively, while still allowing the orthosteric site to be exposed for interaction with an orthosteric ligand (*pure allosteric pose*). Experimental studies and molecular docking simulations conducted with these dualsteric ligands on muscarinic M_2 receptors (Bock et al., 2014; Bock et al., 2016) demonstrated that these hybrid compounds are actually able to bind in two different binding poses, concept that is referred to as *dynamic ligand binding*. It was additionally reported that, for compounds carrying an agonistic orthosteric moiety and an inactivating allosteric fragment, the combination of inactive and active receptor states in a system resulted in overall partial agonism of the studied hybrids. Furthermore, it was shown that the affinity of the fragments for the orthosteric and allosteric sites determines the fraction of compound bound in one or the other pose (Bock et al., 2014).

1.7 Aim of the thesis

The main aim of this thesis was to investigate whether dualsteric hybrid ligands carrying an agonistic orthosteric moiety linked to an antagonistic allosteric moiety may elicit protean agonism at the M_2 receptor subtype. The basis for this investigative direction was the concept that heterobivalent ligands of this kind can adopt two different binding poses, the first leading to receptor activation (dualsteric pose) and the second driving to receptor silencing (pure allosteric pose). This unique ability of dualsteric compounds leads to a potential scenario in which these model derivatives may act as protean agonists (Fig. 1.4): a dualsteric compound which prefers binding in an allosteric binding topography will result in inverse agonism in a system with pronounced spontaneous receptor activity (red curve). However, if this compound is also able to bind in a dualsteric binding pose, functional agonism may occur in a quiescent receptor system (blue curve).

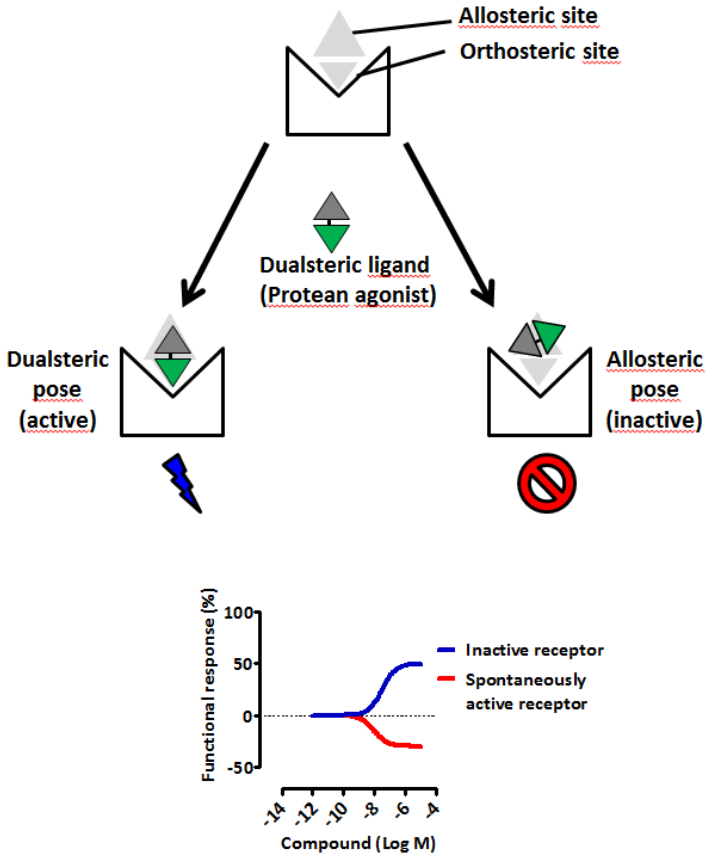

Figure 1.4: Proposed mechanism of action of dualsteric ligands acting as protean agonists. Dualsteric ligands may potentially bind either in a dualsteric binding pose, stimulating receptor signaling, or in a purely allosteric pose, inactivating the receptor (Bock et al., 2014). In this sense, dualsteric binding of protean agonists may lead to a positive signaling output in an inactive receptor system (hypothetical blue curve), whereas the compound may behave as an inverse agonist in a receptor system with spontaneous activity (hypothetical red curve).

Therefore, the purposes of this work were, as listed below:

- To identify the conditions necessary to have two stable receptor systems for the wild type M_2 receptor, i.e. one showing a low amount of spontaneous activity and the second exhibiting high levels of constitutive activity.

- To test in these newly-established systems a set of dualsteric compounds that were composed by an orthosteric moiety, endowed with either agonistic or superagonistic activity and connected through variable linkers to antagonistic allosteric moieties, in the interest of detecting eventual protean agonists.

- To identify structure-activity relationships, in order to define the molecular features required for protean agonism at M_2 receptors among this collection of dualsteric compounds.

- To clarify the molecular mechanism eliciting protean agonism at the M_2 receptor, with the purpose of establishing whether this phenomenon is dependent on the intrinsic efficacy of the compound, as speculated in previous reports, or on a new mechanism dictated by the heterobivalent nature of these compounds.

2. MATERIALS AND METHODS

2.1 Cell culture

Chinese Hamster Ovary (CHO) FlpIn cells stably expressing either the human M_2 or the single mutant $M_2^{422W \rightarrow A}$ receptor were thawed from the nitrogen tank and rapidly seeded in 15 cm culture dishes with Ham's F12 medium (R30) supplemented with 10% FBS (Fetal Bovine Serum, R21), 2 mM L-glutamine (R27), 100 units/ml penicillin, and 100 µg/ml streptomycin (R31). The cells were incubated at 37°C, 5% CO_2 and 96% humidity until they reached 80-90% of confluence. After aspiration of the medium, cells were washed with 10 ml phosphate buffered saline (PBS, R19) to remove residual medium and serum proteins. They were detached by addition of 3 ml of trypsin-EDTA solution (R35). Finally, 7 ml of medium were added to the plate to inactivate trypsin and 1 ml of cells was placed in a new dish containing 18 ml of fresh medium and incubated until confluence was reached. In order to store backup cells with low passage number, cells were frozen and kept in liquid nitrogen. The procedure consisted in harvesting the cells as previously described and centrifuging the suspension at 900 rpm for 4 minutes at 4°C. After removal of the supernatant, the cells were resuspended in fresh medium supplemented with 10% DMSO (Dimethyl sulfoxide), transferred in cryovials (M10) and frozen at -80°C in a container (Mr. Frosty™, T15) allowing a rate of cooling of about -1°C/min. Once the suspension was completely frozen, the cryovials were stored in liquid nitrogen.

2.2 Membrane preparation

Cells which had almost reached confluence were exposed to 14 ml of fresh medium supplemented with 5 mM sodium butyrate (S1) in order to stimulate overexpression of receptors (Kruh, 1982), and incubated for 18-24 hours.

On the day of preparation, the medium from 5 dishes was aspirated and 2.4 ml of ice-cold homogenization buffer (S5) were added to each dish. The cells were then detached with a scraper and the cell suspension was transferred into a glass falcon. Afterwards, 6 ml of homogenization buffer were used to wash the 5 dishes and the liquid was then added to the same falcon as used before. These cycles were done 8 times, for a total of 40 plates.

The cells were homogenized with a Polytron homogenizer (T11), with 2 rounds at level 6, the first time for 25 seconds and the second time for 20 seconds. The homogenates were centrifuged at 40,000 g for 10 minutes at 2°C and then the supernatant was discarded. The pellet was washed twice, adding 20 ml of centrifugation buffer (S6) to each falcon, re-suspending the pellet by gently vortexing and centrifuging with the settings used before. Finally, all the pellets were re-suspended in 40 ml of Tris buffer (S13), aliquoted, and stored in the freezer at -80 °C.

2.3 Protein quantification

The protein content of homogenates was determined by the method of Lowry (Lowry et al., 1951). The homogenates were first pre-treated with copper ion in alkali solution (S2, S9, S10), and after 10 minutes of incubation the Folin reagent (S3) was added. The aromatic amino acids in the treated sample reduced the phosphomolybdatephosphotungstic acid present in the Folin reagent, resulting in a product of the reaction with a blue color. The amount of proteins in the sample could be estimated measuring the absorbance at 500 nm of the end product against a standard curve of a Human Serum Albumin (HSA, R26) solution.

2.4 Radioligand binding studies

In radioligand binding assays, receptors are incubated with a radiolabeled compound for a certain time, usually in the presence of unlabeled ligands or other modulators, and then the label bound to the receptor is separated from the unbound ligand, allowing the bound radioligand to be quantified.

There are two components of radioligand-binding: a “specific” component of binding to the receptor of interest and a “nonspecific” component of binding to other sites. The nonspecific binding is measured in the presence of a concentration of unlabeled ligand sufficient to prevent binding of the radioligand to its specific binding site. Specific binding is calculated from the difference between total and nonspecific binding.

Binding studies were used in an attempt to quantify the parameters of drug-receptor interaction according to a model of drug action. The simplest model is the Law of Mass Action, in which ligands bind reversibly to a single binding site:

$$L + R \underset{k_{off}}{\overset{k_{on}}{\rightleftharpoons}} LR \qquad (1)$$

According to this model, a ligand, L, binds to a receptor, R, with an association rate constant k_{on}, to form a ligand-receptor complex, LR, which is stable for a time but eventually dissociates into free, unchanged receptor and ligand, with a dissociation rate constant k_{off}. Binding reaches equilibrium when the rate of formation of liganded receptor is equal to the rate of dissociation of ligand-receptor complexes:

$$[L] \times [R] \times k_{on} = [LR] \times k_{off} \qquad (2)$$

This equation is rearranged to give two equilibrium constants:

$$\frac{[L] \times [R]}{[LR]} = \frac{k_{off}}{k_{on}} = K_d \qquad (3)$$

where K_d is the equilibrium dissociation constant, i.e. the concentration of the radioligand that results in binding to 50% of the receptors, and

$$\frac{[LR]}{[L] \times [R]} = \frac{k_{on}}{k_{off}} = K_a \qquad (4)$$

where K_a is the equilibrium association constant.

The law of mass action predicts the fractional receptor occupancy at equilibrium as a function of ligand concentration. Fractional occupancy is the fraction of all receptors that have bound to the radioligand.

$$\textbf{Fractional occupancy} = \frac{[LR]}{[R]_{total}} = \frac{[LR]}{[R] + [LR]} \qquad (5)$$

Multiplying both numerator and denominator by [L]/[LR] and substituting the definition of K_d:

$$\textbf{Fractional occupancy} = \frac{[L]}{[L] + K_d} \qquad \textbf{(6)}$$

Equilibrium specific binding (B_{eq}) at a particular radioligand concentration equals fractional occupancy times the total receptor number (B_{max}):

$$B_{eq} = \textbf{Fractional occupancy} \times B_{max} = \frac{B_{max} \times [L]}{K_d + [L]} \qquad \textbf{(7)}$$

2.4.1 Homologous competition binding assays

Homologous competition binding assays have been used to characterize the M_2 receptor in membrane preparations and to obtain the K_d value of the radiolabeled probe for the calculation of the dissociation constant of the orthosteric test compounds (K_i) in heterologous binding experiments (see paragraph 2.4.3).

These experiments are based on the competition between a compound, used in multiple concentrations, and its corresponding radiolabelled compound, used in one single concentration; in this work the antagonist N-methylscopolamine (NMS), tritiated and unlabelled, was used as probe. The aim of these assays is to determine the K_d value as a measure of affinity for NMS, and the receptor number (B_{max}) in the membrane preparations.

A computer program is used to plot the obtained values for [^{3}H]NMS-binding on the ordinate against the logarithm of the concentration of the competitor on the abscissa. Subsequently, nonlinear regression analysis on the basis of the following four parameter logistic function is utilized to calculate a sigmoidal curve that fits best to the set of data points:

$$B_{tot}([X]) = Min + \frac{Max - Min}{1 + (IC_{50} / [X]^{n_H})} \qquad \textbf{(8)}$$

where $B_{tot}([X])$ is [^{3}H]NMS total binding in the presence of a concentration [X] of the inhibitor, Min is the lower plateau of the curve ([^{3}H]NMS unspecific binding), Max is the upper plateau of the curve ([^{3}H]NMS total binding in the absence of inhibitor), IC_{50} is the inflection point of the curve

([^{3}H]NMS specific binding is reduced by 50% if [X]=IC_{50}) and n_H is the Hill slope (a measure of the curve steepness).

This analysis yields three values: the top plateau (Max), which is the total binding of radioligand without competitor, the bottom plateau (Min), which is the nonspecific binding of the radioligand, and the IC_{50}, which represents the concentration of unlabeled ligand that displaces half the specific radioligand binding.

From these data it is also possible to obtain the specific binding of the radioligand (B_{eq}):

$$B_{eq} = Max - Min \quad (9)$$

while the K_d and the B_{max} are calculated as follows.

According to the equation of Cheng and Prusoff (1973):

$$IC_{50} = K_{unlabeled} \times \frac{1 + L}{K_{labeled}} \quad (10)$$

in which $K_{unlabeled}$ and $K_{labeled}$ are the dissociation constants of the unlabeled and labeled ligand respectively, and L is the concentration of radioligand used. The labeled and unlabeled ligands are assumed to bind with the same affinity to the receptors, then $K_{labeled} = K_{unlabeled} = K_d$. Substituting in (10):

$$IC_{50} = K_d \times (1 + L/K_d) \quad (11)$$

$$IC_{50} = K_d + L \quad (12)$$

$$K_d = IC_{50} - L \quad (13)$$

According to the law of mass action:

$$B_{max} = B_{eq} \times \frac{K_d + L}{L} \quad (14)$$

Substituting from (13):

$$B_{max} = B_{eq} \times \frac{IC_{50}}{L} \qquad (15)$$

These equations for K_d and B_{max} calculations, formulated by DeBlasi et al. (1989), are based on four assumptions: that the labeled and unlabeled ligands have identical affinities for the receptor; that only one class of binding site exists; that there is no cooperativity between binding sites and that only a small fraction of the total ligand is bound to the receptors.

2.4.1.1 Experimental procedure

In the performed assays [^{3}H]NMS was added at the concentration of 0.2 nM. The [^{3}H]NMS was used in competition with the unlabeled NMS molecule, in multiple concentrations ranging from 10^{-12} to 10^{-6} M; the nonspecific binding was determined by adding an excess of atropine, in order to occupy all the specific binding sites.

The assays were performed in 96-well plates (M1) either in Tris buffer (S13), Tris NaCl buffer (S14) or Tris KCl buffer (S15) at pH 7.4 and incubated for 3 hours in a shaking water bath (T7) at 24°C. At the end of the incubation, the plates were filtrated in a TomTec filtration device (T24), through glass fibre mats (M14) previously soaked with polyethyleneimine (PEI) solution (S12) for 4-5 minutes to reduce unspecific binding to the filter material. The filters were then dried in a microwave (T18) for 2.5 minutes and transferred to a heating block (T19) after covering them with melt-on scintillator sheets (M12). Finally, they were inserted in a plastic protector (M15) and put into a cassette (M13). A solid scintillator counter (T30) was used to detect and quantify receptor-bound [^{3}H]NMS. The reaction mixture is indicated in the table below (Table 2.1):

	Total binding (µl)	Unspecific binding (µl)	Competition (µl)	Final concentration/well
NMS	-	-	50	Variable
Atropine	-	50	-	10 µM
H_20	50	-	-	-
GDP	50	50	50	100 µM
Membranes	100	100	100	30 µg/ml
Buffer	250	250	250	See above
[^{3}H]NMS	50	50	50	0.2 nM

Table 2.1: Composition of the homologous competition binding assay

2.4.2 Dissociation binding assays

Dissociation binding assays were performed either to better characterize the kinetic properties of the radioligand in the employed buffers, or to analyze an allosteric modulation of the receptor.

2.4.2.1 Complete dissociation

Complete dissociation binding studies were performed with the radioligand [^{3}H]NMS in order to calculate the dissociation rate constant k_{-1} and the half-life of dissociation, which is fundamental to estimate the incubation time for reaching equilibrium in heterologous binding experiments.
In general, a complete dissociation assay is performed in two steps. First, the receptor is pre-labeled to equilibrium with a concentration of radioligand that provides high initial occupancy, and, secondly, the dissociation is induced by the addition of a saturating concentration of unlabeled ligand in order to prevent re-binding of the radiolabeled compound. The time course of dissociation is analyzed using the following exponential function:

$$[RL] = [RL_0]e^{-k_{-1}t} \quad \textbf{(16)}$$

where [RL] is the ligand-receptor complex at a specific time-point after the beginning of dissociation measurement, $[RL_0]$ is the ligand-receptor complex at time zero, k_{-1} is the dissociation

constant of the radioligand-receptor complex and t is the time after the beginning of dissociation measurement.

The half-life of radioligand dissociation ($t_{1/2}$) is calculated with

$$t_{1/2} = \frac{ln2}{k_{-1}} \quad (17)$$

2.4.2.1.1 Experimental procedure

Complete dissociation binding studies were performed to determine the dissociation half-life of [^{3}H]NMS in Tris and Tris NaCl buffer. The assays were performed in 96 well plates. Membrane homogenates were incubated with the radioligand [^{3}H]NMS for 90 min in a shaking water bath at 24^{o}C. The nonspecific binding was determined by adding an excess of atropine. After 90 min of incubation, atropine was added at different time points over a course of 90 min to initiate radioligand dissociation. The filtration and quantification of radioligand binding were performed as described in the previous paragraph (2.4.1.1). The composition of the assay mixture is summarized in the table below (Table 2.2):

	Total binding (µl)	Unspecific binding (µl)	Dissociation (µl)	Final concentration/well
Atropine	-	50	50	10 µM
H_20	50	50	50	-
GDP	50	50	50	1 µM
BSA	50	50	50	0.5%
Membranes	100	100	100	30 µg/ml
Buffer	200	150	150	See 2.4.1.1
[^{3}H]NMS	50	50	50	2 nM

Table 2.2: Composition of complete dissociation binding assay

2.4.2.2 Two-point kinetic experiments

Two-point kinetic experiments are generally used to prove an allosteric modulation of a receptor, demonstrating altered radioligand dissociation in the presence of the allosteric modulator. These assays were used to quantify the allosteric potency; the approach is simpler than recording complete dissociation curves, and it consists in the measurement of the amount of radioligand bound at the start and the amount of residual radioligand bound at a fixed interval after dissociation began.

The residual binding data obtained were then analyzed with a monophasic exponential decay model, described by the equation:

$$B_t = B_0 e^{-k_{-1}t} \qquad \textbf{(18)}$$

where B_t is the amount of specific binding at the time *t*, B_0 is the amount bound at the beginning, and k_{-1} is the rate constant of dissociation. The $EC_{50,diss}$, that is the concentration at which dissociation is retarded by 50%, has then been determined by fitting the values of k_{-1} to a nonlinear regression curve with variable slope.

2.4.2.2.1 Experimental procedure

The assay was performed in 96-well plates in either Tris or Tris NaCl buffer. At first, a mastermix composed of buffer, [^{3}H]NMS and membrane suspensions was prepared and incubated at 24°C to reach the formation of the receptor-NMS complex. The unspecific binding was determined by adding water, buffer, [^{3}H]NMS, membrane suspensions and an excess of atropine directly in the plates, and then incubating them at 24°C for 45 min. Before filtrating, the mastermix was added in the wells of total binding (containing only water), control (containing water and atropine), and test compounds in water, at 12 and 9 minutes before filtration in case of Tris buffer and at 6 and 3 minutes before filtration in Tris NaCl buffer. The filtration and quantification of radioligand binding were performed as described previously (2.4.1.1). The composition of the assay mixture is summarized in the table below (Table 2.3):

	Total binding (µl)	Unspecific binding (µl)	Dissociation (µl)	Final concentration/well
Ligand	-	-	50	Variable
Atropine	-	50	50	10 µM
H_20	100	50	-	-
GDP	50	50	50	1 µM
BSA	50	50	50	0.5%
Membranes	50	50	50	30 µg/ml
Buffer	200	200	200	See 2.4.1.1
[^{3}H]NMS	50	50	50	2 nM

Table 2.3: Composition of the dissociation binding assay

2.4.3 Heterologous competition binding assays

These experiments were used to determine the binding affinity of the tested compounds. The binding of unlabeled ligands is measured indirectly, by the reduction in radioligand binding in the presence of unlabeled ligand. If the unlabeled ligand interacts competitively with the radioligand, then fractional inhibition of radioligand binding can be expressed as:

$$\textbf{Fractional inhibition} = \frac{[I]}{[I] + IC_{50}} \qquad \textbf{(19)}$$

where [I] is the concentration of inhibitor, and IC_{50} is the inhibitor concentration causing 50% inhibition of radioligand binding. Just as the inhibitor competes with the radioligand, so the radioligand competes with the inhibitor and the IC_{50} will usually be larger than the dissociation constant of the inhibitor. This value is calculated from the IC_{50} using the equation of Cheng and Prusoff (1973):

$$K_i = \frac{IC_{50}}{1 + \frac{[L]}{K_d}} \qquad \textbf{(20)}$$

where K_i is the dissociation constant of the inhibitor, and [L] and K_d are the concentration and dissociation constant, respectively, of the radioligand.

Nonlinear regression analysis is used to plot the radioligand binding against the increasing concentrations of the competitor. The analysis is based on the four parameter logistic function (Eq. 8).

In case of experiments performed in the presence of allosteric or dualsteric ligands, the influence of the allosteric component had to be taken into account during data analysis. Indeed, allosteric and dualsteric ligands are able to bind simultaneously with the orthosteric compounds to the receptor, influencing their binding reciprocally. The mutual influence between the two ligands is termed cooperativity (α) and their simultaneous interaction with the receptor can be depicted by the allosteric ternary complex model (ATCM) (Ehlert, 1988):

$$\begin{array}{ccc} [\boldsymbol{A}] + [\boldsymbol{R}] + [\boldsymbol{L}] & \underset{K_L}{\rightleftharpoons} & [\boldsymbol{A}] + [\boldsymbol{RL}] \\ \Updownarrow K_A & & \alpha K_A \Updownarrow \\ [\boldsymbol{AR}] + [\boldsymbol{L}] & \overset{\alpha K_L}{\rightleftharpoons} & [\boldsymbol{ARL}] \end{array} \qquad \textbf{(21)}$$

In this scheme, K_L is the dissociation constant of the radioligand L for its site on the receptor (R), K_A is the dissociation constant of allosteric compound (A) for its site, and LR and AR represent the drug-receptor complexes. At equilibrium, the effect which L has on the affinity of A is equivalent to the effect which A has on the affinity of L and this reciprocal interaction is defined as "cooperativity"; its magnitude is equivalent to the factor (α) by which the two drugs either increase or decrease their respective dissociation constants. Thus, αK_A denotes the dissociation constant for the binding of A to RL, αK_L denotes the dissociation constant for the binding of L to AR, and ARL is the resultant ternary complex.

An allosteric modulator can show positive, negative or neutral cooperativity, namely increasing, decreasing or leaving unaffected the affinity of the orthosteric ligand, respectively. Values of α between 0 and 1 indicate positive cooperativity, while values of α > 1 demonstrate negative cooperativity. When α = 1, the cooperativity is neutral. The following equation was used to calculate the affinity according to the ATCM (Ehlert, 1988):

$$B_L([A]) = \frac{B_0([L] + K_L)}{[L] + K_L\left(\frac{K_A + [A]}{K_A + [A]/\alpha}\right)} \qquad \textbf{(22)}$$

where $B_L([A])$ is the specific binding of the orthosteric ligand L in the presence of an allosteric ligand with concentration [A]. Notably, $B_L([A])$ = [RL] + [ARL]. B_0 is the specific binding of the orthosteric ligand in the absence of the allosteric ligand.

The incubation time to reach the equilibrium in the presence of allosteric and dualsteric ligands was calculated from the results of the dissociation experiments, considering that the time taken to attain 97% of the final equilibrium value is 5 × $t_{1/2}$, where $t_{1/2}$ is the half-life of radioligand dissociation in presence of the allosteric ligand. The $t_{1/2}$ value was calculated according to the following equation (Lazareno and Birdsall, 1995):

$$t_{1/2} = t_{1/2^{off}} \times (1 + \frac{[A]}{EC_{50,\,diss}}) \qquad \textbf{(23)}$$

where $t_{1/2off}$ is the dissociation half-life of the radioligand under control conditions, [A] is the concentration of the allosteric modulator and $EC_{50,diss}$ is the concentration of allosteric modulator that retards radioligand dissociation by 50%.

2.4.3.1 Experimental procedure

The heterologous competition binding assays were carried out as previously described in paragraph 2.4.1.1, with the difference that the nonlabeled compounds used were the test compounds and the reaction mixture contained 100 µM of GDP, to uncouple the receptors from their G proteins and thus ensuring monophasic competition curves.

The reaction composition is illustrated in the table below (Table 2.4):

	Total binding (µl)	Unspecific binding (µl)	Competition (µl)	Final concentration/well
Ligand	-	-	50	Variable
Atropine	-	50	-	10 µM
H_20	50	-	-	-
GDP	50	50	50	100 µM
Membranes	100	100	100	30 µg/ml
Buffer	250	250	250	See 2.4.1.1
[^{3}H]NMS	50	50	50	0.2 nM

Table 2.4: Composition of the heterologous competition binding assay

2.5 [^{35}S]GTPγS binding assays

The [^{35}S]GTPγS binding assay was used to measure the level of G protein activation induced by the test compounds after the binding to the M_2 and the $M_2^{422W\rightarrow A}$ receptors.

The main advantage of this assay is that it measures a functional consequence of receptor occupancy at one of the earliest receptor-mediated events. The assay is based on the mechanism of action of G proteins: activation of receptors by an agonist leads to the dissociation of GDP from the Gα subunit, allowing GTP to bind to Gα. This leads to the functional dissociation of the Gα-GTP and Gβγ subunits, resulting in the activation of their effector systems. The heterotrimer is eventually recreated following GTPase activity of the Gα subunit, forming Gα-GDP and so allowing Gα and Gβγ to reassociate. Agonist activation increases the rate of guanine nucleotide exchange and, therefore, the amount of active Gα-GTP and Gβγ. While this process follows agonist occupation of receptor, receptors may also assume active conformations in the absence of agonist and so constitutively activate G proteins (Lefkowitz et al., 1993).

In the [^{35}S]GTPγS binding assay, [^{35}S]GTPγS replaces endogenous GTP and binds to the Gα subunit following activation of the receptor to form a Gα-[^{35}S]GTPγS species. Since the γ-thiophosphate bond is resistant to hydrolysis by the GTPase of Gα, G protein is prevented from reforming as a heterotrimer and thus [^{35}S]GTPγS labeled Gα subunits accumulate in the membrane and can be measured by counting the amount of [^{35}S]-label incorporated.

The assay requires the addition of exogenous GDP, because it acts by filling empty nucleotide binding sites on the Gα subunit and hence reduces the basal level of [^{35}S]GTPγS binding such that agonist-induced exchange of GDP for [^{35}S]GTPγS can be observed (Harrison and Traynor, 2003).
The [^{35}S]GTPγS assay allows generation of concentration-effect curves and therefore potency (EC_{50}) and maximum effect (E_{max}) measures. However, it has to be taken into account that agonist efficacy determined in this assay is not an absolute measure, and it is then necessary to perform the experiments with at least one reference compound, preferentially a full agonist, in order to be able to discriminate between full and partial agonism activity of the tested compounds.

2.5.1 Experimental procedure

The assay was carried out in 96-well plates, pipetting all the reagents (see Table 2.5) and incubating the plates in a water bath for 60 minutes at 24°C. The filtration was performed as previously described (see 2.4.1.1), with the exception that the glass fiber filters were deposited in distilled water instead of PEI solution.

	Basal binding (µl)	Unspecific binding (µl)	Agonist-induced binding (µl)	Final concentration/well
Ligand	-	-	50	Variable
Atropine	-	50	-	10 µM
H_20	100	50	50	-
GDP	50	50	50	1 µM
BSA	50	50	50	0.5%
Membranes	50	50	50	40 µg/ml
Buffer	200	200	200	See 2.4.1.1
[^{35}S]GTPγS	50	50	50	0.7 nM

Table 2.5: Composition of [^{35}S]GTPγS binding assay

2.6 Statistics

In this study, the data were processed by descriptive statistics and summarized. The values were described by statistical parameters and graphs. As a measure of central tendency, the arithmetic mean ($\bar{x}$) was used:

$$\bar{X} = \frac{1}{n}\sum_{i=1}^{n} X_i \qquad (24)$$

$\bar{x}$: arithmetic mean

n: number of values

x_i: individual value

As a measure of scatter, the variance (s^2) is used; it describes the dispersion of the individual values around the mean, and it represents the sum of the squares of the deviations from the mean of the individual values divided by the number of degrees of freedom:

$$s^2 = \frac{1}{n-1}\sum_{i=1}^{n} (X_i - \bar{X})^2 \qquad (25)$$

The square root of the variance, named standard deviation (s), indicates the average deviation of individual values from the mean:

$$s = \sqrt{\frac{1}{n-1}\sum_{i=1}^{n} (X_i - \bar{X})^2} \qquad (26)$$

In this work, as a measure of scatter, the standard error of the mean (SEM) is used, as a measure of accuracy:

$$\mathrm{SEM} = \frac{s}{\sqrt{n}} \qquad (27)$$

In the result section, a parameter a determined by measurement is in general indicated as $a = \bar{x} \pm$ SEM.

Statistics was also employed to decide, if the means of two normally distributed data sets were equal. This was performed using an independent two sample two-tailed t-test, in which it was assumed that the variances of both data sets were identical. This assumption was previously validated with an F-test. The level of significance p for all hypothesis tests was chosen as p=0.05.

The test statistic of the F-test (F) is the ratio of the variances of the two data sets:

$$F = \frac{s_1^2}{s_2^2} \qquad (28)$$

The null hypothesis is $s_1^2 = s_2^2$ and the alternative hypothesis is therefore $s_1^2 \neq s_2^2$, so both variances are assumed to be identical. If the calculated F-value was greater than the tabulated critical F-value for p, the null hypothesis was rejected.

In case the number of data sets was equal or superior to three, a one-way ANOVA test was used. One-way ANOVA compares three or more unmatched groups, based on the assumption that the populations are Gaussian. The result of this analysis is a P value, which tests the null hypothesis that data from all groups are drawn from populations with identical means. If the overall P value is large, there is no evidence that the means of the data differ. If the overall P value is small, then it is unlikely that the differences observed are due to random sampling. Since a simple one-way ANOVA does not indicate which means differs from every other mean, the Bonferroni post-test was subsequently applied, in order to identify the exact differences throughout the data sets.

2.7 Materials

2.7.1 Technical equipment

In this section, the utilized technical equipment is listed.

Beckman Coulter Inc. (Unterschleißheim, Germany)

T1 Beckman Avanti J-20 XP centrifuge

T2 ϕ 390 pH/Temp/mV/ISE Meter

Beckman Instruments (Palo Alto, USA)

T3 Beckman LS 6500 scintillation counter

Biochrome, Inc. (Cambridge, UK)

T4 Ultrospec 3300 pro, UV/Vis spectrometer

Brand GmbH & Co KG (Wertheim, Germany)

T5 Accu-Jet® pipettor

Carl Zeiss Jena GmbH (Jena, Germany)

T6 Axiovert 25 microscope

Gesellschaft für Labortechnik, mbH (Burgwedel, Germany)

T7 GFL® shaking water bath 1083, 1086

Heraeus (Hilden, Germany)

T8 Herasafe® bench HS15, class II

H+P Labortechnik GmbH (Oberschleissheim, Germany)

T9 Variomag® heatable magnetic stirrer

Ika® Works Inc. (Wilmington, USA)

T10 MS 1 Minishaker

Kinematica AG (Littau-Luzern, Schweiz)

T11 Polytron homogenizer

Mettler Toledo AG (Greifensee, Schweiz)

T12 Balances AG204, B2002-S

Millipore GmbH (Schwalbach, Germany)

T13 Milli-Q® Biocel A10 ultrapure still

T14 Elix® still

Nalgene Company (Rochester, New York, USA)

T15 Mr Frosty 5100 Cyro 1 °C freezing container

Scientific Industries Inc. (Bohemia, New York, USA)

T16 Vortex Genie 2® G-560 E

Scotsman Ice Systems (Bettolino di Pogliano, Milano, Italy)

T17 Scotsman AF 100 AS-E 230/50/1 ice maker

Sharp Electronics Europe GmbH (Hamburg, Germany)

T18 Microwave Sharp P611

Techne (Duxford, Cambridge, UK)

T19 Dri-Block® DB2A

ThermoForma Scientific (Marietta, Ohio, USA)

T20 Thermoforma -80°C fridge

T21 Thermoforma series II water jacketed CO_2-incubator

Thermo Labsystems Oy (Helsinki, Finland)

T22 Finnpipette® digital pipets different sizes

T23 Finnpipette® Multistepper pipet

Tomtec Inc. (Hamden, USA)

T24 Harvester 96© Mach III M (product number: 963-589)

T25 Harvester 96© Mach III M (product number: 990607010)

Taylor Wharton Hasco GmbH (Husum, Germany)

T26 Neubauer counting chamber

T27 Nitrogen tank LS 750

VWR International (Langenfeld, Germany)

T28 Neubauer counting chamber

T29 Cover slips 20×26 mm for Neubauer counting chamber

Wallac (Turku, Finland)

T30 1450-Microbeta Trilux liquid scintillation & luminescence counter

2.7.2 Disposables

In this chapter are listed the expendable items and the manufacturers in the left row and their product number in the right row.

Abgene House (Epsome, UK)

M1 96-well microtiterplate, PP	AB-0564

Brand GmbH & Co KG (Wertheim, Germany)

M2 Pipet tips 0.5-5.0 ml	

Fisher Scientific (Schwerte, Germany)

M3 Scintillation vessel (PE) 21 ml with screw cap	619301

Greiner Bio-One GmbH (Soligen-Wald, Germany)

M4 Cellstar® disposable pipet 10 ml/25 ml	607160/760160
M5 Falcon tubes, sterile, 15 ml/50 ml	227261
M6 Tissue culture plate, sterile 100/20 mm	664160
M7 Tissue culture plate, sterile 145/20 mm	639160

Merck Labor und Chemie Vertrieb GmbH (Bruchsal, Germany)

M8 Syringe filter units (0.22 µM CM membrane; sterile)	5122110

Nalgene Nunc International (Rochester, USA)

M9 Polycarbonate-PC-centrifuge tubes with cap, 50 ml	3138-0050
M10 Cryogenic vials, 1 ml	50001012

Pechiney Plastic Packaging (Menasha, USA)

M11 Parafilm® M laboratory film	PM-996

Perkin Elmer Life Sciences GmbH (Rodgau-Jügesheim, Germany)

M12 MeltiLexTM A scintillation wax	1450-441
M13 Plate cassette	1450-105
M14 Printed filtermat A	1450-441
M15 Sample bag	1450-432

Sarstedt AG & Co. (Nümbrecht, Germany)

M16 Cell scraper, sterile, 25 cm	83.1830
M17 Pipet tips TipOne® 1-200 µl	S1111-0006
M18 Pipet tips TipOne® 101-1000 µl	S1111-2020

ThermoForma Scientific (Marietta, Ohio, USA)

M19 Finnpipette® multistepper pipet tips 1.25 ml, 2.5 ml, 5.0 ml

2.7.3 Reagents

In this section are listed the reagents on the left and the product number on the right.

Acros Organics (Geel, Belgium)

R1 Sodium butyrate	26319
R2 Sodium chloride	207790010

AppliChem (Darmstadt, Germany)

R3 EDTA disodium salt dihydrate	A2937,0100

Grüssing GmbH (Filsum, Germany)

R4 Hydrochloric acid (HCl, 1 M)

Merck KGaA (Darmstadt, Germany)

R5 Folin-Ciocalteu phenol reagent	1.09001.0500
R6 Copper sulfate penta hydrate ($CuSO_4 \times H_2O$) (MW: 249.7 g/mol)	1.02790.0250
R7 Sodium carbonate (Na_2CO_3) (MW: 106.0 g/mol)	1.06392.0500

Millipore GmbH (Schwalbach, Germany)

R8 Aqua destillata (Elix® system)

R9 Aqua pro analysi (Milli Q® system)

Perkin Elmer Life Science GmbH (*Rodgau-Jügesheim, Germany*)

R10 Emulsifier-Safe™	6013389

Riedel-de Haen (Seelze, Germany)

R11 Sodium hydroxide (NaOH 1 mol/l)	06213

Roth (Karlsruhe, Germany)

R12 Hydrochloric acid (HCl 6 mol/l)

R13 Potassium Chloride	6791.3
R14 TRIS Pufferan®	4855.1

Sigma-Aldrich Chemie GmbH (Taufkirchen, Germany)

R15 Atropine sulfate (MW: 676,8 g/mol)	A-0257

R16 Bovine Serum Albumine	A2153
R17 Potassium-sodium tartrate tetrahydrate	379832
($KNaC_4H_4O_6 \times 4H_2O$) (MW: 282.22 g/mol)	
R18 DL-Dithiothreitol	D0632
R19 Dulbecco's phosphate buffered saline (DPBS)	D-5652
R20 Ethylenediaminetetraacetic acid (EDTA)	E-9884
R21 Fetal bovine serum (FBS)	F-7524
R22 Guanosine diphosphate (GDP) ($C_{10}H_{15}N_5O_{11}P_2$) sodium salt	G-7127
(MW: 465 g/mol)	
R23 HEPES sodium salt (MW: 260.3 g/mol)	H-7009
R24 HEPES potassium salt (MW: 276.39 g/mol)	H-0527
R25 HEPES acid (MW: 238.9 g/mol)	H-3375
R26 Human serum albumin	A-1653
R27 L-Glutamine 200mM	G-7513
R28 Magnesium chloride hexahydrate ($MgCl \times 6H_2O$) (MW: 302.3 g/mol)	P-5379
R29 N-methyl-D-glucamine (MW: 195.21 g/mol)	66930
R30 Nutrient mixture F-12 Ham	N-4888
R31 Penicillin-streptomycin solution	P-0781
R32 Polyethylenimine solution (PEI)	P-3143
R33 2-Propanol, 99.5 % (HPLC)	270490
R34 Sodium Bromide	S4547
R35 Trypsin-EDTA-solution (0.5 g/l Trypsin; 0.2 g/l Na_4EDTA)	B-4252

2.7.4 Solutions and buffers

S1 Butyrate stock solution (100 mM)

5.55 g sodium-butyrate (R1) was solved in 500 ml aqua destillata (R8). Storage at 2-8 °C.

S2 Cu_2SO_4 solution 1 %

1 g copper sulphate pentahydrate (R6) was solved in 100 ml aqua destillata (R8). It was stored at room temperature.

S3 Folin-Ciocalteu reagent

The Folin-Ciocalteu reagent (R5) was diluted 1:3 with aqua destillata (R8). It was stored at room temperature.

S4 HEPES stock solution (200 mM) pH 7.4

8.68 g HEPES sodium salt (R23) and 15.89 g HEPES acid (R25) were solved in 500 ml Aqua destillata (R8). The pH was adjusted to 7.4 by the addition of 1 N NaOH (R11). Storage at 2-8°C.

S5 HEPES buffer 1 (20 mM HEPES, 10 mM Na_2EDTA) pH 7.4

50 ml HEPES stock solution (S4) and 50 ml Na_2EDTA standard solution (R8) were added to 400 ml aqua destillata (R8). Storage at 2-8°C.

S6 HEPES buffer 2 (20 mM HEPES, 0.1 mM Na_2EDTA) pH 7.4

50 ml HEPES stock solution (S4) and 0.5 ml Na_2EDTA standard solution (R8) were filled up to 500 ml aqua destillata (R8). Storage at 2-8°C.

S7 HEPES potassium buffer (12.5 mM HEPES, 12.5 mM $MgCl_2$; 125 mM KCl) pH 7.4

9.9 g HEPES acid (R25), 5.4 g HEPES salt (R23), 12.7 g magnesium chloride (R28) and 46.6 g potassium chloride (R13) were solved in 5000 ml distilled water (R8). The pH was adjusted to 7.4 with 1 N NaOH (R11). Storage at 2-8 °C.

S8 HEPES low cations buffer (12.5 mM HEPES, 12.5 mM $MgCl_2$) pH 7.4

9.9 g HEPES acid (R25), 5.4 g HEPES salt (R23) and 12.7 g magnesium chloride (R28) were solved in 5000 ml distilled water (R8). The pH was adjusted to 7.4 with 1 N NaOH (R11). Storage at 2-8 °C.

S9 $KNaC_4H_4O_6$ solution 2 %

2 g potassium-sodium tartrate tetrahydrate (R17) were solved in 100 ml aqua destillata (R8). Storage at room temperature.

S10 Na_2CO_3 solution 2 %

2 g of sodium carbonate (R7) were solved in 100 ml 0.1 N NaOH.

S11 Nutrient mixture F12-Ham

50 ml fetal bovine serum (R21), 5 ml penicillin-streptomycin solution (R31) and 4 ml glutamine solution (R27) were added to 500 ml Ham's F12 medium (R30). Storage at 2-8°C.

S12 Polyethylenimine solution

10 g Polyethylenimine solution (R32) was filled up to 507 g with aqua destillata (R8). Storage at 2-8°C.

S13 Tris buffer

1.9 g Tris (R14), 0.127 g magnesium chloride (R28), 0.116 g Na_2EDTA (R3) and 0.048 g DTT (R18) were solved in 250 ml distilled water (R8). The pH was adjusted to 7.4 with 1 M HCl (R4). Storage at 2-8 °C.

S14 Tris NaCl buffer

1.9 g Tris (R14), 0.127 g magnesium chloride (R28), 0.116 g Na_2EDTA (R3), 0.048 g DTT (R18) and 3.65 g NaCl (R2) were solved in 250 ml distilled water (R8). The pH was adjusted to 7.4 with 1 M HCl (R4). Storage at 2-8 °C.

S15 Tris KCl buffer

1.9 g Tris (R14), 0.127 g magnesium chloride (R28), 0.116 g Na_2EDTA (R3), 0.048 g DTT (R18) and 4.66 g KCl (R13) were solved in 250 ml distilled water (R8). The pH was adjusted to 7.4 with 1 M HCl (R4). Storage at 2-8 °C.

S16 Tris NaBr buffer

1.9 g Tris (R14), 0.127 g magnesium chloride (R28), 0.116 g Na_2EDTA (R3), 0.048 g DTT (R18) and 6.43 g NaBr (R34) were solved in 250 ml distilled water (R8). The pH was adjusted to 7.4 with 1 M HCl (R4). Storage at 2-8 °C.

S17 Tris NMDGCl buffer

1.9 g Tris (R14), 0.127 g magnesium chloride (R28), 0.116 g Na_2EDTA (R3), 0.048 g DTT (R18) and 12.2 g NMDG (R29) were solved in 250 ml distilled water (R8). The pH was adjusted to 7.4 with 1 M HCl (R4). Storage at 2-8 °C.

S18 Tris wash buffer

30.29 g Tris (R14) and 5.08 g magnesium chloride (R28) were solved in 5000 ml distilled water (R8). The pH was adjusted to 7.4 with 6 M HCl (R11). Storage at 2-8 °C.

S19 HEPES incubation buffer (12.5 mM HEPES, 12.5 mM $MgCl_2$; 125 mM NaCl) pH 7.4

9.9 g HEPES acid (R25), 5.4 g HEPES salt (R23), 12.7 g magnesium chloride (R28) and 36.5 g sodium chloride (R2) were solved in 5000 ml distilled water. The pH was adjusted to 7.4 with 1 N NaOH (R11). Storage at 2-8 °C.

2.7.5 Ligands of the M_2 receptor and test compounds

Orthosteric agonists

Acetylcholine iodide
Molecular weight: 273.1 g/mol
Supplier: Sigma-Aldrich Chemie GmbH
(Steinheim, Germany)
Product number: A-7000
Endogenous ligand of the muscarinic receptors.

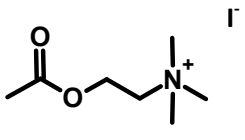

Iperoxo iodide
Molecular weight: 324.2 g/mol
Provided by Prof. Dr. H. Holzgrabe and coworkers
(University of Würzburg)
Super-high affinity agonist of muscarinic receptors.

Isox iodide
Molecular weight: 322.2 g/mol
Provided by Prof. Dr. H. Holzgrabe and coworkers
(University of Würzburg)
Agonist at muscarinic receptors.

Pilocarpine hydrochloride
Molecular weight: 244.72 g/mol
Supplier: Sigma-Aldrich Chemie GmbH
(Steinheim, Germany)
Product number: P6503
Partial agonist at muscarinic receptors.

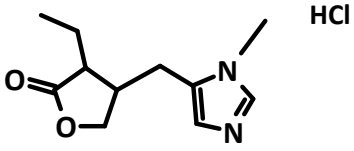

OOM iodide
Molecular weight: 324.16 g/mol
Provided by Prof. Dr. M. De Amici and coworkers
(University of Milan)
Agonist of muscarinic receptors.

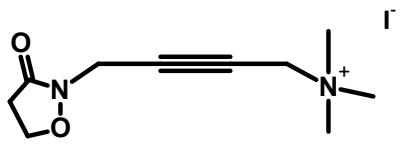

Figure 2.1: Description and chemical structure of the employed orthosteric agonists.

Orthosteric antagonists

N-methylscopolamine bromide
Molecular weight: 398.3 g/mol
Supplier: Sigma-Aldrich Chemie GmbH
(Steinheim, Germany)
Product number: S-8502
Inverse agonist of muscarinic receptors.

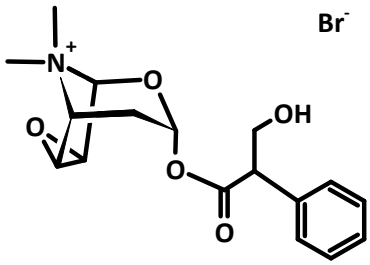

Atropine sulfate
Molecular weight: 676.8 g/mol
Supplier: Sigma-Aldrich Chemie GmbH
(Steinheim, Germany)
Product number: A-0257
Inverse agonist of muscarinic receptors.

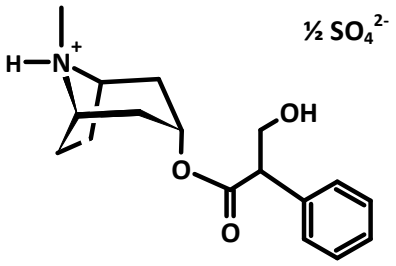

Figure 2.2: Description and chemical structure of the employed inverse agonists N-methylscopolamine and atropine.

Dualsteric compounds

ALB3 bromide
Molecular weight: 670.48 g/mol
Provided by Prof. Dr. M. De Amici
and coworkers (University of Milan).

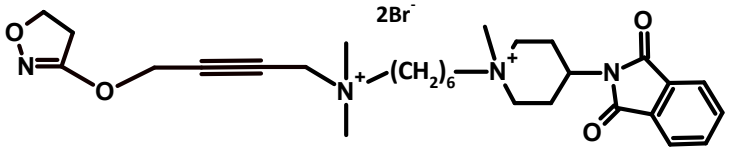

ALB4 bromide
Molecular weight: 720.54 g/mol
Provided by Prof. Dr. M. De Amici
and coworkers (University of Milan).

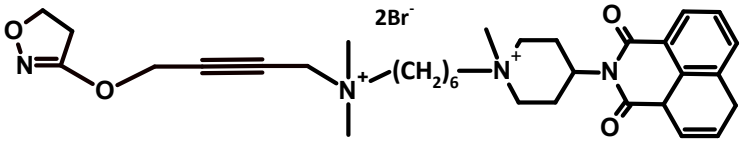

Isox-0-naph chloride
Molecular weight: 481.97 g/mol
Provided by Prof. Dr. M. De Amici
and coworkers (University of Milan).

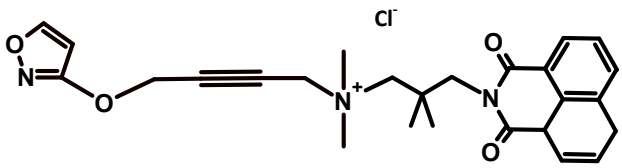

Isox-4-naph bromide
Molecular weight: 706.51 g/mol
Provided by Prof. Dr. M. De Amici
and coworkers (University of Milan).

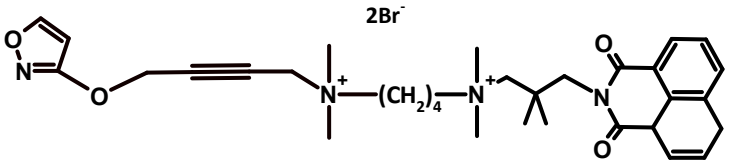

Isox-6-naph bromide
Molecular weight: 734.6 g/mol
Provided by Prof. Dr. M. De Amici
and coworkers (University of Milan).

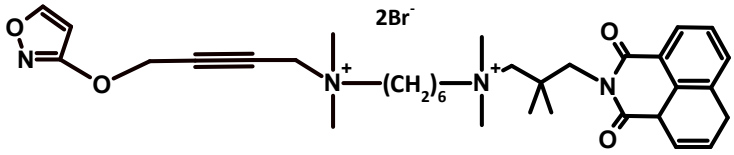

Isox-8-naph bromide
Molecular weight: 762.61 g/mol
Provided by Prof. Dr. M. De Amici
and coworkers (University of Milan).

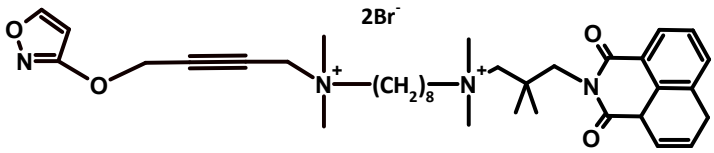

Iper-0-naph chloride
Molecular weight: 486 g/mol
Provided by Prof. Dr. H. Holzgrabe
and coworkers (University of Würzburg).

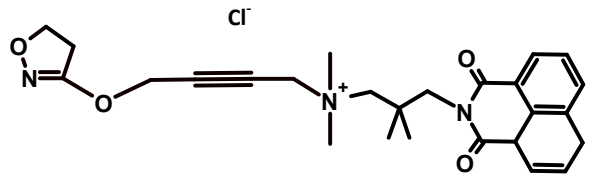

Iper-4-naph bromide
Molecular weight: 708.5 g/mol
Provided by Prof. Dr. H. Holzgrabe
and coworkers (University of Würzburg).

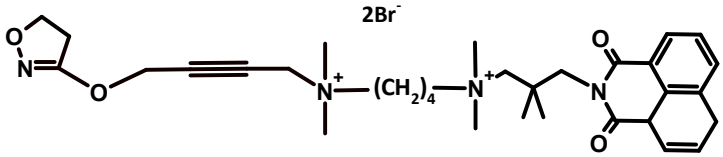

Iper-6-naph bromide
Molecular weight: 736.6 g/mol
Provided by Prof. Dr. H. Holzgrabe
and coworkers (University of Würzburg).

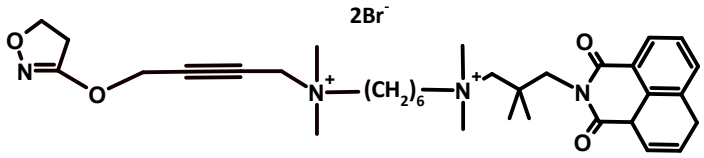

Iper-8-naph bromide
Molecular weight: 764.61 g/mol
Provided by Prof. Dr. H. Holzgrabe
and coworkers (University of Würzburg).

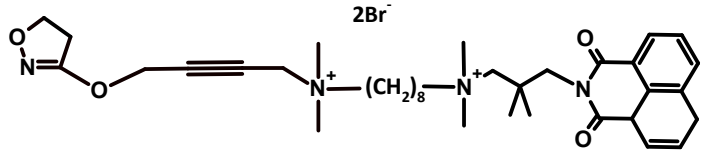

OOM-6-naph bromide
Molecular weight: 736.6 g/mol
Provided by Prof. Dr. M. De Amici
and coworkers (University of Milan).

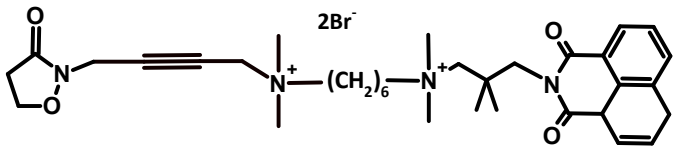

Isox-6-phth bromide
Molecular weight: 656.5 g/mol
Provided by Prof. Dr. H. Holzgrabe
and coworkers (University of Würzburg).

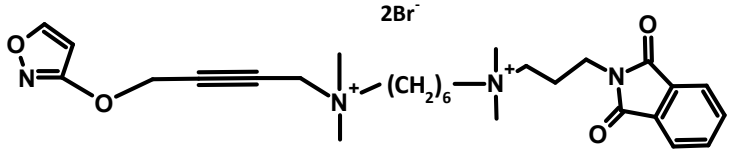

Iper-6-phth bromide
Molecular weight: 658.5 g/mol
Provided by Prof. Dr. H. Holzgrabe
and coworkers (University of Würzburg).

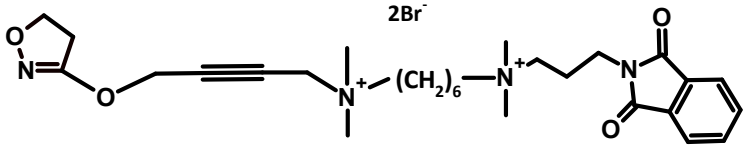

OOM-6-phth bromide
Molecular weight: 682.5 g/mol
Provided by Prof. Dr. M. De Amici
and coworkers (University of Milan).

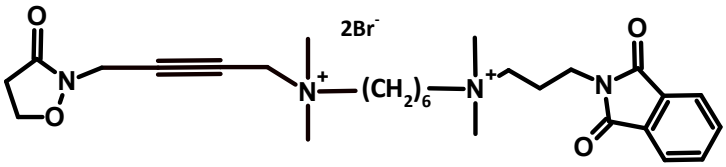

Figure 2.3: Description and chemical structure of the dualsteric compounds employed in this study. They were generously provided by Prof. Dr. M. De Amici and coworkers (Istituto di Chimica Farmaceutica e Tossicologica, Universitá degli Studi di Milano, Italy) and Prof. Dr. H. Holzgrabe and coworkers (Pharmaceutical and Medicinal Chemistry, University of Würzburg, Germany).

Allosteric fragments

6-naph bromide
Molecular weight: 627.49 g/mol
Provided by Prof. Dr. H. Holzgrabe
and coworkers (University of Würzburg).

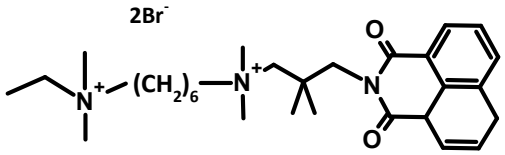

8-naph bromide
Molecular weight: 655.49 g/mol
Provided by Prof. Dr. H. Holzgrabe
and coworkers (University of Würzburg).

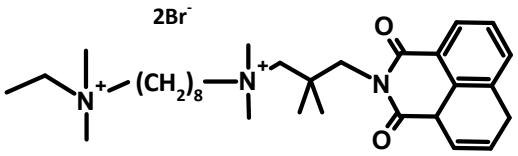

6-phth bromide
Molecular weight: 549.4 g/mol
Provided by Prof. Dr. H. Holzgrabe
and coworkers (University of Würzburg).

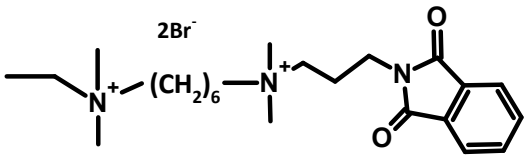

PCy-6-Et bromide
Molecular weight: 561.39 g/mol
Provided by Prof. Dr. M. De Amici
and coworkers (University of Milan).

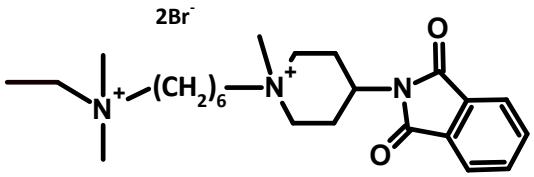

NCy-6-Et bromide
Molecular weight: 611.45 g/mol
Provided by Prof. Dr. M. De Amici
and coworkers (University of Milan).

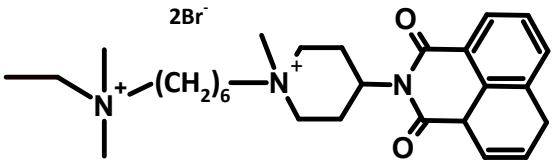

Figure 2.4: Description and chemical structure of the allosteric fragments employed in this study. They were generously provided by Prof. Dr. M. De Amici and coworkers (Istituto di Chimica Farmaceutica e Tossicologica, Universitá degli Studi di Milano, Italy) and Prof. Dr. H. Holzgrabe and coworkers (Pharmaceutical and Medicinal Chemistry, University of Würzburg, Germany).

2.7.6 Nucleotides

GDP (Guanosine 5'-diphosphate) sodium salt
Molecular weight: 465.2 g/mol
Supplier: Sigma-Aldrich Chemie GmbH
(Taufkirchen, Germany)
Product number: G-7127

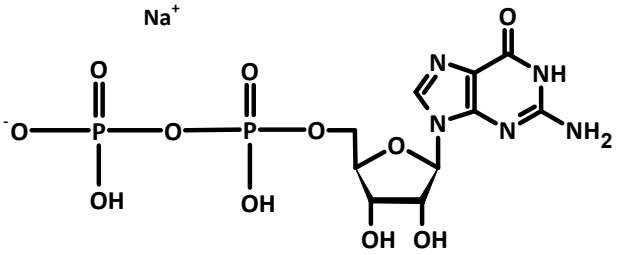

Figure 2.5: Description and chemical structure of the employed nucleotide GDP.

2.7.7 Radioactively labeled compounds

[^{3}H]N-methylscopolamine chloride
Molecular weight: 353.8 g/mol
Specific activity: 84.1 Ci/mol
Supplier: PerkinElmer Life Sciences (Boston, USA)
Product number: NET636001MC

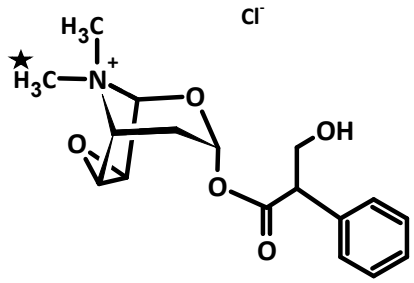

[^{35}S]GTPγS
Molecular weight: 539.2 g/mol
Specific activity: 1250 Ci/mol
Supplier: PerkinElmer Life Sciences
(Boston, USA)
Product number: NEG030H250UC

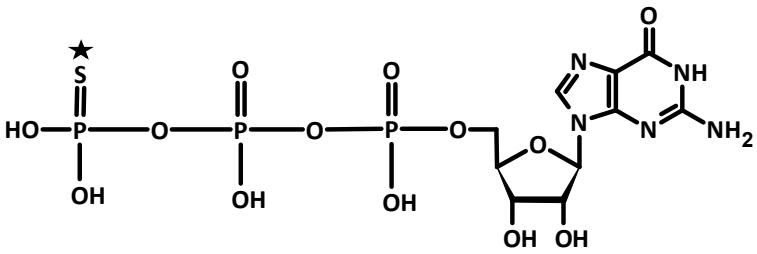

Figure 2.6: Description and chemical structure of the employed radiolabeled compounds [^{3}H]N-methylscopolamine and [^{35}S]GTPγS.

2.7.8 Computer software

GraphPad Prism® (Version 5.03; GraphPad® Software, San Diego, USA)
ChemSketch® (Version 12.01; Advanced Chemistry Development Inc., Toronto, Canada)
MathType® (Version 6.9b; Design Science Inc., Longbeach, California, USA)
Microsoft® Word (Version 2010; Microsoft Corporation, Redmond, USA)
Microsoft® Excel (Version 2010; Microsoft Corporation, Redmond, USA)
Microsoft® PowerPoint (Version 2010; Microsoft Corporation, Redmond, USA)

3 RESULTS

3.1 Determination of the level of spontaneous activity of the wild type M_2 receptor in different buffers

3.1.1 Sodium ions removal in HEPES buffer does not stimulate spontaneous activity

Generally, G_i-signalling is investigated in [^{35}S]GTPγS binding experiments performed in HEPES sodium buffer containing 100 mM NaCl (S19) supplemented with 10 µM GDP and 40 µg/ml membrane proteins, and incubated for 60 min at 30°C (Schrage et al., 2013; Bock et al., 2014). In this buffer, the spontaneous activity of the receptor is not reproducible as its level changes dramatically within a same set of experiments (Fig. 3.1).

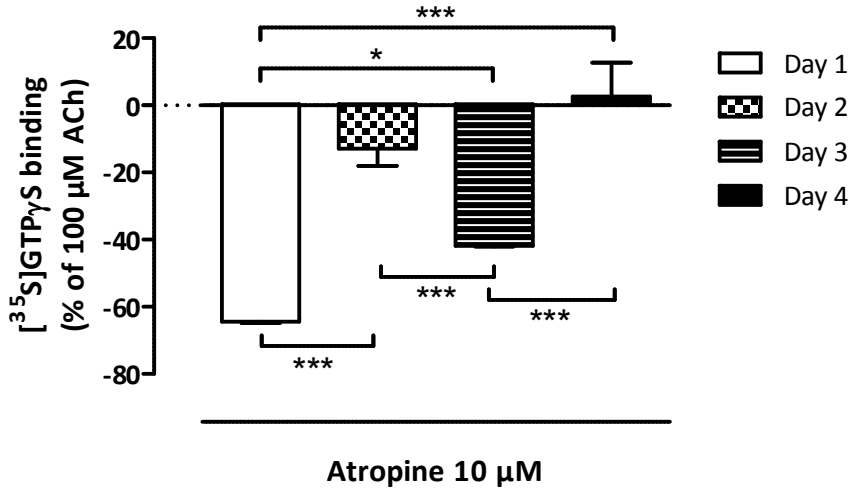

Figure 3.1: [^{35}S]GTPγS binding inhibited by 10 µM atropine. Ordinate: percentage of [^{35}S]GTPγS binding, normalized on maximum effect elicited by 100 µM ACh (set 100%). 0% corresponds to basal [^{35}S]GTPγS binding. The assay was performed in HEPES sodium buffer with an incubation time of 60 minutes at 30°C. The bar diagram shows mean ± SEM of single experiments performed in triplicate. *, **, ***: significantly different ($p<0.05$, 0.01, 0.001) according to one-way ANOVA with Bonferroni's multiples comparison test.

The parameters derived from these experiments are presented in Table 3.1.

Day	*E_{max} (%)*	*n*
1	-64 ± 1	1
2	-13 ± 5	1
3	-42 ± 1	1
4	3 ± 10	1

Table 3.1: Parameter values derived from Figure 3.1; E_{max}: maximum level of [^{35}S]GTPγS binding in percent normalized on 100 µM ACh, which was set to 100%; n: number of performed experiments. The table shows mean values ± SEM of single experiments carried out in triplicate.

Thus, different HEPES buffers were tested, in order to identify the appropriate conditions to establish a stable M_2 receptor system, which was either always spontaneously active or inactive. The constitutive activity of the M_2 receptor, revealed with a single concentration of atropine (10 µM), was quantified in HEPES potassium buffer (S7) and in an HEPES buffer with low cation concentration (S8), maintaining the same concentration of membrane protein and GDP, as well as identical temperature and incubation time. Even if sodium depletion is known to stimulate receptor constitutive activity in several systems (Costa and Herz, 1989; Tian et al., 1994), this was not the case for the M_2 receptor. Indeed, as shown in Fig. 3.2, 10 µM atropine did not decrease [^{35}S]GTPγS binding to a significant level, i.e. the receptor was inactive in both buffers.

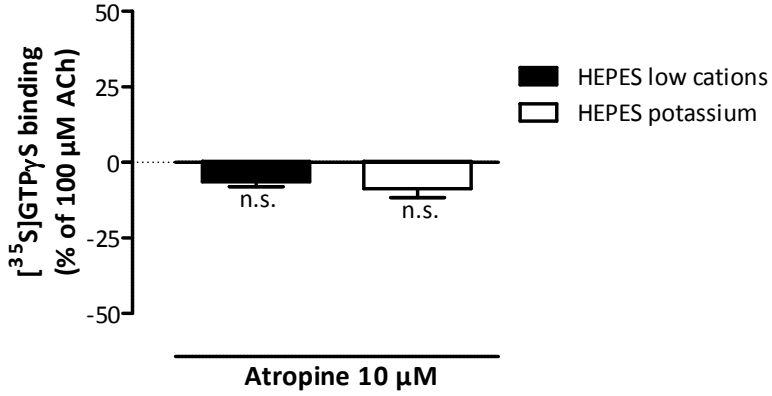

Figure 3.2: [^{35}S]GTPγS binding induced in the presence of 10 µM atropine. Ordinate: percentage of [^{35}S]GTPγS binding, normalized on maximum effect elicited by 100 µM ACh (set to 100%). 0% corresponds to basal [^{35}S]GTPγS binding. The assay was performed with an incubation time of 60 minutes at 30°C. The bar diagram shows mean ± SEM of 3 experiments performed in triplicate. n.s.: not significantly different from basal [^{35}S]GTPγS binding according to a two-tailed t-test.

A summary of the parameters derived from the data analysis is presented in Table 3.2.

Buffer	*E_{max} (%)*	*n*
HEPES low cations	-6 ± 2	3
HEPES potassium	-9 ± 3	3

Table 3.2: Parameter values derived from Figure 3.2; E_{max}: maximum level of [^{35}S]GTPγS binding in percent normalized on 100 µM ACh which was set to 100%; n: number of performed experiments. The table shows mean values ± SEM of 3 independent experiments carried out in triplicate.

Taken together, this system was not appropriate to generate spontaneous M_2 receptor activity.

3.1.2 Testing of M_2AChR spontaneous activity in different experimental settings

Taken into consideration that a stable spontaneous receptor system could not be obtained in the previously applied conditions (see 3.1.1), protein concentration, GDP, incubation time and temperature were individually changed in order to test the level of constitutive receptor activity in different settings. At first, the concentration of GDP was varied in HEPES potassium buffer, since this nucleotide is known to uncouple the receptor from the G protein (Chang and Snyder, 1980; De Lean et al., 1980; Lohse et al., 1984; Stiles, 1988) and might therefore have an influence on spontaneous activity. As shown in Fig. 3.3, at the GDP concentration of 10 µM (Log[GDP]= -5), the level of spontaneous activity was too small to have a measuring window for inverse agonism. Contrarily, at 1 µM (Log[GDP]= -6) and 0.3 µM (Log[GDP]= -6.5) of GDP, the constitutive activity was increased (i.e. the system was sensitive to atropine), together with the efficacy of the full agonist ACh. At lower GDP concentrations, the spontaneous activity was either absent (at 0.1 µM GDP (Log[GDP]= -7) as well as without any GDP) or the endogenous agonist was not showing a significant efficacy compared to the basal activity of the receptor (at Log[GDP]= -8).

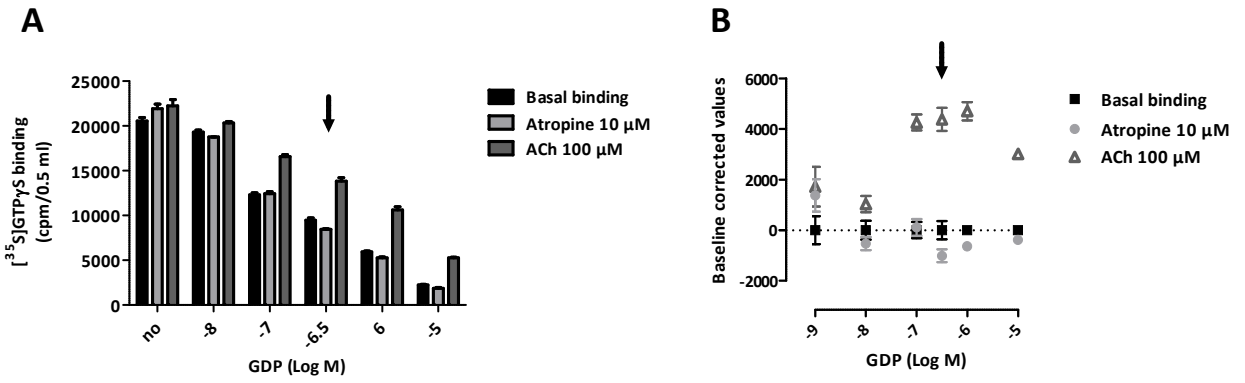

Figure 3.3: [^{35}S]GTPγS binding in control conditions (basal) and in the presence of ACh 100 µM and atropine 10 µM. (A) Ordinate: [^{35}S]GTPγS binding, expressed as counts per minute (cpm). (B) Ordinate: [^{35}S]GTPγS binding, corrected on the basal [^{35}S]GTPγS binding of each GDP concentration. Abscissa: concentration of GDP. The assay was performed in HEPES potassium buffer with an incubation time of 60 minutes at 30°C. The graph shows mean ± SEM of a representative experiment performed in triplicate.

Considering that the previous results indicated 0.3 µM GDP as the ideal concentration to allow visualization of both positive and negative agonism, a representative curve for atropine and ACh was obtained in HEPES potassium buffer with 0.3 µM GDP. As shown in Fig. 3.4, the resulting amount of spontaneous activity was too small to attain a concentration-effect curve for the inverse agonist atropine. Apparently, HEPES potassium buffer had the same limitations that the previously tested HEPES sodium buffer had, i.e. an unstable level of spontaneous activity that is difficult to control.

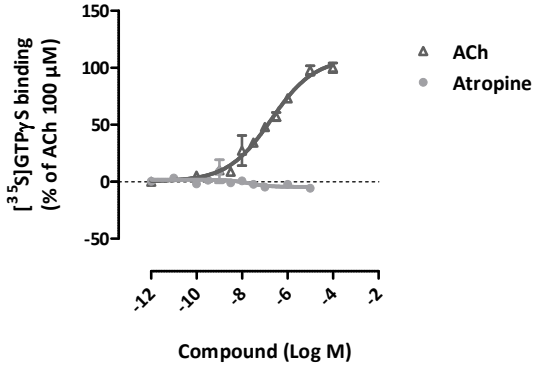

Figure 3.4: Test compound-induced [^{35}S]GTPγS binding to membrane suspensions from FlpIn CHO-M_2 cells in HEPES potassium buffer supplemented with 0.3 µM GDP. Ordinate: percentage of [^{35}S]GTPγS binding, normalized on the effect of 100 µM ACh which was set to 100%. The upper plateau of ACh does not significantly differ from 100%. 0% corresponds to the lower plateau (basal [^{35}S]GTPγS binding). Abscissa: logarithm of the concentrations of the compounds. The assay was performed with an incubation time of 60 minutes at 30°C. The graph shows the mean values ± SEM of a representative experiment performed in triplicate. Curve fitting: "Four-parameter logistic equation" (Eq. 8).

Since the studies in HEPES buffer did not allow the attainment of a stable spontaneously active system, a different buffer composition was chosen for testing. Given that several experimental papers studying GPCRs constitutive activity and salt influence reported the use of a Tris buffer for the experiments (Rosenberger et al., 1980; Hilf and Jakobs, 1989; Malmberg and Mohell, 1995), the following [^{35}S]GTPγS assays were carried out in a low osmolarity Tris buffer (S13) with 10 µM GDP. The washing steps in the filtration phase were performed with a Tris washing buffer (S18), as described in the literature (Rosenberger et al., 1980; Selley et al., 2000). At first, the concentration of membrane proteins was chosen as the variable factor (Fig. 3.5).

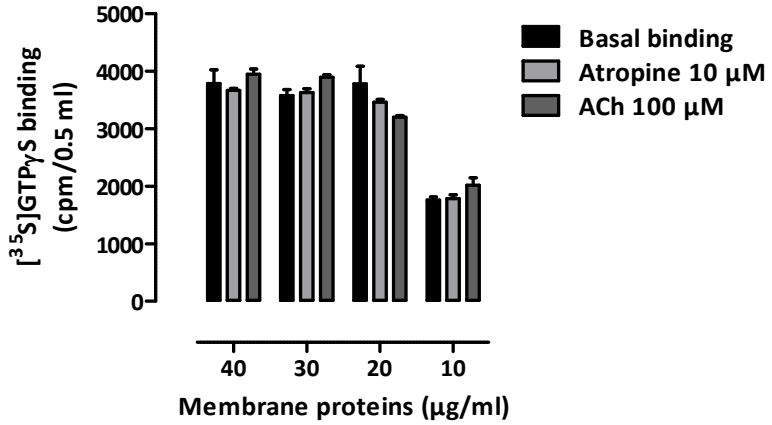

Figure 3.5: [^{35}S]GTPγS binding in control conditions (basal) and in the presence of ACh 100 µM and atropine 10 µM. Ordinate: [^{35}S]GTPγS binding, expressed as counts per minute (cpm). Abscissa: concentration of membrane proteins. The assay was performed in Tris buffer with 10 µM GDP with an incubation time of 60 minutes at 30°C. The bar diagram shows mean ± SEM of a representative experiment performed in triplicate.

Notably, hardly any difference is observable at the different protein concentrations. As next step, the GDP was applied at 1 µM, and different protein concentrations were also investigated (Fig. 3.6).

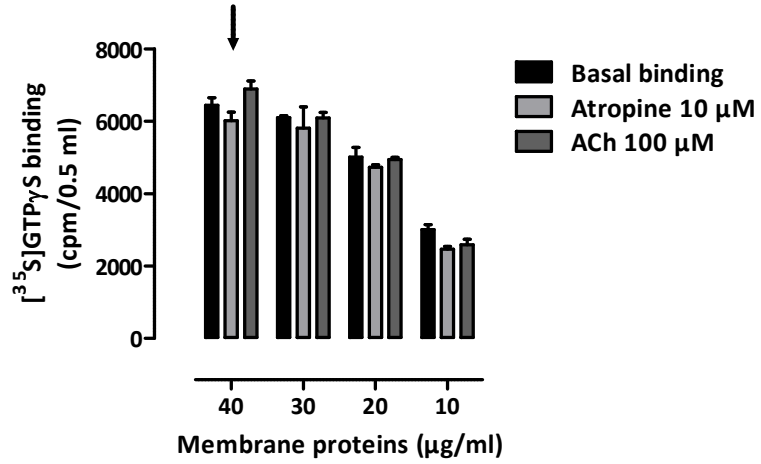

Figure 3.6: [^{35}S]GTPγS binding in control conditions (basal) and in the presence of ACh 100 µM and atropine 10 µM in Tris buffer with 1 µM GDP. Ordinate: [^{35}S]GTPγS binding, expressed as counts per minute (cpm). Abscissa: concentration of membrane proteins. The assay was performed with an incubation time of 60 minutes at 30°C. The bar diagram shows mean ± SEM of a representative experiment performed in triplicate.

As indicated by the arrow, at 40 µg/ml of protein there appears to be an acceptable measuring window for both agonism and inverse agonism. In order to reduce the high counts number, the incubation temperature was lowered to 24°C and three different time points (15, 30 and 60 min) were tested (Fig. 3.7).

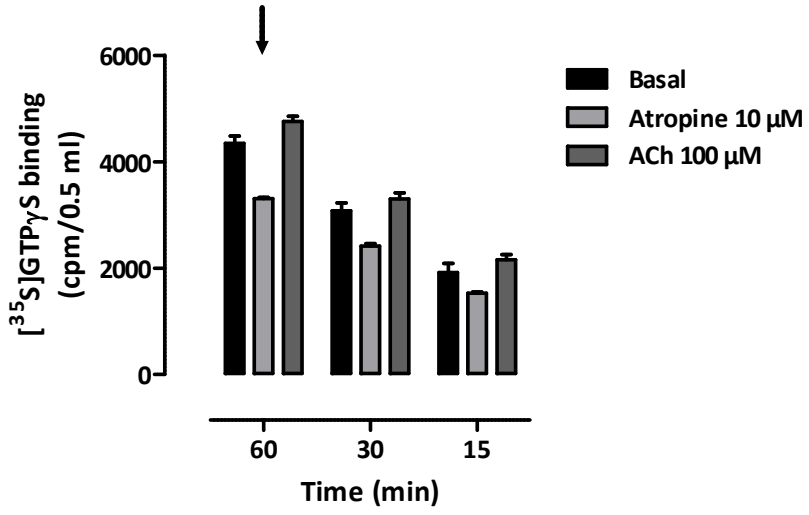

Figure 3.7: [^{35}S]GTPγS binding in control conditions (basal) and in the presence of ACh 100 µM and atropine 10 µM in Tris buffer with 1 µM GDP and 40 µg/ml of membrane proteins. The incubation was performed at 24°C for 15, 30 and 60 min. Ordinate: [^{35}S]GTPγS binding, expressed as counts per minute (cpm). Abscissa: incubation time expressed in minutes. The bar diagram shows mean ± SEM of a representative experiment performed in triplicate.

As shown in Fig. 3.7, the incubation at a lower temperature (24°C instead of 30°C) reduced the total cpm, and allowed a better definition of the differences between basal [^{35}S]GTPγS binding and [^{35}S]GTPγS binding measured in the presence of atropine and ACh. At each time point, the presence of spontaneous activity is notable, but an incubation time of 60 min seems to be the ideal time to better amplify the measuring windows for both agonism and inverse agonism.
Since the cpm were still very high, bovine serum albumin (BSA) was applied at a concentration of 0.5% and 1% with the objective of reducing the background noise.

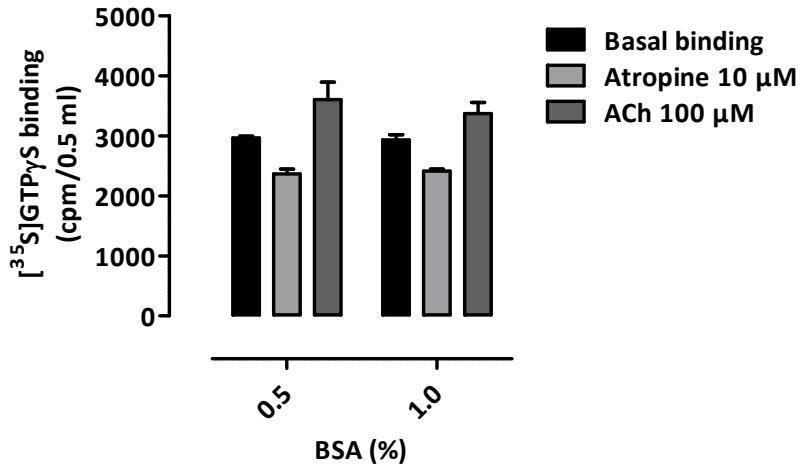

Figure 3.8: [^{35}S]GTPγS binding in control conditions (basal) and in the presence of ACh 100 µM and atropine 10 µM in Tris buffer with 1 µM GDP, 40 µg/ml of membrane proteins and a variable concentration of BSA. Ordinate: [^{35}S]GTPγS binding, expressed as counts per minute (cpm). Abscissa: concentration of BSA. The assay was performed with an incubation time of 60 minutes at 24°C. The bar diagram shows mean ± SEM of a representative experiment performed in triplicate.

As reported in Fig. 3.8, adding BSA to the buffer mixture contributed to significantly lower the cpm. Since the level of constitutive activity was comparable at 0.5% and 1% of BSA and a better agonism window was observed at 0.5% BSA, this latter concentration was elected for the following studies.

3.1.3 Addition of a high concentration of salts inhibits the spontaneous activity in Tris buffer

One of the main requirements of this thesis was the establishment of two wild type M_2 receptor systems that were either spontaneously active or quiescent. Thus, since a constitutive system had been settled (see 3.1.2), the following effort was aimed at investigating the conditions required for abolishing the low osmolarity Tris buffer-induced constitutive activity. It was known from previous

studies (Wu et al., 2012; Zhang et al., 2012; Fenalti et al., 2014; Miller-Gallacher et al., 2014) that Na^+ acts as negative allosteric modulator for class A GPCRs, contributing to keep the receptor in a quiescent state when present at significant concentrations. Hence, this salt, together with other salts as KCl and NaBr, and with the osmotically equivalent NMDGCl (Pihlavisto et al., 1998; Barann et al., 2004; Billups et al., 2006; Vivo et al., 2006) was tested for its ability to inhibit M_2 spontaneous activity. Figure 3.9 shows that in Tris buffer (S13) 10 µM atropine significantly decreased the basal [^{35}S]GTPγS binding of about 50%, demonstrating that the constitutive activity of the receptor is stimulated in these conditions, as anticipated from the preliminary studies (see 3.1.2). 200 mM of NaCl abolished the constitutive activity of the receptor, as understandable from the [^{35}S]GTPγS binding elicited in the presence of 10 µM atropine, that was not significantly different from basal binding (set at 0%). Accordingly, 200 mM of NaBr had the same effect of silencing the receptor, given that this salt also presents sodium as cation. The surprising result was that 200 mM of KCl and NMDGCl, that do not contain sodium, were also able to keep the receptor in the quiescent conformation (Fig. 3.9). As a consequence, we recognized that every change of osmolarity led to an annulment of constitutive activity.

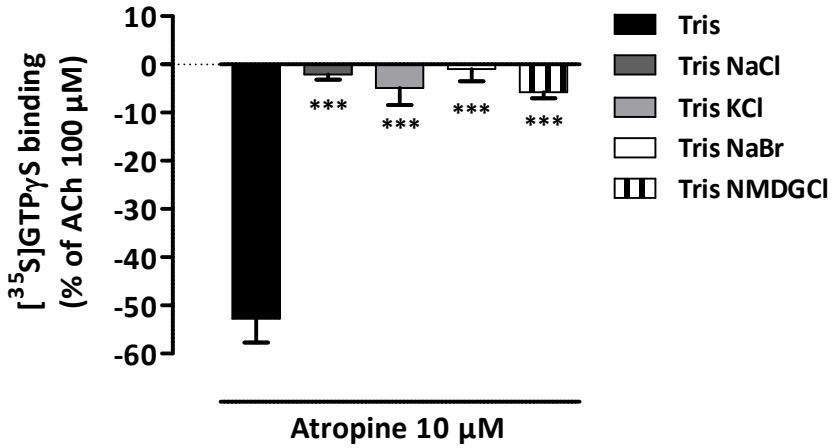

Figure 3.9: [^{35}S]GTPγS binding induced by 10 µM atropine in the presence of 200 mM of the indicated salts and the molecule NMDGCl. Ordinate: percentage of [^{35}S]GTPγS binding, normalized on maximum effect elicited by 100 µM ACh (set 100%). 0% corresponds to basal [^{35}S]GTPγS binding. The assay was performed with an incubation time of 60 minutes at 24°C. The bar diagram shows mean ± SEM of 3-7 experiments performed in triplicate. ***: $p<0.001$, significantly different from the value reported in Tris buffer according to one-way ANOVA with Bonferroni's multiples comparison test.

A summary of the parameters derived from the data analysis is presented in Table 3.3.

Buffer	*E_{max} (%)*	*n*
Tris	-53 ± 5	7
Tris NaCl	-2 ± 1	7
Tris KCl	-5 ± 4	7
Tris NaBr	-1 ± 3	7
Tris NMDGCl	-6 ± 1	3

Table 3.3: Parameter values derived from Figure 3.9; E_{max}: maximum level of [^{35}S]GTPγS binding in percent normalized on 100 µM ACh which was set to 100%; n: number of performed experiments. The table shows mean values ± SEM of 3-7 independent experiments carried out at least in triplicate.

In order to better characterize the influence of NaCl and KCl on the spontaneous activity of the M_2AChR, receptor activation was investigated at increasing salt concentrations. As shown in Fig. 3.10, the constitutive activity progressively diminished and was then completely abolished at the highest salt concentration (200 mM). Additionally, [^{35}S]GTPγS binding stimulated by the endogenous agonist ACh decreased almost equidistant to basal [^{35}S]GTPγS binding, thus maintaining the window for agonism measurement constant over the different NaCl concentrations (Fig. 3.10A). The same experiment was performed in the presence of increasing concentrations of KCl, with very similar outcomes (Fig.3.10B).

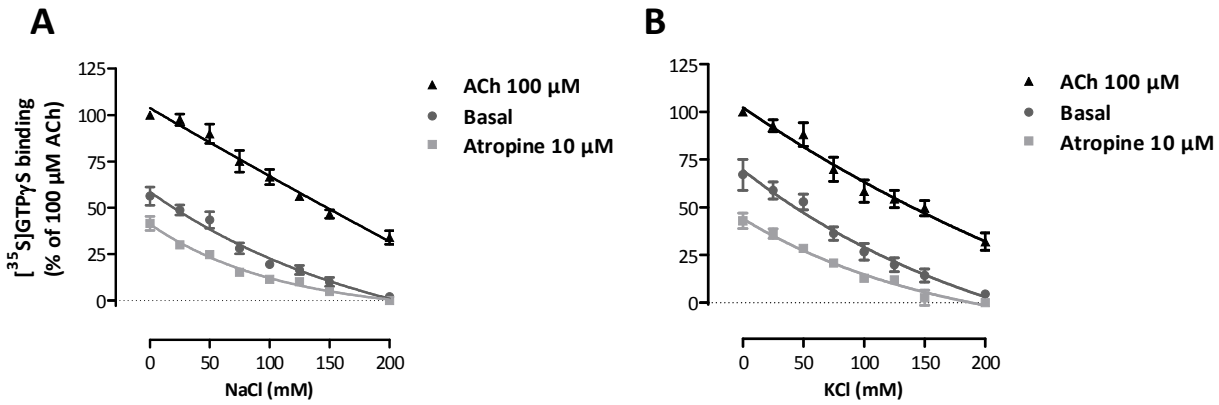

Figure 3.10: Influence of increasing concentrations of NaCl (A) and KCl (B) on basal [^{35}S]GTPγS binding and binding induced by 100 µM ACh and 10 µM atropine. Maximum stimulation induced by 100 µM ACh was set to 100%. Maximum inhibition induced by atropine was set to 0%. The assay was performed with an incubation time of 60 minutes at 24°C. Data: mean ± SEM of 3-5 independent experiments.

Taken together, these results indicated that NaCl and KCl have similar effect on the level of spontaneous activity of the M_2 receptor.

3.2 Influence of salts and spontaneous activity on orthosteric signaling

3.2.1 NaCl and KCl decrease the potency of ACh, iperoxo, isox and OOM

The influence of NaCl and KCl on signaling stimulated by the orthosteric agonists ACh, iperoxo, isox and OOM was evaluated in [^{35}S]GTPγS binding assays, in order to determine an eventual modification of agonist activity in the absence or presence of constitutive activity of the receptor. As shown in Fig. 3.11, both salts had significant effects on agonist signaling. Both KCl and NaCl shifted the inflection point of the curves (pEC_{50}) to lower values, indicating that these monovalent cations reduced the agonist potency. Additionally, the effect of NaCl was stronger than that of KCl in decreasing the pEC_{50} values of all agonists (Table 3.4).

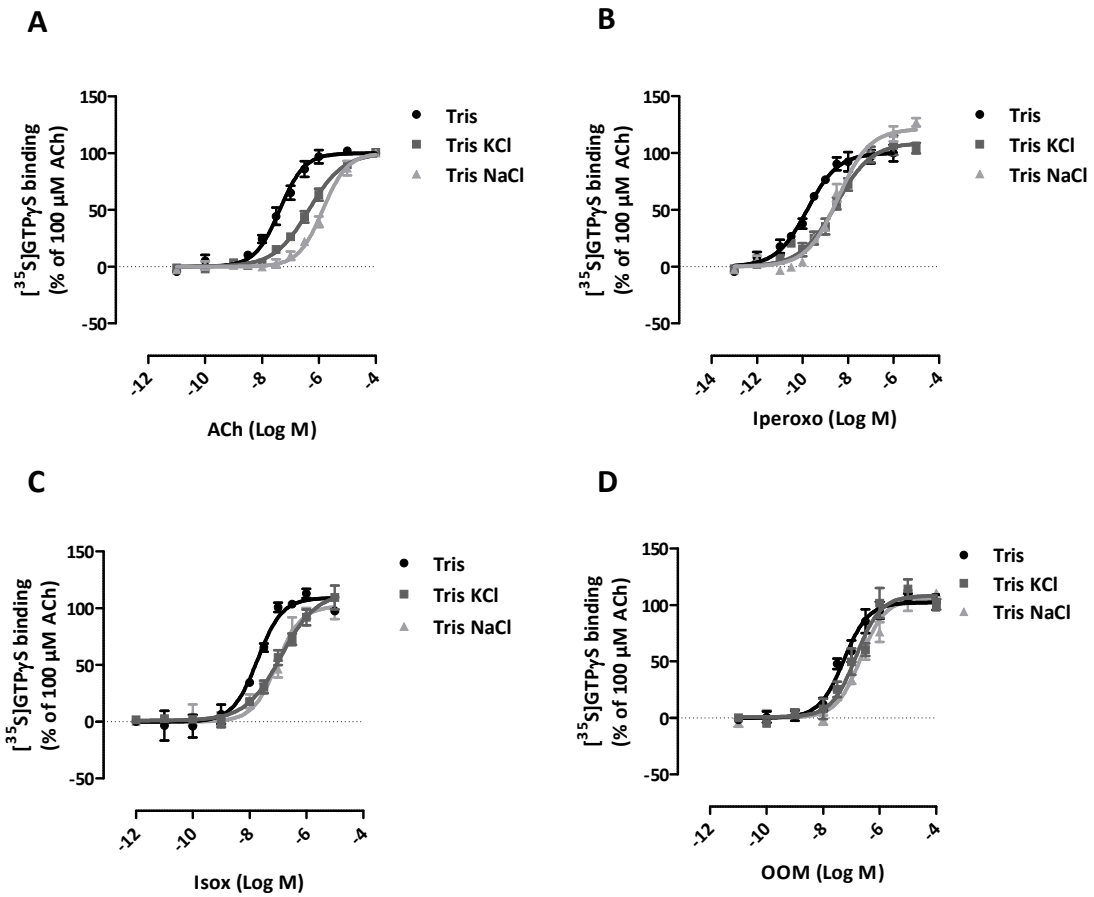

Figure 3.11: Test compound-induced [^{35}S]GTPγS binding to membrane suspensions from FlpIn CHO-M_2 cells in the indicated buffers. Ordinate: percentage of [^{35}S]GTPγS binding, normalized on the maximum effect of 100 µM ACh which was set to 100%. 0% corresponds to the lower plateau (basal [^{35}S]GTPγS binding). Abscissa: logarithm of the concentrations of the compounds. The assay was performed with an incubation time of 60 minutes at 24°C. The graph shows the mean values ± SEM of 3-7 experiments performed in triplicate. Curve fitting: "Four-parameter logistic equation" (Eq. 8).

The E_{max} values also appeared slightly affected, even though there was no statistical significance. In case of iperoxo, there was a tendency pointing to higher values upon salt addition, while for isox the E_{max} imperceptibly decreased. There was no difference reported for ACh, since the upper plateau of the curve for the endogenous agonist (and reference ligand) was fixed at 100% in all buffers.

Compound	*Buffer*	*pEC_{50}*	*E_{max} (%)*	*n*
ACh	Tris	7.71 ± 0.13	100	5
	Tris KCl	6.34 ± 0.06***	100	4
	Tris NaCl	5.83 ± 0.04$^{***/a}$	100	3
Iperoxo	Tris	9.84 ± 0.11	98 ± 6	4
	Tris KCl	8.51 ± 0.14***	110 ± 8	5
	Tris NaCl	7.90 ± 0.09$^{***/a}$	127 ± 6	3
Isox	Tris	7.75 ± 0.02	118 ± 4	7
	Tris KCl	6.99 ± 0.10***	109 ± 14	4
	Tris NaCl	7.08 ± 0.13***	101 ± 6	5
OOM	Tris	7.25 ± 0.10	102 ± 4	4
	Tris KCl	6.79 ± 0.11	109 ± 4	4
	Tris NaCl	6.63 ± 0.16*	107 ± 5	4

Table 3.4: Parameter values derived from Figure 3.11; pEC_{50}: negative common logarithm of the concentration of test compound causing a half maximum effect; E_{max}: maximum level of [^{35}S]GTPγS binding in percent normalized on ACh which was set to 100%; n: number of performed experiments. The table shows mean values ± SEM of 3-7 independent experiments carried out in triplicate. *,**,***: significantly different ($p<0.05$, 0.01, 0.001) from the value reported in Tris buffer according to one-way ANOVA with Bonferroni's multiples comparison test. ^{a}: significantly different ($p<0.05$) from the value reported in Tris KCl buffer according to one-way ANOVA with Bonferroni's post test.

Taken together, a lower level of receptor spontaneous activity, achieved with a high osmolarity buffer, causes a decrease in potency of the orthosteric full agonists and the superagonist.

3.2.2 The spontaneously active system has elevated basal activity and maximum achievable activation

We were interested in the nature of the M_2 receptor system with high rates of spontaneous activity (Tris buffer) in comparison to a quiescent M_2 receptor system (Tris supplemented with 200 mM NaCl or KCl). We hypothesized that high spontaneous M_2 activity may either increase the basal level of [^{35}S]GTPγS binding without altering the maximum inducible effect of the system (Fig. 3.12A), or could lead to an increase in basal [^{35}S]GTPγS binding and also a higher potential E_{max} of the system (Fig.3.12B).

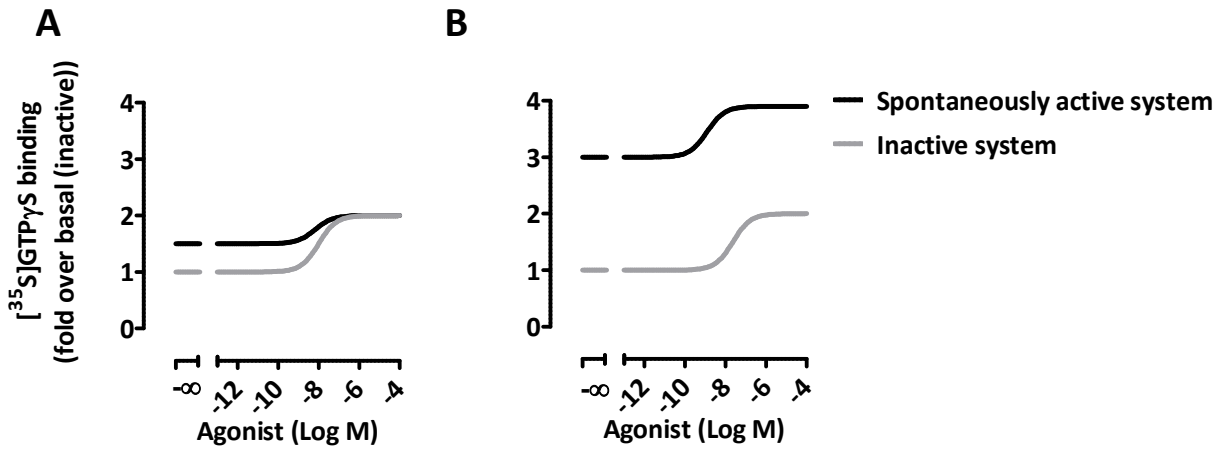

Figure 3.12: Hypothetical concentration-effect curves in a spontaneously active system (e.g. [^{35}S]GTPγS binding in Tris buffer) in comparison to systems without spontaneous activity (e.g. [^{35}S]GTPγS binding in Tris buffer supplemented with NaCl or KCl). (A) Option 1: All systems share the same maximum effect achievable and differ only in the basal level of receptor activation. (B) Option 2: Not only the basal signaling is elevated but also the achievable maximum effect is higher in the spontaneously active system.

To approach these hypotheses experimentally, [^{35}S]GTPγS binding was measured in CHO-M_2 membranes induced by the endogenous agonist ACh (Fig. 3.13A) and the muscarinic superagonist iperoxo (Fig. 3.13B) in one system where the receptor was spontaneously active (Tris) and two systems where no spontaneous activity was apparent (Tris KCl and Tris NaCl).

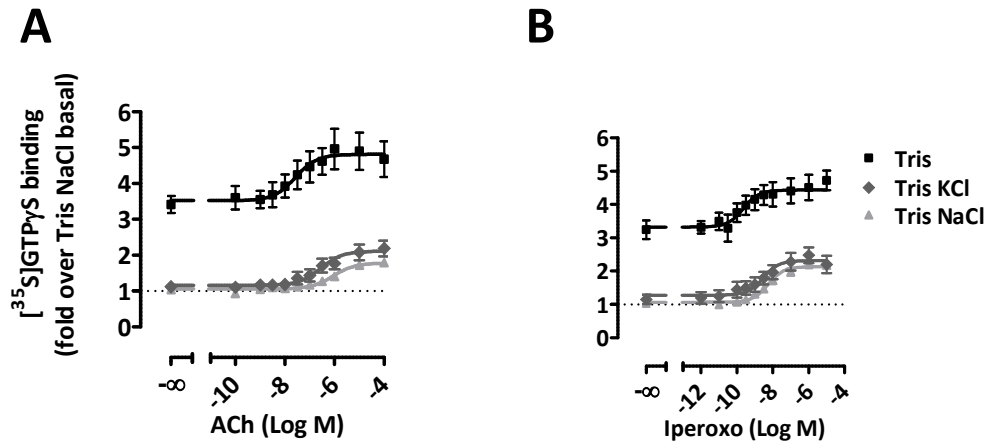

Fig. 3.13: Test compound-induced [^{35}S]GTPγS binding to membrane suspensions from FlpIn CHO-M_2 cells in the indicated buffers. Ordinate: [^{35}S]GTPγS binding, normalized on fold over basal binding measured in Tris NaCl buffer. Ordinate value = 1 corresponds to the lower plateau in Tris NaCl buffer (basal [^{35}S]GTPγS binding in NaCl). Abscissa: logarithm of the concentrations of the compounds. The assay was performed with an incubation time of 60 minutes at 24°C. The graph shows the mean values ± SEM of 4-7 experiments performed in triplicate. Curve fitting: "Four-parameter logistic equation" (Eq. 8).

Clearly, not only the basal amount of receptor activity was enhanced but also the maximum inducible effect of the system (E_{max}) was increased in the spontaneously active system in comparison to the inactive system. This goes in line with the hypothesis that both basal and maximal [^{35}S]GTPγS binding are enhanced in a low osmolarity Tris buffer (Fig.3.12B).

3.2.3 NaCl has no influence on pEC_{50} and E_{max} of pilocarpine

Pilocarpine is a partial agonist at M_2 receptor that is known to bind to the orthosteric binding pocket. G_i-signaling stimulated by this ligand was investigated in [^{35}S]GTPγS binding assays in order to determine whether orthosteric full agonists and partial agonists are similarly influenced by NaCl addition and by the level of spontaneous activity. As shown in Fig. 3.14, neither the potency nor the maximum effect of pilocarpine was affected by the addition of NaCl.

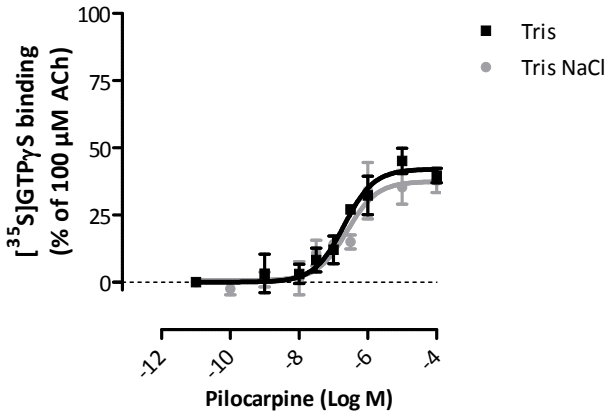

Figure 3.14: Pilocarpine-induced [^{35}S]GTPγS binding to membrane suspensions from FlpIn CHO-M_2 cells in the indicated buffers. Ordinate: percentage of [^{35}S]GTPγS binding, normalized on the maximum effect of 100 µM ACh which was set to 100%. 0% corresponds to the lower plateau (basal [^{35}S]GTPγS binding). Abscissa: logarithm of the concentrations of the compounds. The assay was performed with an incubation time of 60 minutes at 24°C. The graph shows the mean values ± SEM of 3-5 experiments performed in triplicate. Curve fitting: "Four-parameter logistic equation" (Eq. 8).

The partial agonist stimulated about 40% of the maximum effect produced by ACh, which was set to 100%. A summary of the parameters derived from the data analysis is presented in Table 3.5.

Compound	*Buffer*	*pEC_{50}*	*E_{max} (%)*	*n*
Pilocarpine	Tris	6.72 ± 0.14	42 ± 4	3
	Tris NaCl	6.41 ± 0.20	42 ± 5	5

Table 3.5: Parameter values derived from Figure 3.14; pEC_{50}: negative common logarithm of the concentration of test compound causing a half maximum effect; E_{max}: maximum level of [^{35}S]GTPγS binding in percent normalized on ACh which was set to 100%; n: number of performed experiments. The table shows mean values ± SEM of 3-5 independent experiments carried out in triplicate.

Taken together, orthosteric full and partial agonists are differentially influenced by the addition of 200 mM to the buffer. Indeed, neither the efficacy nor the potency of the partial agonist pilocarpine was modified by the salt addition, while the potency of the full agonists was reported to be lowered in the presence of NaCl (see 3.2.1).

3.2.4 Atropine displays its inverse agonism in the spontaneously active system

Atropine is known as an antagonist or inverse agonist at the muscarinic M_2 receptor. To test the effect of this ligand in both experimental systems, [^{35}S]GTPγS assays were performed in Tris and Tris NaCl buffer. The results of these experiments are shown in Fig. 3.15.

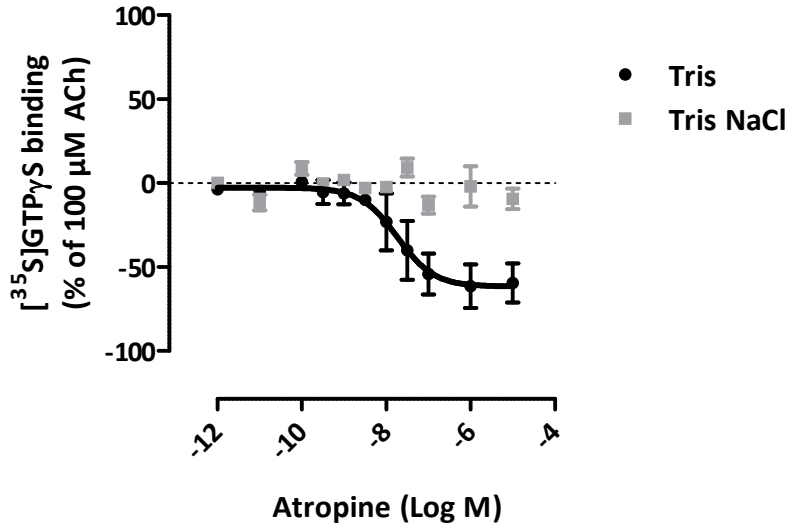

Figure 3.15: Atropine-inhibited [^{35}S]GTPγS binding to membrane suspensions from FlpIn CHO-M_2 cells in the indicated buffers. Ordinate: percentage of [^{35}S]GTPγS binding, normalized on the maximum effect of 100 µM ACh which was set to 100%. 0% corresponds to basal [^{35}S]GTPγS binding. Abscissa: logarithm of the concentrations of the compounds. The assay was performed with an incubation time of 60 minutes at 24°C. The graph shows the mean values ± SEM of 3 experiments performed in triplicate. Curve fitting: "Four-parameter logistic equation" (Eq. 8).

A summary of the parameters derived from the data analysis is presented in Table 3.6.

Compound	*Buffer*	*pEC_{50}*	*E_{max} (%)*	*n*
Atropine	Tris	7.74 ± 0.23	-62 ± 6	3
	Tris NaCl	n. d.	n. d.	3

Table 3.6: Parameter values derived from Figure 3.15; pEC_{50}: negative common logarithm of the concentration of test compound causing a half maximum effect; E_{max}: maximum level of [^{35}S]GTPγS binding in percent normalized on 100 µM ACh which was set to 100%; n: number of performed experiments. The table shows mean values ± SEM of 3 independent experiments carried out in triplicate.

Atropine behaved as an inverse agonist in Tris buffer and as a neutral antagonist in Tris NaCl buffer. This result is not unexpected, considering that an inverse agonist is predicted to decrease receptor activation in the presence of constitutive activity, but to have no effect if the receptor protein is quiescent.

3.3 Influence of salts on orthosteric ligand binding

3.3.1 NaCl decreases the half-life of dissociation of the radioantagonist

The dissociation of [^{3}H]NMS was investigated in complete dissociation binding assays. These experiments allow the determination of the half-life of dissociation, providing an indication of the speed of dissociation of the radioligand from the receptor. It was previously reported that NaCl causes an acceleration of radiagonist dissociation in opioid receptors (Pert and Snyder, 1973). Here, we investigated how NaCl influences the radioantagonist dissociation from the M_2 receptor. As shown in Fig. 3.16, the dissociation kinetics are almost 4-fold faster in Tris NaCl compared to Tris buffer.

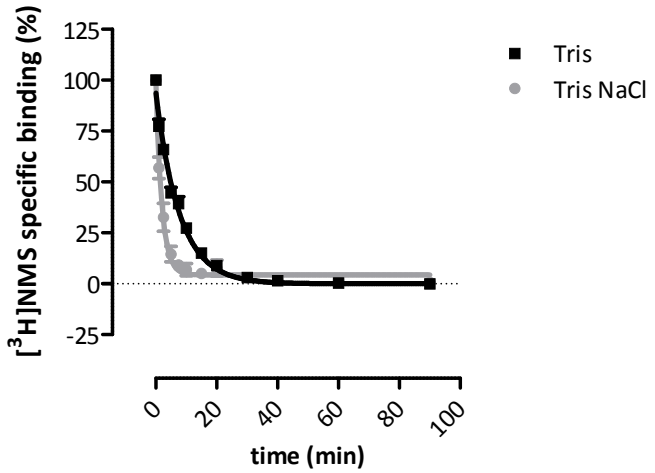

Figure 3.16: Time-effect curves of [^{3}H]NMS dissociation. Ordinate: [^{3}H]NMS specific binding expressed as percentage of [^{3}H]NMS binding at time zero. Abscissa: incubation time of [^{3}H]NMS-bound receptors with the compound. Data points: mean ± SEM of 3-4 assays performed in triplicate. Curve fitting was performed according to equation (16). The dissociation binding assay was conducted in Tris and Tris NaCl buffer and incubated at 24°C.

The parameter values obtained with these experiments are summarized in table 3.7.

Buffer	$t_{1/2}$ *(min)*	*n*
Tris	5.40 ± 0.44	3
Tris NaCl	1.50 ± 0.23***	4

Table 3.7: Parameter values derived from Figure 3.16; $t_{1/2}$: half-life of radioligand dissociation expressed in minutes; n: number of performed experiments. The table shows mean values ± SEM of 3-4 independent experiments carried out in triplicate. ***: significant difference to the value reported in Tris buffer ($p<0.001$).

Thus, the muscarinic M_2 system behaves similarly to the opioid receptors, which are also classified as class A GPCRs.

3.3.2 NaCl has no effect on NMS affinity and B_{max}

Homologous binding experiments performed with radiolabeled and non-radiolabeled [^{3}H]NMS were employed to investigate the affinity of the inverse agonist NMS and to estimate the total receptor number (B_{max}) of the utilized membrane preparations. It is known that NaCl may have an influence on the affinity of antagonists for GPCRs. This salt can increase (Malmberg and Mohell, 1995), decrease (Rosenberger et al., 1980) or leave unaffected (U'Prichard and Snyder, 1978) the affinity of antagonists. In order to better characterize the effect that NaCl and KCl have on the affinity of NMS, concentration-effect curves were obtained in Tris, Tris KCl and Tris NaCl buffer. As shown in Fig. 3.17, the addition of 200 mM KCl or NaCl had no effect on the affinity of NMS.

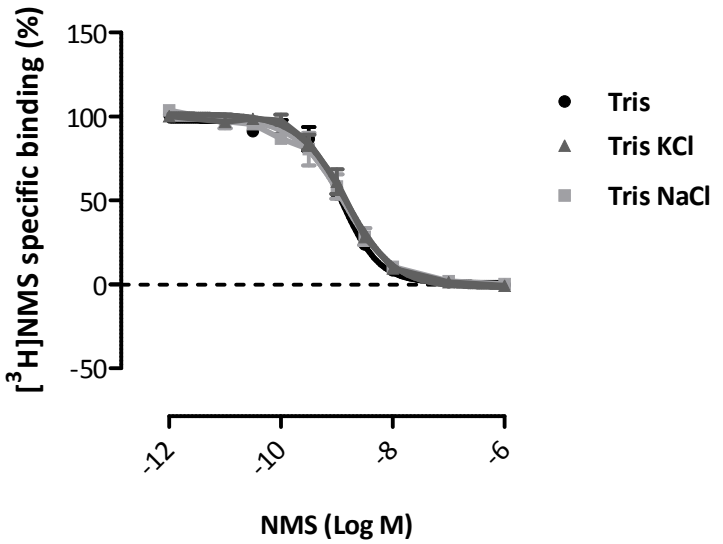

Figure 3.17: Homologous competition binding with 0.2 nM [^{3}H]NMS as tracer. Ordinate: [^{3}H]NMS binding expressed as percentage of the [^{3}H]NMS binding in absence of unlabeled NMS. Abscissa: logarithm of the concentration of unlabeled NMS. Curve fitting: "Four-parameter logistic equation" (Eq. 8) with constant Hill coefficient n= -1. Data points: mean ± SEM of 4 assays performed in triplicate. The experiments were carried out in Tris, Tris KCl and Tris NaCl buffer and incubated for 150 min at 24°C.

The total receptor number (B_{max}) was calculated with equation (7) and is represented in Fig. 3.18. The addition of NaCl and KCl to the Tris buffer did not influence this parameter. The affinity of NMS was calculated according to equation (13).

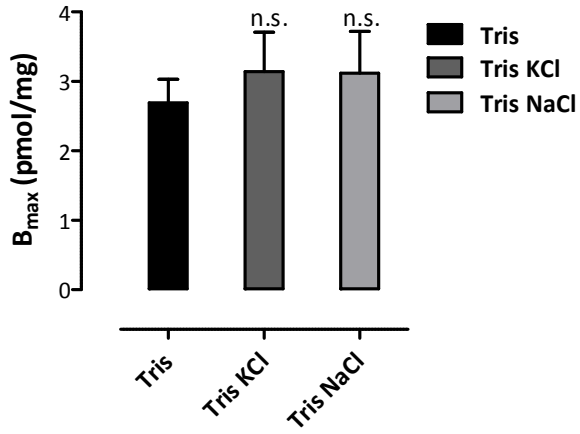

Figure 3.18: B_{max} values of the same membrane preparation tested in Tris, Tris KCl and Tris NaCl buffer. n.s.: not significantly different from B_{max} values reported in Tris buffer according to one-way ANOVA with Bonferroni's post test.

The parameter values obtained with these experiments are summarized in table 3.8.

Buffer	*pK_d*	*B_{max} (pmol/mg)*	*n*
Tris	9.01 ± 0.09	2.69 ± 0.34	4
Tris KCl	8.90 ± 0.10	3.14 ± 0.57	4
Tris NaCl	8.96 ± 0.14	3.12 ± 0.60	4

Table 3.8: Parameter values derived from Figure 3.17 and 3.18; pK_d: affinity of NMS for M_2 receptor calculated with equation (13). B_{max}: number of binding sites according to equation (7); n: number of performed experiments. The table shows mean values ± SEM of 4 independent experiments carried out in triplicate.

These results indicate that 200 mM of NaCl and KCl influence neither NMS affinity nor the number of binding sites of the M_2 receptors.

3.3.3 NaCl and KCl decrease the affinity of orthosteric full agonists and the superagonist

[^{3}H]NMS equilibrium binding assays were carried out to determine the affinities of the orthosteric agonists for the NMS-unoccupied receptor. All ligands completely displaced [^{3}H]NMS, with significantly lower affinities upon addition of salts (Figure 3.19). Curve fitting was based on equation (8), and the compound's affinity for the receptor was calculated from the inflection point of the concentration-effect curve applying equation (20).

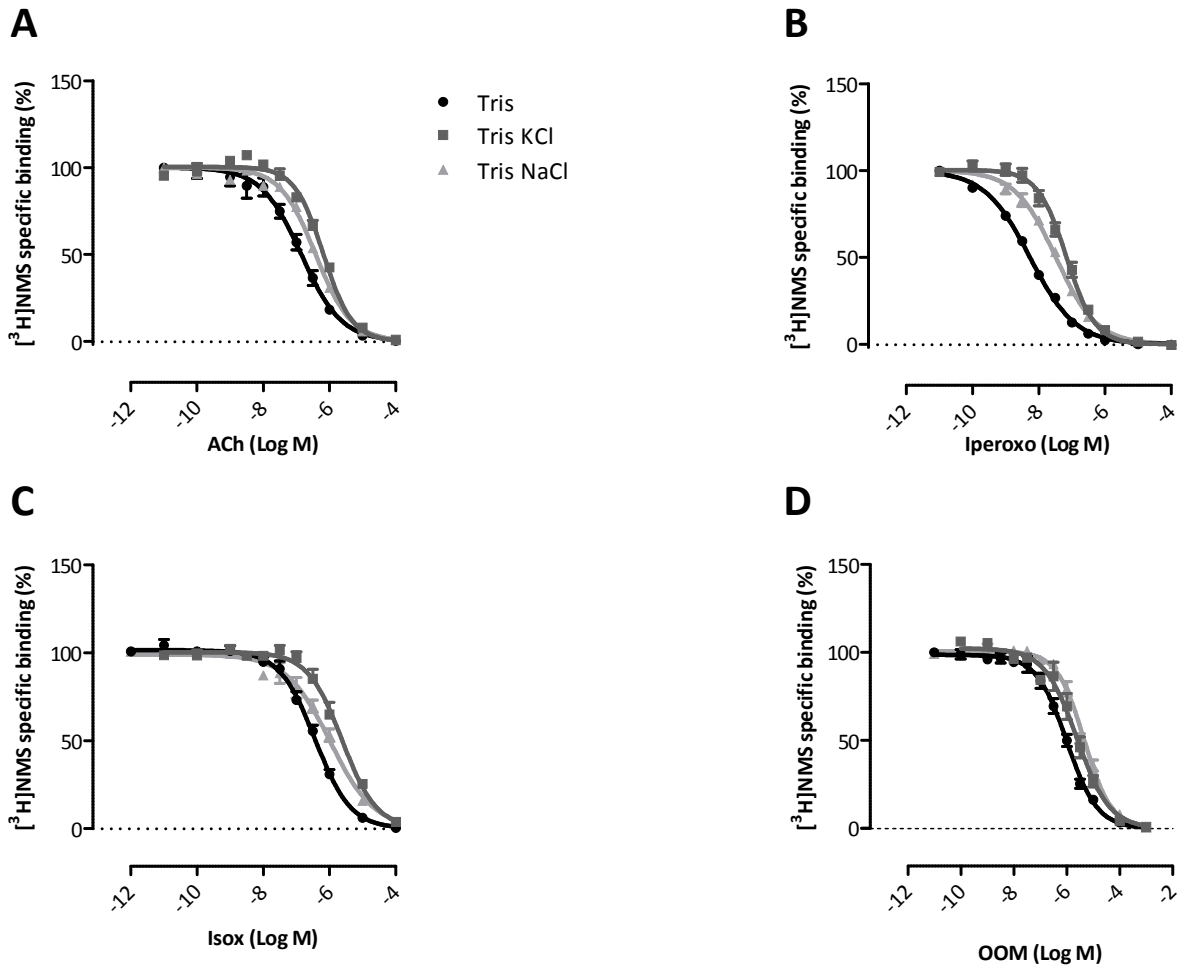

Figure 3.19: [^{3}H]NMS equilibrium binding assays. Ordinate: [^{3}H]NMS binding expressed as percentage of [^{3}H]NMS binding in absence of compound. Abscissa: logarithm of the concentration of test compounds. The experiments were carried out in Tris, Tris KCl and Tris NaCl buffer supplemented with 100 µM GDP and incubated for 150 minutes at 24°C. Data points: mean ± SEM of 3-7 assays performed at least in duplicate. Curve fitting: "Four-parameter logistic equation" (Eq. 8).

The parameter values obtained with these experiments are summarized in table 3.9.

Compound	*Buffer*	*pK_i*	*n_H*	*n*
ACh	Tris	7.04 ± 0.09	-0.70 ± 0.09	5
	Tris KCl	6.31 ± 0.03***	-1 (-0.88 ± 0.07)	3
	Tris NaCl	6.53 ± 0.04**	-0.89 ± 0.07	4
Iperoxo	Tris	8.58 ± 0.10	-0.61 ± 0.04	6
	Tris KCl	7.31 ± 0.07***	-1 (-0.88 ± 0.06)	6
	Tris NaCl	7.58 ± 0.04***	-0.74 ± 0.05	4
Isox	Tris	6.69 ± 0.09	-0.83 ± 0.04	4
	Tris KCl	5.79 ± 0.14**	-1 (-0.83 ± 0.07)	4
	Tris NaCl	6.12 ± 0.13*	-0.66 ± 0.06	4
OOM	Tris	6.31 ± 0.08	-0.77 ± 0.08	7
	Tris KCl	5.72 ± 0.16**	-0.71 ± 0.08	4
	Tris NaCl	5.50 ± 0.09***	-1.11 ± 0.26	7

Table 3.9: Parameter values derived from Figure 3.19; pK_i: negative common logarithm of the dissociation binding constant of the test compounds. n_H: Hill slope of the curve. If it did not significantly differ from unity, a value of -1 was assumed and the exact value reported in brackets; n: number of performed experiments. The table shows mean values ± SEM of 3-7 independent experiments carried out in triplicate. *, **, ***: significant difference to the pK_i value reported in Tris buffer ($p<0.05$, 0.01, 0.001).

Taken together, these data show that receptor spontaneous activity and/or salt concentration significantly influence the affinity of all the orthosteric full agonists and the superagonist investigated in this study.

3.3.4 NaCl lightly decreases the affinity of pilocarpine

The partial agonist pilocarpine was tested in [^{3}H]NMS equilibrium binding assays in order to determine the affinity of this ligand for the NMS-unoccupied receptor. Pilocarpine completely displaced [^{3}H]NMS, with an affinity that was slightly lower in Tris NaCl buffer compared to Tris buffer (Figure 3.20). Curve fitting was based on equation (8), and the compound's affinity for the

receptor was calculated from the inflection point of the concentration-effect curve applying equation (20).

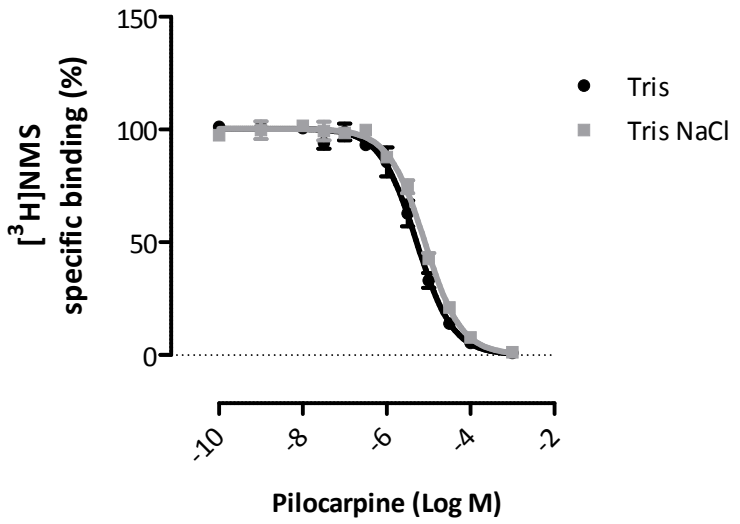

Figure 3.20: [^{3}H]NMS equilibrium binding assays. Ordinate: [^{3}H]NMS binding expressed as percentage of [^{3}H]NMS binding in absence of compound. Abscissa: logarithm of the concentration of pilocarpine. The experiments were carried out in Tris and Tris NaCl buffer supplemented with 100 µM GDP and incubated for 150 minutes at 24°C. Data points: mean ± SEM of 5 assays performed in triplicate. Curve fitting: "Four-parameter logistic equation" (Eq. 8).

The parameter values obtained with these experiments are summarized in table 3.10.

Compound	*Buffer*	*pK_i*	*n_H*	*n*
Pilocarpine	Tris	5.20 ± 0.05	-1 (-1.12 ± 0.12)	5
	Tris NaCl	5.53 ± 0.12*	-1 (-1.11 ± 0.10)	5

Table 3.10: Parameter values derived from Figure 3.20; pK_i: negative common logarithm of the dissociation binding constant of pilocarpine. n_H: Hill slope of the curve. If it did not significantly differ from unity, a value of -1 was assumed and the exact value reported in brackets; n: number of performed experiments. The table shows mean values ± SEM of 5 independent experiments carried out in triplicate. *: significant difference to the pK_i value reported in Tris buffer ($p<0.05$).

3.4 Influence of salts and spontaneous activity on allosteric signaling

3.4.1 Allosteric compounds act either as inverse agonists or neutral antagonists depending on the level of spontaneous activity of M_2

In order to determine the effects that a constitutively active and an inactive M_2 receptor system have on signaling stimulated by allosteric molecules, five allosteric ligands were tested in [^{35}S]GTPγS binding studies, in both Tris and Tris NaCl buffer. As shown in Fig. 3.21, all the ligands were able to reduce [^{35}S]GTPγS binding, acting as inverse agonists in the spontaneously active system. Contrarily, they had no effect in the presence of 200 mM NaCl, showing neutral antagonism.

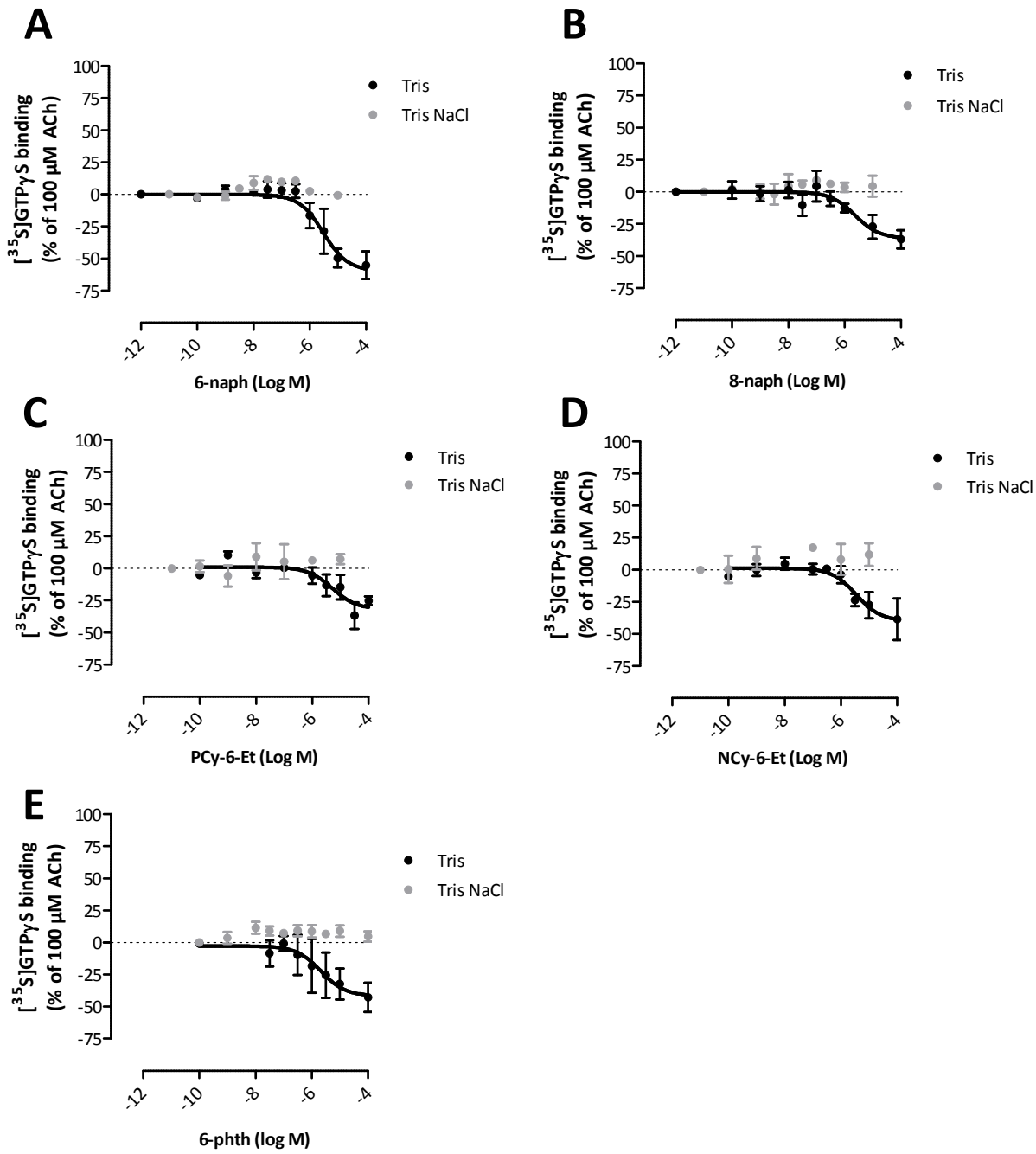

Figure 3.21: Test compound-induced [^{35}S]GTPγS binding to membrane suspensions from FlpIn CHO-M_2 cells in the indicated buffers. Ordinate: percentage of [^{35}S]GTPγS binding, normalized on the maximum effect of 100 µM ACh which was set to 100%. 0% corresponds to the lower plateau (basal [^{35}S]GTPγS binding). Abscissa: logarithm of the concentrations of the compounds. The assay was performed with an incubation time of 60 minutes at 24°C. The graph shows the mean values ± SEM of 3-5 experiments performed in triplicate. Curve fitting: "Four-parameter logistic equation" (Eq. 8).

The parameter values obtained with these experiments are summarized in table 3.11.

Compound	*Buffer*	*pEC_{50}*	*E_{max} (%)*	*n*
6-naph	Tris	5.52 ± 0.20	-68 ± 11	5
	Tris NaCl	n.d.	n.d.	4
8-naph	Tris	5.28 ± 0.5	-46 ± 7	3
	Tris NaCl	n.d.	n.d.	3
PCy-6-Et	Tris	5.14 ± 0.45	-33 ± 1	3
	Tris NaCl	n.d.	n.d.	3
Ncy-6-Et	Tris	5.41 ± 0.04	-41 ± 16	3
	Tris NaCl	n.d.	n.d.	3
6-phth	Tris	5.48 ± 0.49	-45 ± 10	3
	Tris NaCl	n.d.	n.d.	6

Table 3.11: Parameter values derived from Figure 3.21; pEC_{50}: negative common logarithm of the concentration of test compound causing a half maximum effect; E_{max}: maximum level of [^{35}S]GTPγS binding in percent normalized on 100 µM ACh which was set to 100%; n: number of performed experiments. The table shows mean values ± SEM of 3-6 independent experiments carried out in triplicate.

These results indicate that all the tested fragments are allosteric antagonists at the M_2 receptor.

3.5 Influence of NaCl on allosteric ligand binding

3.5.1 Addition of 200 mM of NaCl decreases the allosteric potency of the allosteric ligands

The tested allosteric compounds are fragments of the dualsteric ligands that were studied in this thesis. In order to estimate the allosteric affinity and the influence of NaCl on allosteric interactions, dissociation binding studies were performed. It is known from previous literature that the action of allosteric agents depends on the ionic composition of the buffer (Ellis et al., 1991) and, in particular, that the affinity of alkane-bis-ammonium-type compounds is increased in low osmolarity buffers (Tränkle et al., 1996; Schröter et al., 2000). These experiments allowed the determination of the allosteric potency of the test compounds in both high and low osmolarity, analyzing the delay in the dissociation time of the orthosteric radioligand [^{3}H]NMS.

The parameter value obtained was the $pEC_{50,diss}$ of the test compounds, i.e. the concentration of compound that inhibits the dissociation of the orthosteric radioligand by 50%. This parameter reflects the affinity of the test compounds for the radioligand-occupied receptor, i.e. the affinity for the allosteric site of the M_2 receptor. Fig. 3.22 shows an exemplifying experiment performed in Tris buffer at increasing concentrations of the allosteric ligand 6-naph. At increasing concentrations of the compound, the dissociation of [^{3}H]NMS is gradually decreased and then abolished at the highest tested concentration of allosteric modulator (10 µM).

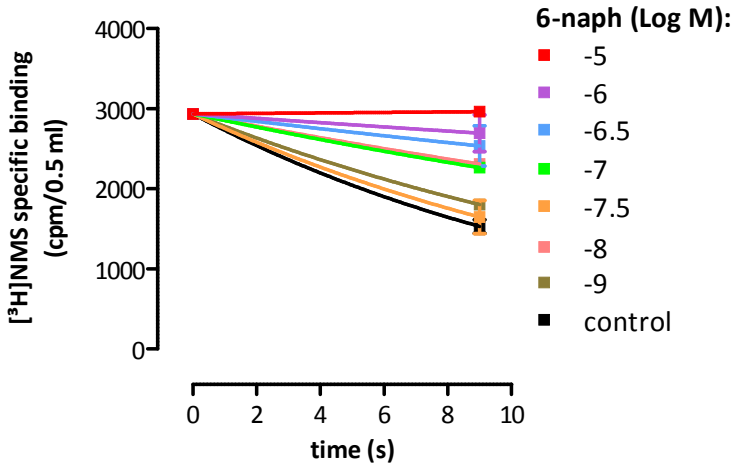

Figure 3.22: Representative array of curves of the delay of [^{3}H]NMS dissociation induced by 6-naph binding to M_2 receptors orthosterically-bound with [^{3}H]NMS in Tris buffer. Ordinate: [^{3}H]NMS binding in cpm/0.5 ml. Abscissa: incubation time of [^{3}H]NMS-bound receptors with the compound.

These results are converted in concentration-effect curves showing the dissociation rate constant (k_{-1}) calculated for every single concentration of allosteric modulator (Fig 3.23).

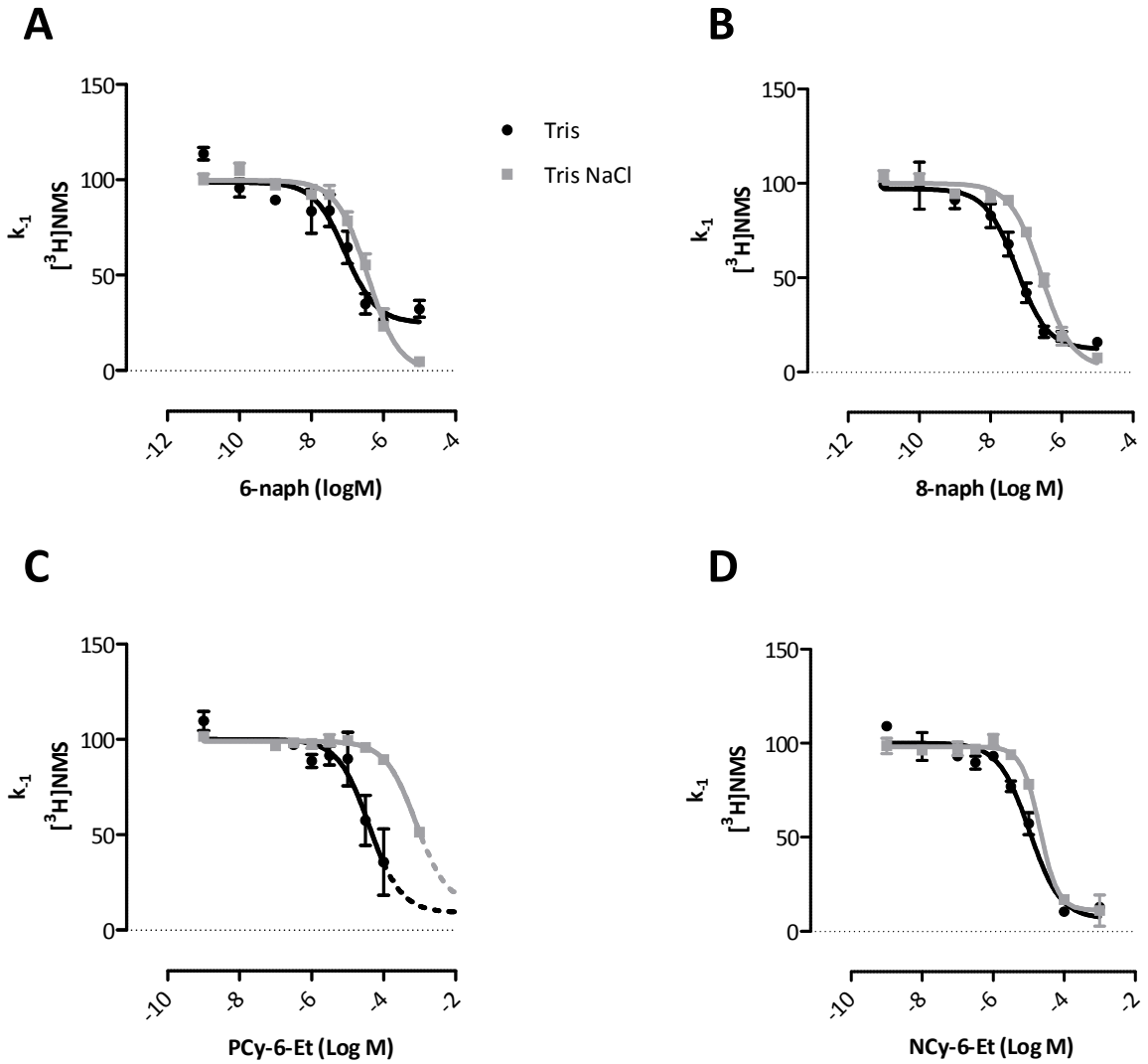

Figure 3.23: Concentration-effect curves of the delay of [^{3}H]NMS dissociation induced by the test compounds. Ordinate: apparent rate constant of radioligand dissociation expressed as percentage of the rate constant in absence of compound. Abscissa: logarithm of the numerical value of the concentrations of the tested compounds. Data points: mean ± SEM of 3-4 assays performed in duplicate. Curve fitting: "Four-parameter logistic equation" (Eq. 8). The dissociation binding assay was conducted in Tris and Tris NaCl buffer and incubated at 24°C.

Figure 3.23 shows the graphs derived from the two-point kinetic assays with the four allosteric ligands. All the tested ligands are able to partially or totally inhibit the dissociation of the orthosteric radioantagonist. The addition of 200 mM NaCl to the buffer causes a rightward shift of the curves, denoting a decrease in the allosteric affinity of all the compounds.

The parameter values obtained with these experiments are summarized in table 3.12.

Compound	*Buffer*	*$pEC_{50,diss}$*	*Bottom plateau (%)*	*n*
6-naph	Tris	6.93 ± 0.38	25 ± 7	3
	Tris NaCl	6.36 ± 0.08	0 ± 6	3
8-naph	Tris	7.37 ± 0.15	12 ± 3	4
	Tris NaCl	6.51 ± 0.03**	2 ± 3	3
PCy-6-Et	Tris	4.46 ± 0.18	15 ± 14	3
	Tris NaCl	3.09 ± 0.26*	13 ± 24	3
NCy-6-Et	Tris	4.95 ± 0.11	5 ± 3	3
	Tris NaCl	4.55 ± 0.09*	3 ± 7	3

Table 3.12: Parameter values derived from Figure 3.23; $pEC_{50,diss}$: negative common logarithm of the concentration of test compound causing a half maximum delay of radioligand dissociation; n: number of performed experiments. The table shows mean values ± SEM of 3-4 independent experiments performed in duplicate. *,**,***: ($p<0.05$, 0.01, 0.001), significantly different from the value reported in Tris buffer according to a two-tailed t-test.

In sum, the allosteric modulators showed a decrease in affinity for the allosteric binding site of M_2 when investigated in the high osmolarity buffer, as expected from previous data reported in literature (Tränkle et al., 1996; Schröter et al., 2000).

3.5.2 PCy-6-Et and NCy-6-Et showed negative cooperativity with [^{3}H]NMS

[^{3}H]NMS equilibrium binding assays were carried out to determine the affinities of the allosteric compounds for the NMS-unoccupied receptor. The compound's affinity for the receptor was calculated applying equation (22), derived from the ATCM model (Ehlert, 1988).

As shown above, the allosteric ligands inhibited, at least partially, [^{3}H]NMS dissociation (3.5.1) in dissociation studies. Therefore, the incubation time to reach equilibrium was calculated according to Lazareno and Birdsall (Eq. 23). For the highest concentrations of PCy-6-Et and NCy-6-Et used in the heterologous binding experiments, the calculated incubation time was 5 hours in Tris buffer and 1.5 hours in Tris NaCl buffer. An incubation time of 6 hours was therefore applied in both buffers. Figure 3.24 shows the displacement curves of PCy-6-Et and NCy-6-Et in the [^{3}H]NMS equilibrium binding assays, performed in Tris and Tris NaCl.

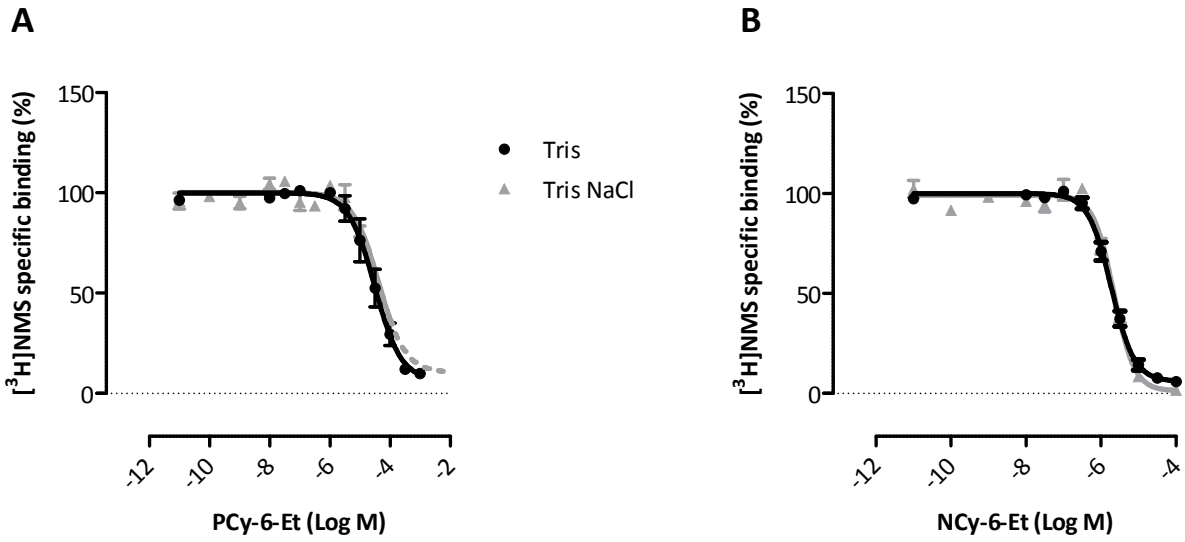

Figure 3.24: [^{3}H]NMS equilibrium binding assays. Ordinate: [^{3}H]NMS binding expressed as percentage of [^{3}H]NMS binding in absence of compound. Abscissa: logarithm of the concentration of test compounds. The experiments were carried out in Tris and Tris buffer supplemented with 100 µM GDP and incubated for 6 hours at 24°C. Data points: mean ± SEM of 3-4 assays performed in triplicate. Curve fitting: "Four-parameter logistic equation" (Eq. 8).

Both allosteric fragments were able to displace the radioligand. NCy-6-Et reached full [^{3}H]NMS displacement in both buffers, while PCy-6-Et only achieved partial displacement. In both buffers PCy-6-Et had a similar affinity, while NCy-6-Et lost affinity in Tris NaCl compared to Tris buffer.

The data obtained from these experiments are summarized in table 3.13.

Compound	*Buffer*	*pK_A*	*Lower plateau (%)*	*n_H*	*n*
PCy-6-Et	Tris	4.91 ± 0.20	7 ± 2	-1 (-1.02 ± 0.20)	4
	Tris NaCl	4.42 ± 0.23	10 ± 14	-2.51 ± 2.48	3
NCy-6-Et	Tris	5.98 ± 0.05	6 ± 2	-1.42 ± 0.12	4
	Tris NaCl	5.77 ± 0.04*	1 ± 3	-1.60 ± 0.21	3

Table 3.13: Parameter values derived from Figure 3.24. pK_A: negative common logarithm of the affinity values of the test compounds; n_H: Hill slope of the curve; if it did not significantly differ from unity, a value of -1 was assumed and the exact value reported in brackets. n: number of performed experiments. The table shows mean values ± SEM of 3-4 independent experiments performed in triplicate. *: ($p<0.05$), significantly different from the value reported in Tris buffer according to a two-tailed t-test.

Altogether, the results indicate that the two allosteric fragments are negative cooperative with [^{3}H]NMS.

3.5.3 6-naph and 8-naph showed conflicting results in equilibrium binding studies

[^{3}H]NMS equilibrium binding assays were also carried out to determine the affinities of the allosteric compounds 6-naph and 8-naph for the NMS-unoccupied receptor. The incubation time to reach equilibrium was calculated according to Lazareno and Birdsall (Eq. 23). For the concentrations of the compounds used in the heterologous binding experiments, the highest incubation time for reaching equilibrium was 17 hours. Therefore, an incubation time of 18 hours was chosen. Figure 3.25 shows the binding curves of 6-naph and 8-naph in Tris and Tris NaCl. Notably, the results of these experiments are contradictory. In some assays, the ligands acted as positive allosteric modulators, increasing the binding of [^{3}H]NMS (Fig. 3.25A,B). In others, the same compounds were negative allosteric modulators, partially displacing [^{3}H]NMS binding (Fig. 3.25C,D).

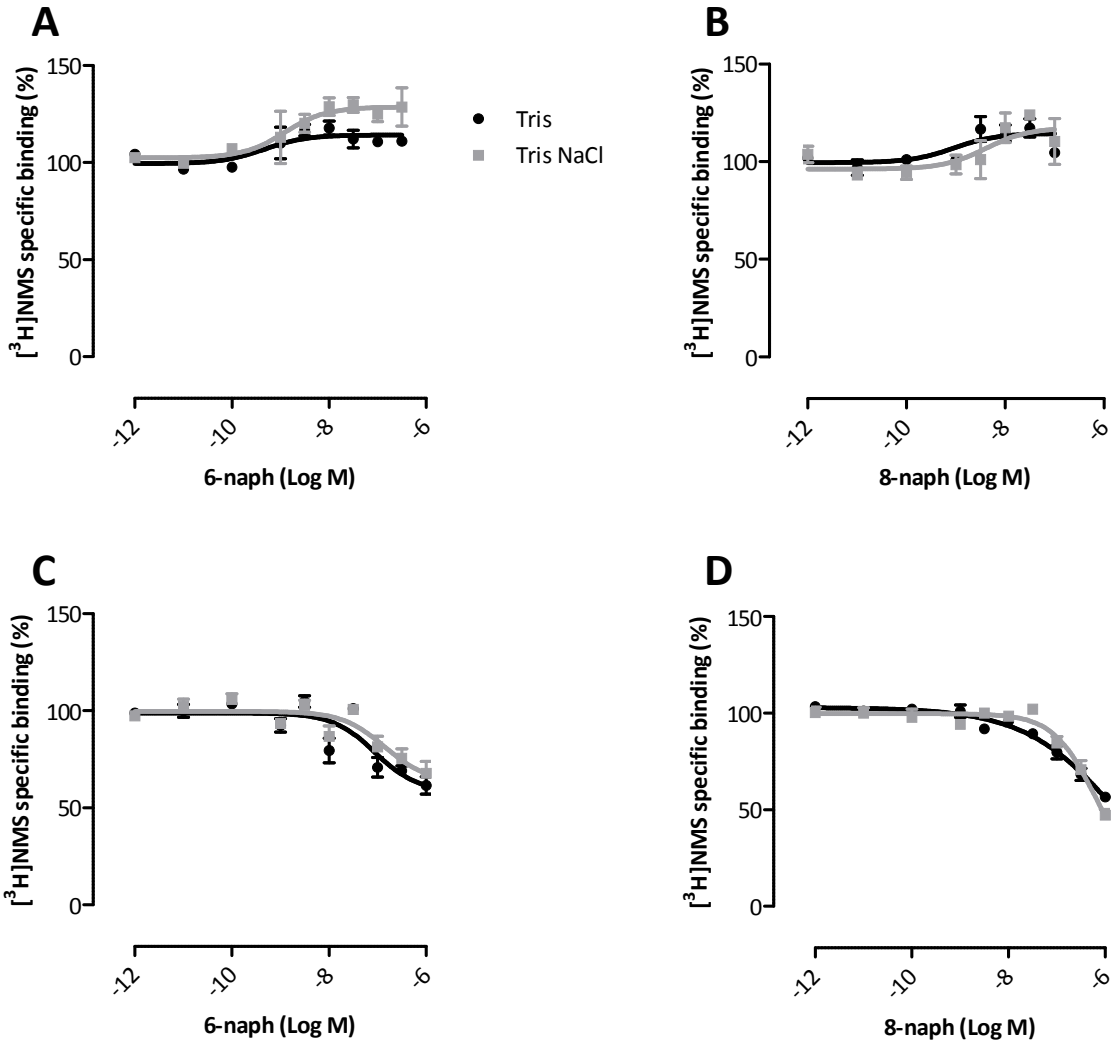

Figure 3.25: [^{3}H]NMS equilibrium binding assays. Ordinate: [^{3}H]NMS binding expressed as percentage of [^{3}H]NMS binding in absence of compound. Abscissa: logarithm of the concentration of test compounds. The experiments were carried out in Tris and Tris buffer supplemented with 100 µM GDP and incubated for 18 hours at 24°C. (A,B): Mean curve of experiments that resulted in enhancement of [^{3}H]NMS binding. (C,D): Mean curve of experiments that resulted in decrease of [^{3}H]NMS binding. Data points: mean ± SEM of 2-6 assays performed in triplicate. Curve fitting: "Four-parameter logistic equation" (Eq. 8).

Given that the compounds are allosteric modulators, data analysis was performed according to equation (22). The results indicated that the affinity of 6-naph and 8-naph is significantly higher in case they act as positive allosteric modulators (up to 100-times) rather than partial displacers of [^{3}H]NMS.

The data obtained from these experiments are summarized in table 3.14.

Compound	*Buffer*	*pK_A*	*Lower plateau (%)*	*Upper plateau (%)*	*n*
(A) 6-naph	Tris	9.17 ± 0.17	100 ± 2	113 ± 3	3
	Tris NaCl	9.04 ± 0.40	102 ± 4	130 ± 5*	4
(B) 8-naph	Tris	8.74 ± 018	100 ± 2	115 ± 2	3
	Tris NaCl	8.41 ± 0.49	96 ± 4	118 ± 12	2
(C) 6-naph	Tris	7.18 ± 0.11	58 ± 3	99 ± 3	6
	Tris NaCl	6.94 ± 0.22	63 ± 7	100 ± 2	6
(D) 8-naph	Tris	7.03 ± 0.07	52 ± 4	103 ± 2	2
	Tris NaCl	6.36 ± 0.10*	26 ± 6	100 ± 1	6

Table 3.14: Parameter values derived from Figure 3.25. pK_A: negative common logarithm of the affinity values of the test compounds; n: number of performed experiments. The table shows mean values ± SEM of 2-6 independent experiments performed in triplicate. *,**,***: ($p<0.05$, 0.01, 0.001), significantly different from the value reported in Tris buffer according to a two-tailed t-test.

Taken together, it was not possible to get a uniform result for 6-naph and 8-naph and given the results of this set of experiments it cannot be determined whether these compounds are positive or negative cooperative with [^{3}H]NMS.

3.6 Influence of salts and spontaneous activity on dualsteric signaling

3.6.1 Iper-X-naph dualsteric ligands show partial or protean agonism

The five test compounds composed by the superagonist iperoxo and a naphmethonium-derived allosteric fragment connected with a linker of different length (see 2.7.5), were evaluated in [^{35}S]GTPγS binding experiments. These assays were conducted in order to determine potency and efficacy of the test compounds in the G_i pathway in the presence and absence of spontaneous activity.

The inflection point of the concentration-effect curve (pEC_{50}) was taken to reflect the potency of the compounds, while the maximum effect (E_{max}) was considered as a measure of intrinsic activity or efficacy of the compounds. The known full agonist acetylcholine was evaluated in the same

assay to define the maximum effect. A single concentration of atropine (10 µM) was used to determine the amount of spontaneous activity of the receptor as this ligand is a full inverse agonist and thus it prevents ligand-independent [^{35}S]GTPγS binding.

As shown in Fig. 3.26, iper-0-naph showed a very peculiar behavior. This ligand was an inverse agonist in the presence of spontaneous activity (Tris buffer) and a partial agonist in the absence of constitutive activity (Tris NaCl). The results are shown as normalized either on basal [^{35}S]GTPγS binding (Fig. 3.26A) or on the value reported in the presence of 10 µM atropine (Fig. 3.26B). The parameter data are derived from Fig. 3.26A for better comparison with the other hybrid ligands.

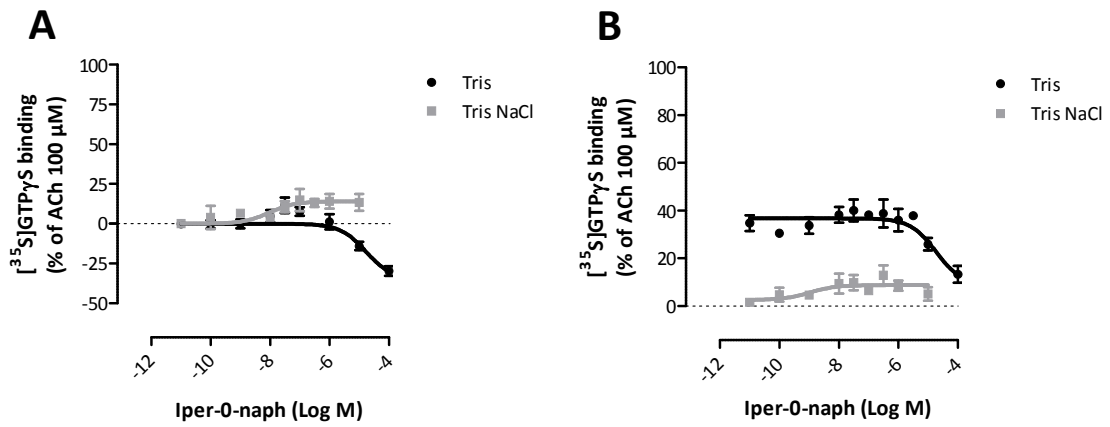

Figure 3.26: Iper-0-naph-induced [^{35}S]GTPγS binding to membrane suspensions from FlpIn CHO-M_2 cells. Abscissa: logarithm of the concentrations of the compounds. Ordinate: percentage of [^{35}S]GTPγS binding, normalized on the maximum effect of 100 µM ACh which was set to 100%. **(A)** 0% corresponds to the lower plateau (basal [^{35}S]GTPγS binding). **(B)** 0% corresponds to the [^{35}S]GTPγS binding in the presence of 10 µM atropine. The assay was performed in Tris and Tris NaCl buffer with an incubation time of 60 minutes at 24°C. The graphs show the mean values ± SEM of 3-6 experiments performed in triplicate. Curve fitting: "Four-parameter logistic equation" (Eq. 8).

The other four compounds were partial agonists in both buffers, as shown in Fig. 3.27.

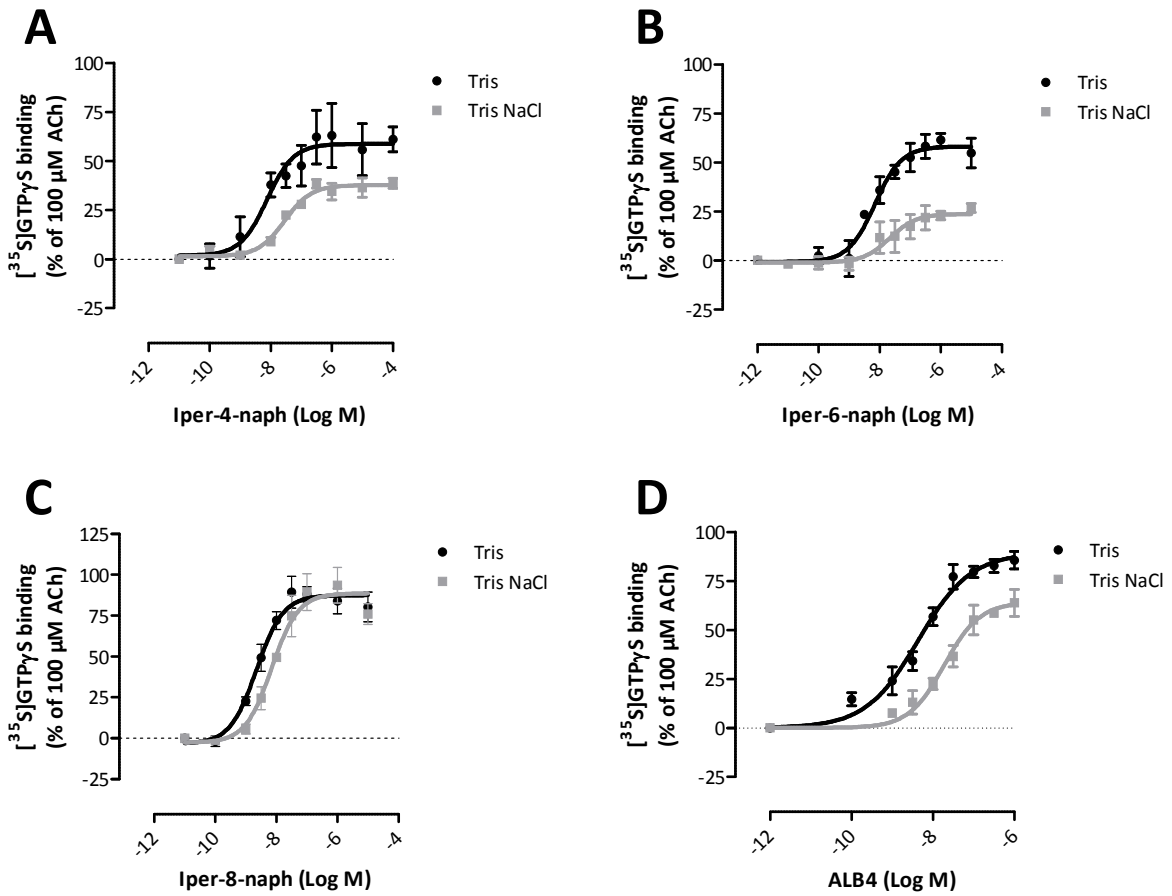

Figure 3.27: Test compound-induced [^{35}S]GTPγS binding to membrane suspensions from FlpIn CHO-M_2 cells. Ordinate: percentage of [^{35}S]GTPγS binding, normalized on the maximum effect of 100 µM ACh which was set to 100%. 0% corresponds to the lower plateau (basal [^{35}S]GTPγS binding). Abscissa: logarithm of the concentrations of the compounds. The assay was performed in Tris and Tris NaCl buffer with an incubation time of 60 minutes at 24°C. The graph shows the mean values ± SEM of 3-6 experiments performed in triplicate. Curve fitting: "Four-parameter logistic equation" (Eq. 8).

The parameter values derived from Fig. 3.26 and 3.27 are summarized in Table 3.15.

Compound	*Buffer*	*pEC_{50}*	*E_{max} (%)*	*n*
Iper-0-naph	Tris	5.19 ± 0.31	-32 ± 6	4
	Tris NaCl	7.73 ± 0.21**	9 ± 2**	3
Iper-4-naph	Tris	8.14 ± 0.27	60 ± 12	3
	Tris NaCl	7.56 ± 0.10	38 ± 4	3
Iper-6-naph	Tris	8.26 ± 0.26	57 ± 5	3
	Tris NaCl	7.43 ± 0.47	27 ± 1***	4
Iper-8-naph	Tris	8.64 ± 0.07	86 ± 6	5
	Tris NaCl	8.21 ± 0.06**	85 ± 8	3
ALB4	Tris	8.51 ± 0.14	81 ± 2	6
	Tris NaCl	7.70 ± 0.07**	65 ± 8*	4

Table 3.14: Parameter values derived from Figure 3.26A and 3.27; pEC_{50}: negative common logarithm of the concentration of test compound causing a half maximum effect; E_{max}: maximum level of [^{35}S]GTPγS binding in percent normalized on 100 µM ACh which was set to 100%; n: number of performed experiments. The table shows mean values ± SEM of 3-6 independent experiments carried out in triplicate. *, **, ***: ($p<0.05$, 0.01, 0.001), significantly different from the value reported in Tris buffer according to a two-tailed t-test.

3.6.2 Isox-X-naph dualsteric ligands show distinct patterns of receptor activation

The five test compounds composed by the full agonist isox and a naphmethonium-derived allosteric fragment, connected with a linker of different length, were evaluated in [^{35}S]GTPγS binding experiments. The aim of these assays was to determine whether there were differences in signaling activation in comparison to the corresponding iperoxo-derivatives.

The compound with a hexamethylene chain, isox-6-naph, showed protean agonism, similarly to the already described iper-0-naph hybrid. As shown in Fig. 3.28, it decreased [^{35}S]GTPγS binding in Tris buffer and it stimulated [^{35}S]GTPγS binding in Tris NaCl buffer. The results are shown as normalized either on basal [^{35}S]GTPγS binding (Fig. 3.28A) or to 10 µM atropine (Fig. 3.28B). The parameter data are derived from Fig. 3.28A for better comparison with the other hybrid ligands.

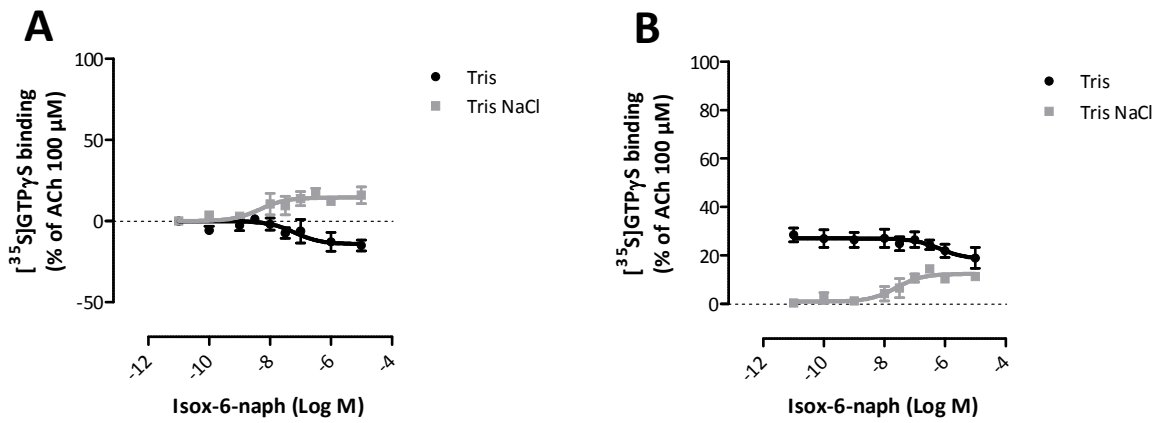

Figure 3.28: Isox-6-naph-induced [^{35}S]GTPγS binding to membrane suspensions from FlpIn CHO-M_2 cells. Ordinate: percentage of [^{35}S]GTPγS binding, normalized on the maximum effect of 100 µM ACh which was set to 100%. **(A)** 0% corresponds to the lower plateau (basal [^{35}S]GTPγS binding). **(B)** 0% corresponds to the maximum inhibition of [^{35}S]GTPγS binding induced by 10 µM atropine. Abscissa: logarithm of the concentrations of the compounds. The assay was performed in Tris and Tris NaCl buffer with an incubation time of 60 minutes at 24°C. The graph shows the mean values ± SEM of 5-7 experiments performed in triplicate. Curve fitting: "Four-parameter logistic equation" (Eq. 8).

The results obtained for the other dualsteric ligands are shown in Fig. 3.29.

Isox-0-naph was an inverse agonist in the spontaneously active system and a neutral antagonist in the quiescent system. Isox-4-naph and isox-8-naph were partial agonists in both systems. Upon addition of NaCl to the buffer and decrease of the constitutive receptor activity, the E_{max} of both compounds was significantly reduced.

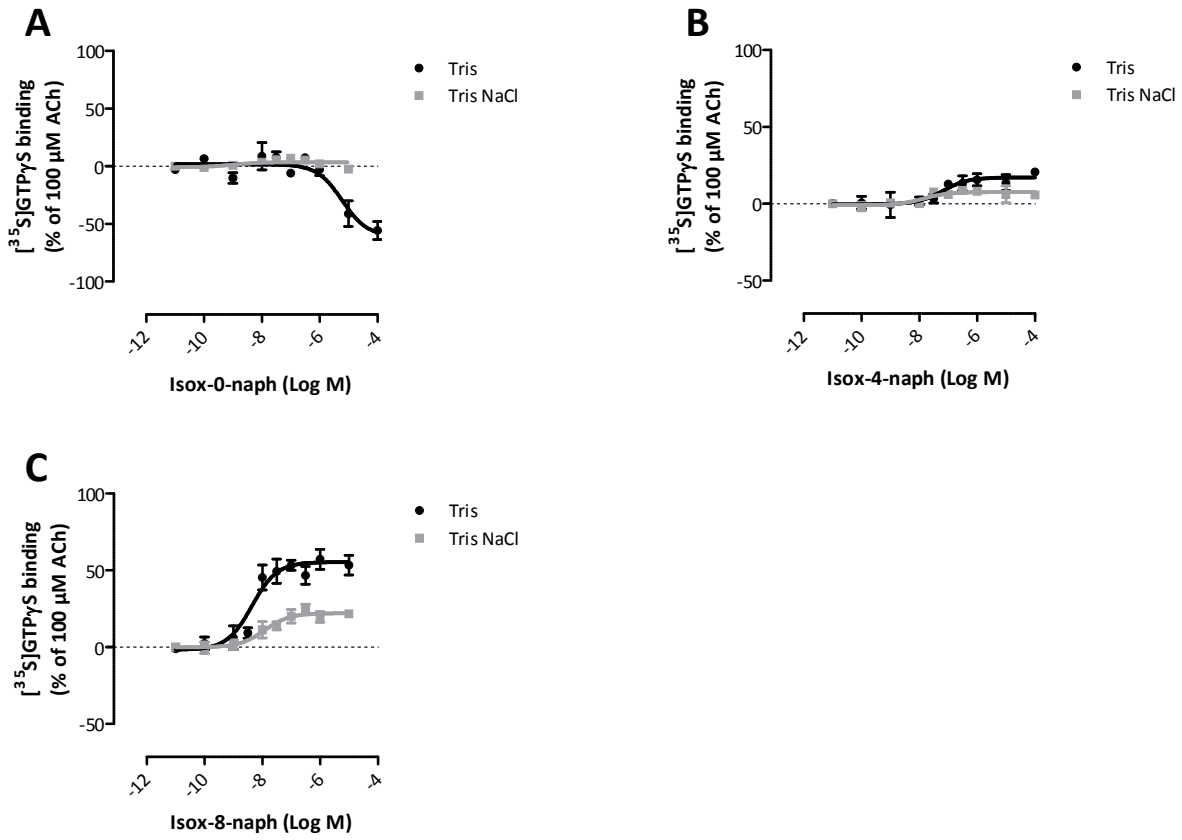

Figure 3.29: Test compound-induced [^{35}S]GTPγS binding to membrane suspensions from FlpIn CHO-M_2 cells. Ordinate: percentage of [^{35}S]GTPγS binding, normalized on the maximum effect of 100 µM ACh which was set to 100%. 0% corresponds to the lower plateau (basal [^{35}S]GTPγS binding). Abscissa: logarithm of the concentrations of the compounds. The assay was performed in Tris and Tris NaCl buffer with an incubation time of 60 minutes at 24°C. The graph shows the mean values ± SEM of 3-5 experiments performed in triplicate. Curve fitting: "Four-parameter logistic equation" (Eq. 8).

The parameter values inferred from these experiments are summarized in Table 3.16.

Compound	*Buffer*	*pEC_{50}*	*E_{max} (%)*	*n*
Isox-0-naph	Tris	4.76 ± 0.35	-56 ± 7	3
	Tris NaCl	n.d.	n.d.	3
Isox-4-naph	Tris	7.28 ± 0.03	17 ±3	3
	Tris NaCl	7.71 ± 0.21*	8 ±2	3
Isox-6-naph	Tris	6.50 ± 0.34	-17 ±4	7
	Tris NaCl	7.81 ± 0.38**	16 ± 3**	5
Isox-8-naph	Tris	8.38 ± 0.28	58 ± 4	5
	Tris NaCl	8.02 ± 0.32	22 ± 2***	3

Table 3.15: Parameter values derived from Figure 3.28 and 3.29; pEC_{50}: negative common logarithm of the concentration of test compound causing a half maximum effect; E_{max}: maximum level of [^{35}S]GTPγS binding in percent normalized on 100 µM ACh which was set to 100%; n: number of performed experiments. *, **, ***: significantly different ($p<0.05$, 0.01, 0.001) from the value reported in Tris buffer according to a two-tailed t-test. The table shows mean values ± SEM of 3-7 independent experiments carried out in triplicate.

3.6.3 OOM-6-naph shows protean agonism at M_2

OOM-6-naph is a dualsteric ligand composed of an allosteric moiety derived from naphmethonium linked through a 6-methylene linker to an oxotremorine-like orthosteric moiety. This compound was tested for receptor activation in order to determine whether it behaved similarly to iper-6-naph, i.e. as a partial agonist, or similar to isox-6-naph, i.e. a protean agonist. As shown in Fig. 3.30, OOM-6-naph was able to activate M_2 receptors in a quiescent system, while inactivating signaling of spontaneously active receptors, thus behaving as a protean ligand.

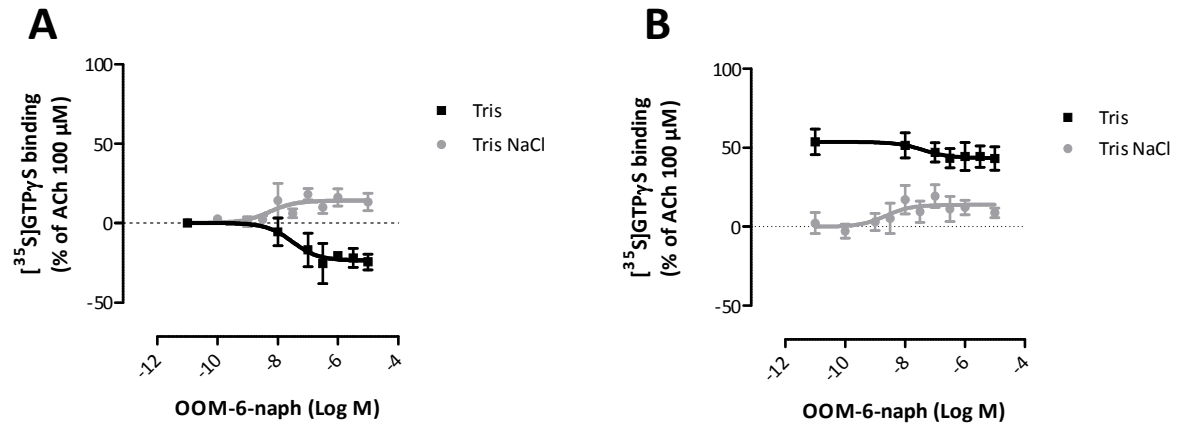

Figure 3.30: OOM-6-naph-induced [^{35}S]GTPγS binding to membrane suspensions from FlpIn CHO-M_2 cells. Ordinate: percentage of [^{35}S]GTPγS binding, normalized on the maximum effect of 100 µM ACh which was set to 100%. **(A)** 0% corresponds to the lower plateau (basal [^{35}S]GTPγS binding). **(B)** 0% corresponds to the [^{35}S]GTPγS binding in the presence of 10 µM atropine. Abscissa: logarithm of the concentrations of the compounds. The assay was performed in Tris and Tris NaCl buffer with an incubation time of 60 minutes at 24°C. The graph shows the mean values ± SEM of 3-4 experiments performed in triplicate. Curve fitting: "Four-parameter logistic equation" (Eq. 8).

The parameter values inferred from Fig. 3.30A are summarized in Table 3.17.

Compound	*Buffer*	*pEC_{50}*	*E_{max} (%)*	*n*
OOM-6-naph	Tris	7.22 ± 0.60	-26 ± 5	3
	Tris NaCl	7.40 ± 0.49	17 ± 4**	4

Table 3.17: Parameter values derived from Figure 3.30A; pEC_{50}: negative common logarithm of the concentration of test compound causing a half maximum effect; E_{max}: maximum level of [^{35}S]GTPγS binding in percent normalized on 100 µM ACh which was set to 100%; n: number of performed experiments. The table shows mean values ± SEM of 3-4 independent experiments carried out in triplicate. **: significantly different ($p<0.01$) from the value reported in Tris buffer according to a two-tailed t-test.

3.6.4 Iper-X-phth dualsteric ligands show partial agonism in both spontaneously active and quiescent system

As previously described, three compounds derived from iperoxo, isox and OOM showed protean agonism at M_2 receptors. All of the previously tested ligands had the same allosteric fragment, i.e. naphmethonium-derived (naph-). Here, dualsteric ligands with a different allosteric moiety, i.e.

W84-derived (phth-), were studied for comparison. The aim of these experiments was to determine whether phth-compounds could elicit protean agonism as their naph-counterparts.
The compounds ALB3, iper-6-phth, isox-6-phth and OOM-6-phth were analyzed in [^{35}S]GTPγS assays and the results are shown in Fig. 3.31.

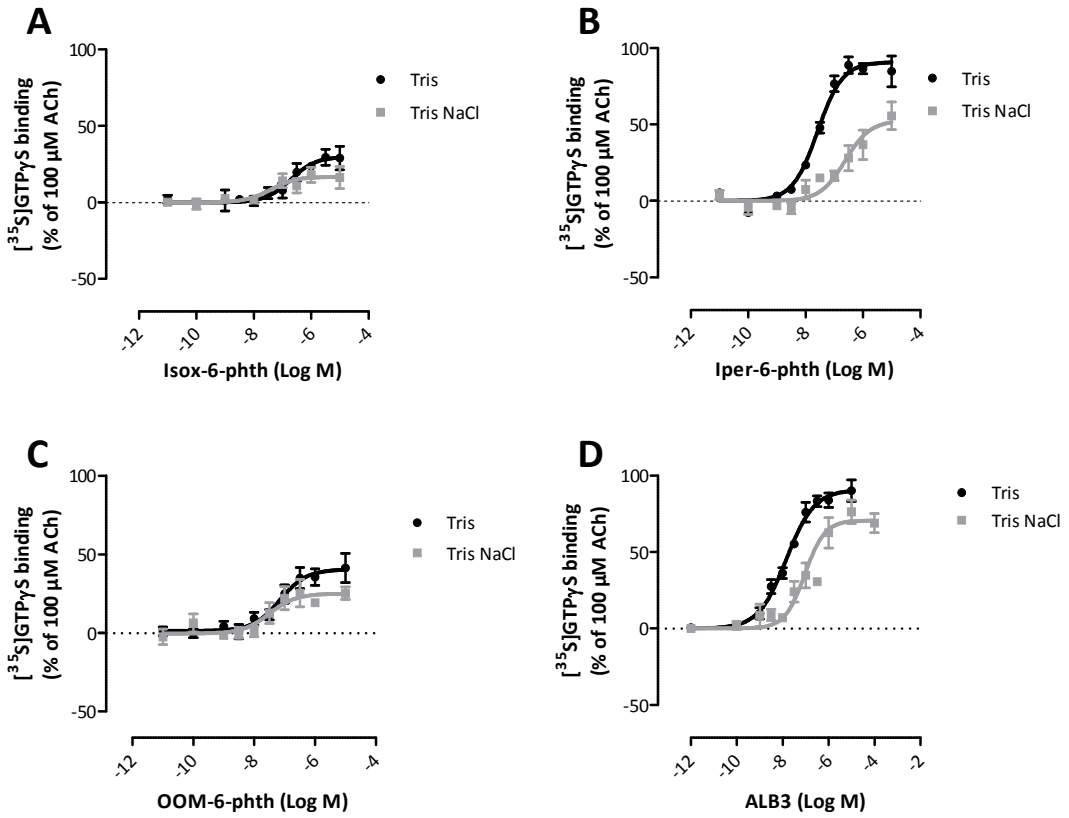

Figure 3.31: Test compound-induced [^{35}S]GTPγS binding to membrane suspensions from FlpIn CHO-M_2 cells. Ordinate: percentage of [^{35}S]GTPγS binding, normalized on the maximum effect of 100 µM ACh which was set to 100%. 0% corresponds to the lower plateau (basal [^{35}S]GTPγS binding). Abscissa: logarithm of the concentrations of the compounds. The assay was performed in Tris and Tris NaCl buffer with an incubation time of 60 minutes at 24°C. The graph shows the mean values ± SEM of 3-5 experiments performed in triplicate. Curve fitting: "Four-parameter logistic equation" (Eq. 8).

All of the compounds were partial agonists in both Tris and Tris NaCl buffers. The iperoxo-derived ligands showed a significantly lower potency in Tris NaCl compared to Tris buffer, while the potency of isox- and OOM-derivatives were not reported to be different in the two buffers. In regard to the efficacy, only the E_{max} of iper-6-phth was significantly decreased when the high osmolarity buffer was applied. The parameter values inferred from these experiments are summarized in Table 3.18.

Compound	*Buffer*	*pEC_{50}*	*E_{max} (%)*	*n*
Iper-6-phth	Tris	7.59 ± 0.04	91 ± 5	4
	Tris NaCl	6.40 ± 0.38*	60 ± 10*	3
Isox-6-phth	Tris	6.67 ± 0.40	33 ± 5	5
	Tris NaCl	7.20 ± 0.37	19 ± 5	4
ALB3	Tris	7.92 ± 0.06	86 ± 5	5
	Tris NaCl	7.20 ± 0.29*	71 ± 7	5
OOM-6-phth	Tris	7.19 ± 0.29	44 ± 7	5
	Tris NaCl	7.16 ± 0.45	27 ± 3	5

Table 3.18: Parameter values derived from Figure 3.31 ; pEC_{50}: negative common logarithm of the concentration of test compound causing a half maximum effect; E_{max}: maximum level of [^{35}S]GTPγS binding in percent normalized on 100 µM ACh which was set to 100%; n: number of performed experiments. *: significantly different ($p<0.05$) from the value reported in Tris buffer according to a two-tailed t-test. The table shows mean values ± SEM of 3-5 independent experiments carried out in triplicate.

3.7 Influence of NaCl on dualsteric ligand binding

3.7.1 Six dualsteric ligands lose allosteric affinity in Tris NaCl buffer

Isox-6-naph, iper-6-naph, iper-8-naph, ALB3 and ALB4 are heterobivalent ligands composed of an orthosteric and an allosteric moiety. To check for allosteric interaction, dissociation binding studies were performed. The assays were carried out in Tris and Tris NaCl buffer to verify if the presence of NaCl had an influence on the allosteric potency of the listed compounds. Fig. 3.32 shows the results of these experiments.

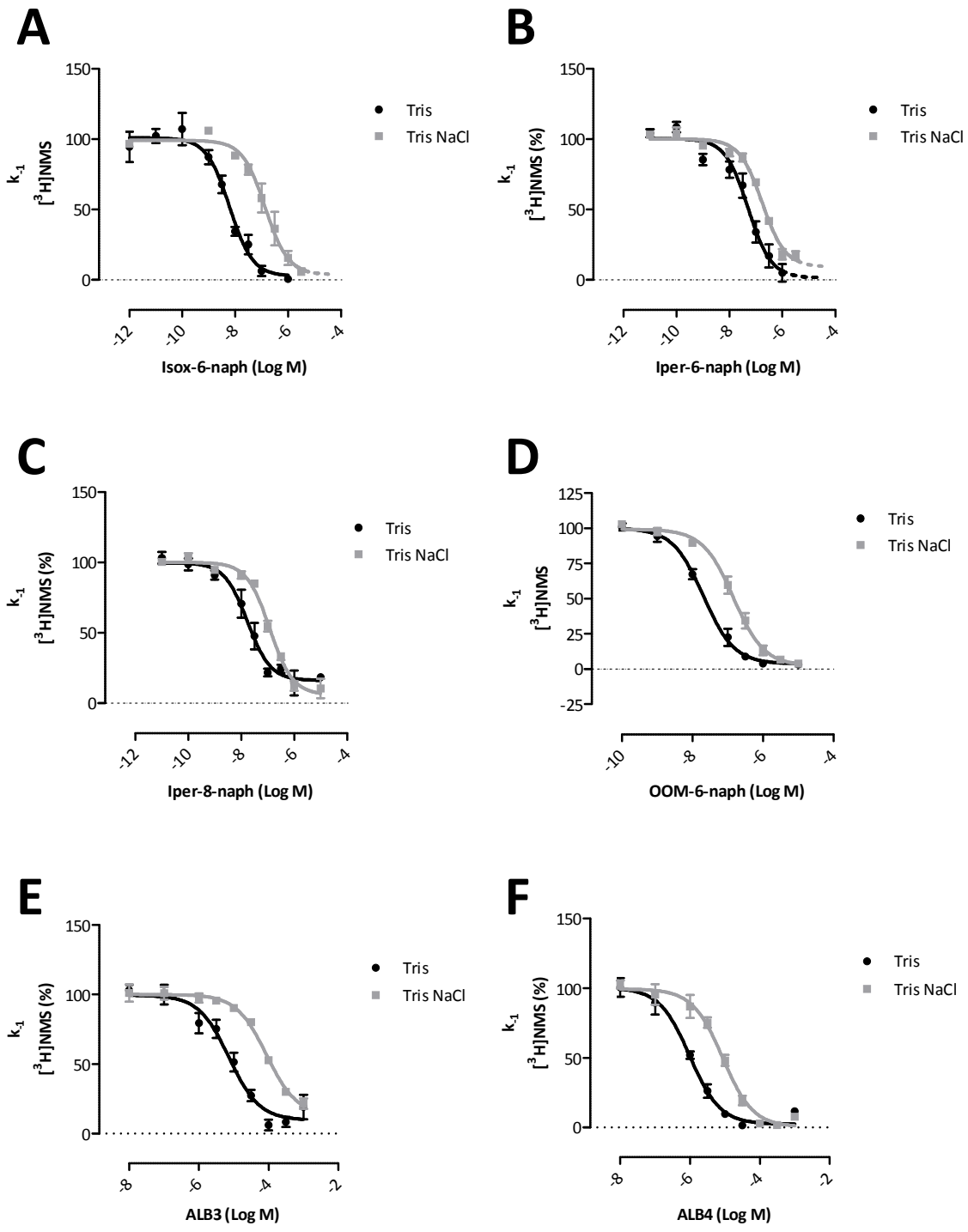

Figure 3.32: Concentration-effect curves of the delay of [^{3}H]NMS dissociation induced by the test compounds. Ordinate: apparent rate constant of radioligand dissociation expressed as percentage of the rate constant in absence of compound. Abscissa: logarithm of the numerical value of the concentrations of the compounds. Data points: mean ± SEM of 3-6 assays performed in duplicate. Curve fitting: "Four-parameter logistic equation" (Eq. 8). The dissociation binding assay was conducted in Tris and Tris NaCl buffer and incubated at 24°C. The bottom plateaus that did not differ significantly from zero were constrained to 0.

The six dualsteric ligands are able to partially or totally inhibit the dissociation of the orthosteric radioantagonist [^{3}H]NMS; all compounds displayed a dose-response curve that was rightward-shifted in the presence of NaCl, indicating that sodium decreases the allosteric affinity of the compounds.

The parameter values obtained with these experiments are summarized in table 3.19.

Compound	*Buffer*	*$pEC_{50,diss}$*	*Bottom plateau (%)*	*n*
Isox-6-naph	Tris	8.10 ± 0.11	3 ± 5	3
	Tris NaCl	6.78 ± 0.22**	4 ± 5	3
Iper-6-naph	Tris	7.31 ± 0.13	1 ± 6	5
	Tris NaCl	6.75 ± 0.04***	9 ± 3	4
Iper-8-naph	Tris	7.77 ± 0.21	15 ± 4	3
	Tris NaCl	6.91 ± 0.04***	5 ± 3	4
OOM-6-naph	Tris	7.61 ± 0.12	4 ± 3	6
	Tris NaCl	6.83 ± 0.11***	2 ± 3	6
ALB3	Tris	5.14 ± 0.11	9 ± 4	3
	Tris NaCl	4.05 ± 0.05	13 ± 3	3
ALB4	Tris	5.98 ± 0.08	1 ± 2	3
	Tris NaCl	5.06 ± 0.08	0 ± 2	3

Table 3.19: Parameter values derived from Figure 3.32; $pEC_{50,diss}$: negative common logarithm of the concentration of test compound causing a half maximum delay of radioligand dissociation; n: number of performed experiments. The table shows mean values ± SEM of 3-6 independent experiments performed in duplicate. *, **, ***: ($p<0.05$, 0.01, 0.001), significantly different from Tris buffer according to a two-tailed t-test.

3.7.2 The allosteric potency of iper-0-naph and isox-8-naph is left unaltered by NaCl addition

Two additional dualsteric ligands were analyzed in dissociation experiments, in order to estimate their allosteric potency and an eventual effect of NaCl on their allosteric affinity. As shown in Fig. 3.33, iper-0-naph and isox-8-naph were able to inhibit the dissociation [^{3}H]NMS, totally and

partially, respectively. Upon addition of NaCl, the $pEC_{50,diss}$ was not shifted, pinpointing that NaCl had no influence on the allosteric affinity of these two ligands.

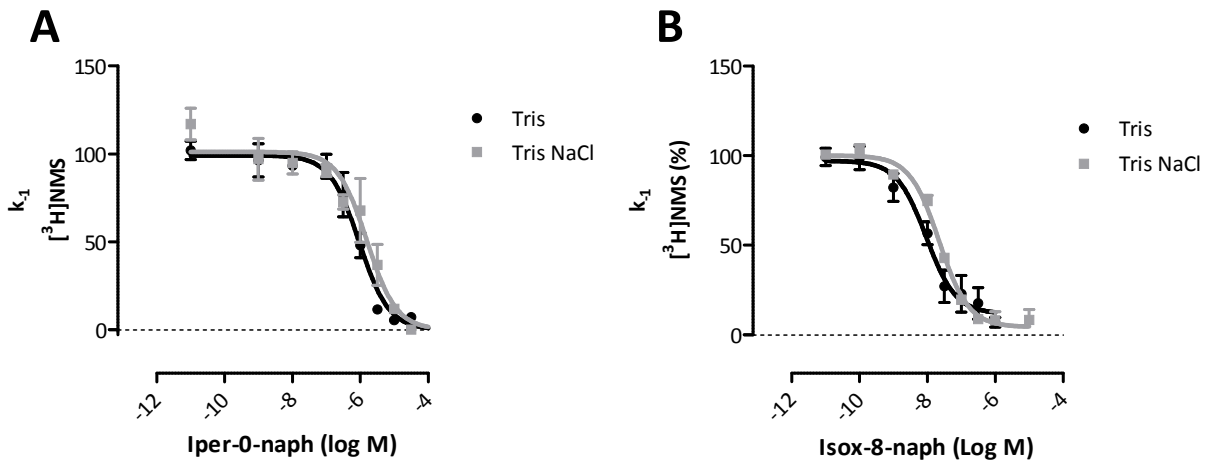

Figure 3.33: Concentration-effect curves of the delay of [^{3}H]NMS dissociation induced by the test compounds. Ordinate: apparent rate constant of radioligand dissociation expressed as percentage of the rate constant in absence of compound. Abscissa: logarithm of the numerical value of the concentrations of the compounds. Data points: mean ± SEM of 3-4 assays performed in duplicate. Curve fitting: "Four-parameter logistic equation" (Eq. 8). The dissociation binding assay was conducted in Tris and Tris NaCl buffer and incubated at 24°C. The bottom plateaus that did not differ significantly from zero were constrained to 0.

The parameter values obtained with these experiments are summarized in table 3.20.

Compound	*Buffer*	*$pEC_{50,diss}$*	*Bottom plateau (%)*	*n*
Iper-0-naph	Tris	5.95 ± 0.27	-4 ± 7	4
	Tris NaCl	5.77 ± 0.27	-2 ± 10	3
Isox-8-naph	Tris	7.88 ± 0.10	12 ± 5	4
	Tris NaCl	7.63 ± 0.03	4 ± 2	4

Table 3.20: Parameter values derived from Figure 3.33; $pEC_{50,diss}$: negative common logarithm of the concentration of test compound causing a half maximum delay of radioligand dissociation; n: number of performed experiments. The table shows mean values ± SEM of 3-4 independent experiments performed in duplicate.

3.7.3 Iperoxo-derived dualsteric hybrids displace [^{3}H]NMS

[^{3}H]NMS equilibrium binding assays were carried out to determine the affinities of the allosteric compounds for the NMS-unoccupied receptor. All experiments resulted in monophasic concentration-effect curves since they were performed in the presence of 100 µM GDP. Iper-6-naph, iper-8-naph, iper-0-naph, ALB3 and ALB4 displaced [^{3}H]NMS either partially (iper-6-naph, iper-8-naph, iper-0-naph) or completely (ALB3 and ALB4). The compound's affinity for the receptor was calculated applying equation (22), derived from the ATCM model (Ehlert, 1988) or equation (20), depending on partial or total radioligand displacement, respectively.

As shown previously (see 3.7.2), the dualsteric compounds inhibited [^{3}H]NMS dissociation. Therefore, the incubation time to reach equilibrium was calculated according to Lazareno and Birdsall (Eq. 23). For the highest concentrations of the compounds used in the heterologous binding experiments, the incubation time was set to 18 hours for iper-6-naph, iper-8-naph and iper-0-naph, given their high allosteric affinity, while an incubation time of 6 hours was chosen for ALB3 and ALB4, since these ligands have a lower affinity for the allosteric site. Figure 3.34 shows the displacement curves of the iperoxo-derived test compounds in the [^{3}H]NMS equilibrium binding assays.

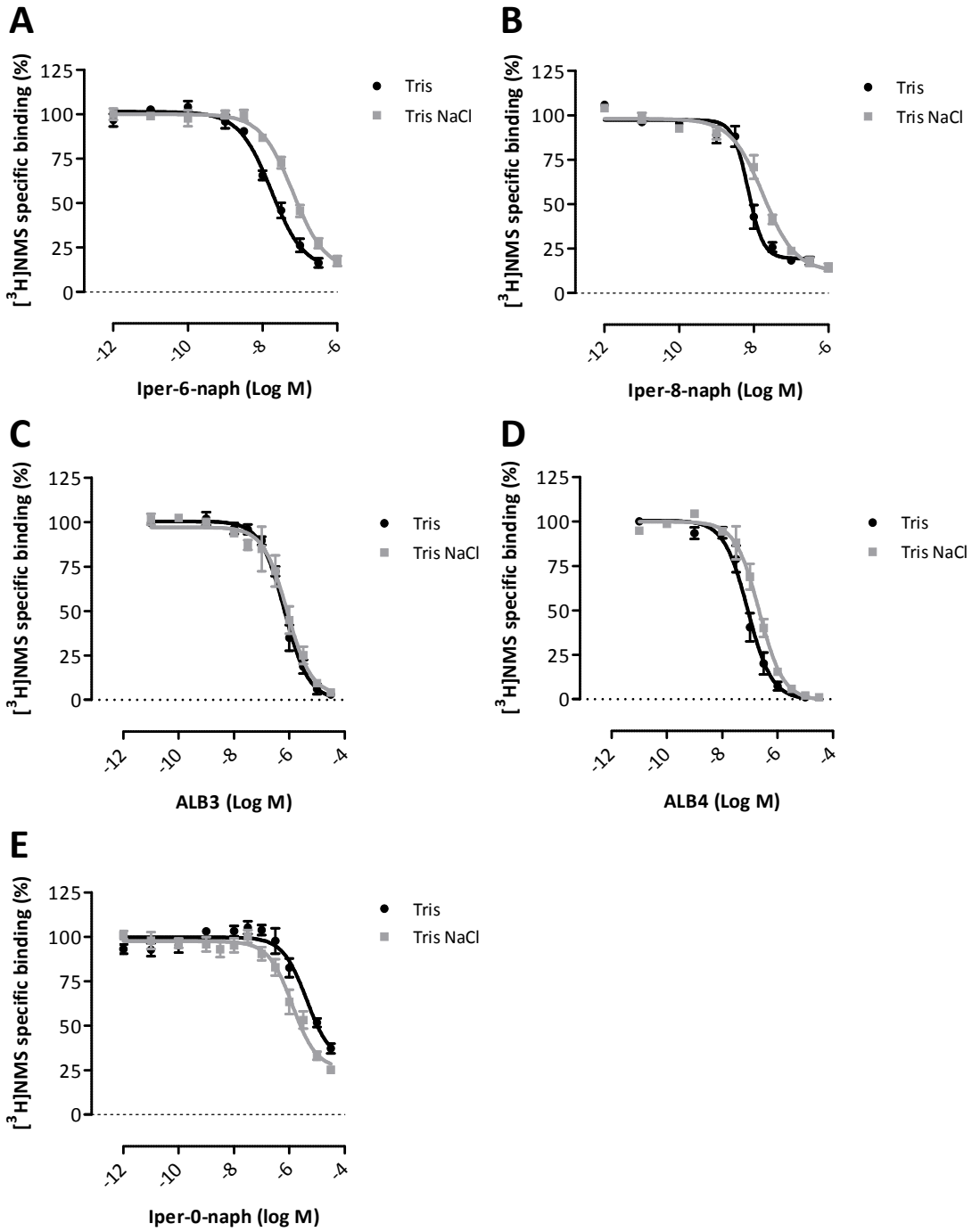

Figure 3.34: [^{3}H]NMS equilibrium binding assays with membrane suspensions of CHO-hM_2 cells. Ordinate: [^{3}H]NMS binding expressed as percentage of [^{3}H]NMS binding in absence of compound. Abscissa: logarithm of the concentration of test compounds. The experiments were carried out in Tris or Tris NaCl buffer supplemented with 100 µM GDP and incubated for 6 or 18 hours at 24°C. Data points: mean ± SEM of 3-6 assays performed in triplicate. Curve fitting: "Four-parameter logistic equation" (Eq. 8).

The data obtained from these experiments are summarized in table 3.21.

Compound	*Buffer*	*pK_A*	*Hill slope*	*Bottom plateau (%)*	*n*
Iper-6-naph	Tris	7.96 ± 0.08	-1 (-0.93 ± 0.15)	12 ± 3	4
	Tris NaCl	7.27 ± 0.05***	-1 (-1.09 ± 0.07)	12 ± 2	4
Iper-8-naph	Tris	8.34 ± 0.10	-2.38 ± 0.75	12 ± 1	4
	Tris NaCl	7.89 ± 0.09*	-1 (-1.13 ± 0.36)	13 ± 2	3
ALB3	Tris	6.24 ± 0.07	-1 (-1.30 ± 0.17)	0 ± 2	3
	Tris NaCl	6.19 ± 0.18	-1 (-0.87 ± 0.20)	2 ± 2	3
ALB4	Tris	7.15 ± 0.14	-1 (-1.38 ± 0.11)	-1 ± 1	3
	Tris NaCl	6.75 ± 0.11	-1 (-1.11 ± 0.14)	-1 ± 1	3
Iper-0-naph	Tris	5.48 ± 0.21	-1 (-1.18 ± 0.14)	28 ± 2	4
	Tris NaCl	5.96 ± 0.15	-1 (-1.03 ± 0.12)	22 ± 1	6

Table 3.21: Parameter values derived from Figure 3.34. pK_A: negative common logarithm of the affinity values of the test compounds; n_H: Hill slope; if it did not significantly differ from unity, a value of -1 was assumed and the exact value reported in brackets. The table shows mean values ± SEM of 3-6 independent experiments performed at least in duplicate. *,**,***: ($p<0.05$, 0.01, 0.001), significantly different from the value reported in Tris buffer according to a two-tailed t-test.

3.7.4 Isox- and OOM-derived dualsteric hybrids are positive, neutral or negative cooperative with [^{3}H]NMS

[^{3}H]NMS equilibrium binding assays were carried out to determine the affinities of isox- and OOM-derived compounds for the NMS-unoccupied receptor. The calculated incubation time for the highest concentrations of compounds used in these experiments was 17 hours. An incubation time of 18 hours was therefore selected. The compound's affinity for the receptor was calculated applying equation (22), derived from the ATCM model (Ehlert, 1988), for isox-6-naph, while it was not possible to calculate the affinity of isox-8-naph (incomplete curve) and OOM-6-naph (neutral cooperativity with the radioligand) (Fig. 3.35).

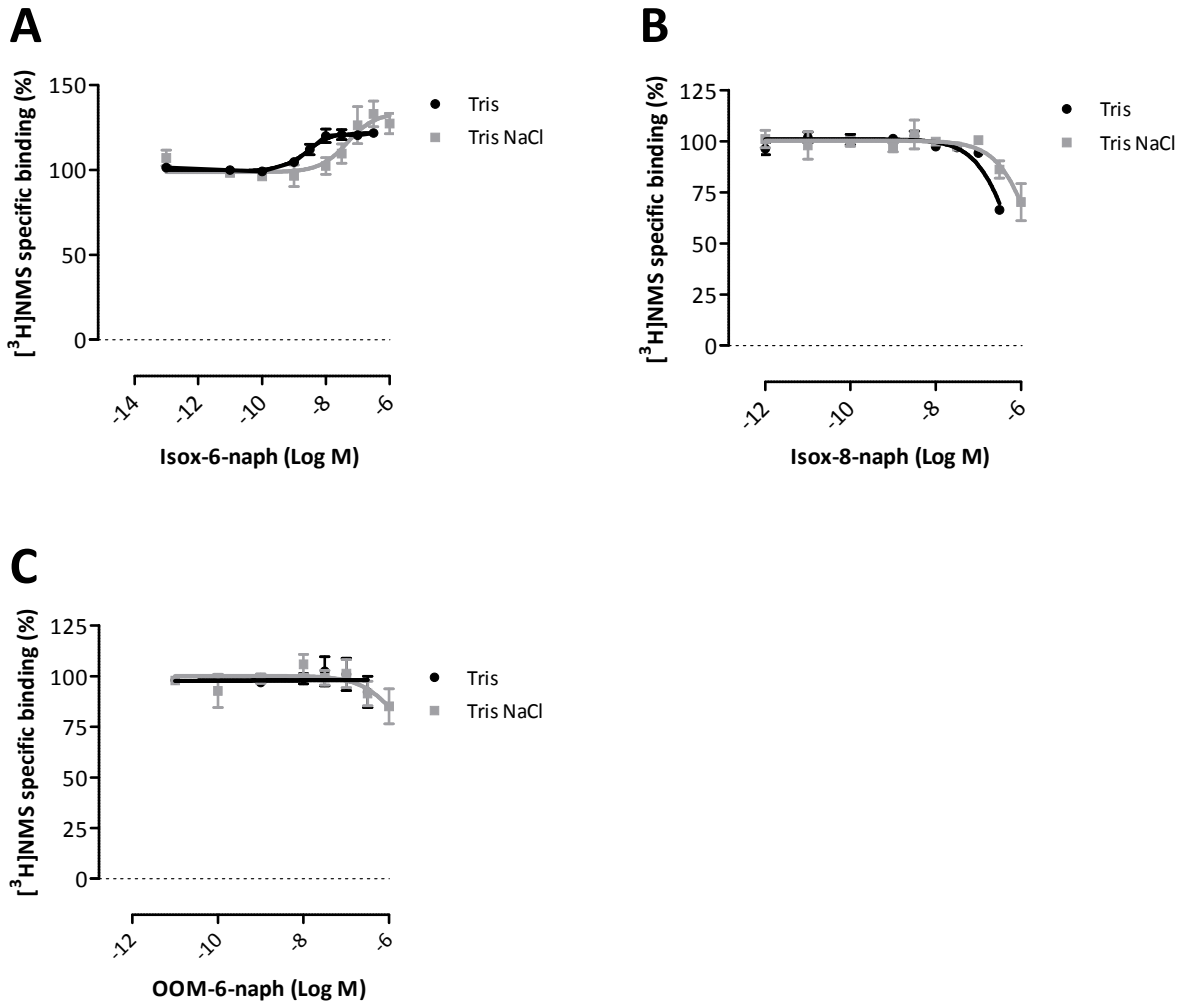

Figure 3.35: [^{3}H]NMS equilibrium binding assays with membrane suspensions of CHO-hM_2 cells. Ordinate: [^{3}H]NMS binding expressed as percentage of [^{3}H]NMS binding in absence of compound. Abscissa: logarithm of the concentration of test compounds. The experiments were carried out in Tris or Tris NaCl buffer supplemented with 100 µM GDP and incubated for 18 hours at 24°C. Data points: mean ± SEM of 3-6 assays performed in triplicate. Curve fitting: "Four-parameter logistic equation" (Eq. 8).

The data obtained from these experiments are summarized in table 3.22.

Compound	*Buffer*	*pK_A*	*Hill slope*	*Bottom plateau (%)*	*Top plateau (%)*	*n*
Isox-6-naph	Tris	8.47 ± 0.10	-1 (-1.63 ± 0.62)	100 ± 1	121 ± 3	4
	Tris NaCl	7.95 ± 0.16*	-2.30 ± 1.90	99 ± 3	138 ± 5*	5
Isox-8-naph	Tris	7.91 ± 0.01	n. d.	n. d.	100 ± 1	4
	Tris NaCl	7.71 ± 0.02***	n. d.	n. d.	100 ± 2	3
OOM-6-naph	Tris	n. d.	n. d.	n. d.	n. d.	6
	Tris NaCl	n. d.	n. d.	n. d.	100 ± 2	4

Table 3.22: Parameter values derived from Figure 3.35. pK_A: negative common logarithm of the affinity values of the test compounds; n_H: Hill slope; if it did not significantly differ from unity, a value of -1 was assumed and the exact value reported in brackets. *, **, ***: ($p<0.05$, 0.01, 0.001), significantly different from the value reported in Tris buffer according to a two-tailed t-test. The table shows mean values ± SEM of 3-6 independent experiments performed in triplicate.

As shown in Fig. 3.35, isox-6-naph enhances radioligand binding both in Tris and Tris NaCl buffer, displaying a significantly higher affinity in Tris, but a greater top plateau in Tris NaCl. Concerning the ligand isox-8-naph, it appears that this compound decreases [^{3}H]NMS binding, even though it is not able to reach a full displacement in the applicable range of concentrations. OOM-6-naph showed neutral cooperativity with the radioligand in Tris buffer and slightly negative cooperativity in Tris NaCl buffer.

3.8 Determination of the level of spontaneous activity of the single mutant $M_2^{422W\rightarrow A}$ receptor in different buffers

The single mutant $M_2^{422W\rightarrow A}$ was described in previous work (Prilla et al., 2006) as an allosteric loss-of-affinity mutant (see 1.5.1). Since the influence of the allosteric binding site on the efficacy of the test ligands was one of the principal interests in this study, this mutant receptor was tested in functional studies. First, the level of spontaneous activity was investigated in Tris and Tris NaCl buffer, with the aim of understanding whether these two buffers were able to assure a reliable spontaneously active and inactive receptor system, respectively. The results of these experiments are shown in Fig. 3.36.

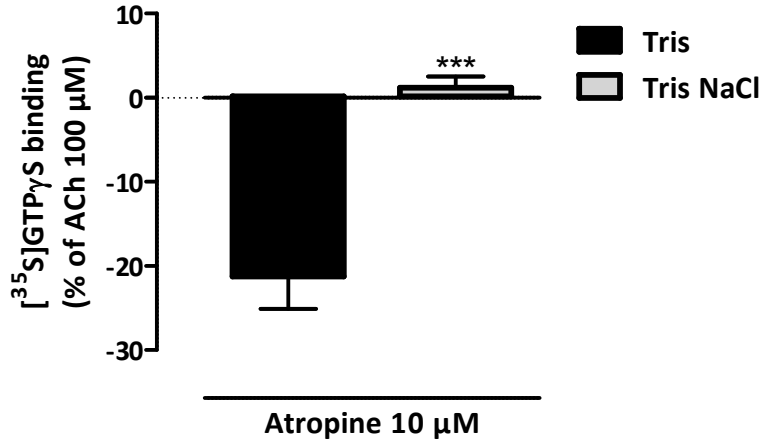

Figure 3.36: [^{35}S]GTPγS binding measured in the presence of 10 µM atropine in experiments performed either in Tris or Tris NaCl buffer. Ordinate: percentage of [^{35}S]GTPγS binding, normalized on maximum effect elicited by 100 µM ACh (set to 100%). 0% corresponds to basal [^{35}S]GTPγS binding. The bar diagram shows mean ± SEM of 5-7 experiments performed in triplicate. ***: p<0.001, significantly different from the value reported in Tris buffer according to a two-tailed t-test.

The statistical parameters derived from these experiments are listed in table 3.23.

Buffer	*E_{max} (%)*	*n*
Tris	-21 ± 4	7
Tris NaCl	1 ± 1***	5

Table 3.23: Parameter values derived from Figure 3.35; E_{max}: maximum level of [^{35}S]GTPγS binding in percent normalized on 100 µM ACh which was set to 100%; n: number of performed experiments. The table shows mean values ± SEM of 5-7 independent experiments carried out in triplicate. ***: p<0.001, significantly different from the value reported in Tris buffer according to a two-tailed t-test.

In Tris buffer the mutant receptor maintains its spontaneous activity, even though at a lower level compared to the wild type M_2. When the buffer containing 200 mM NaCl was used, the spontaneous activity was abolished and the receptor resulted inactivated.

3.9 Influence of NaCl and spontaneous activity on orthosteric signaling at $M_2^{422W\rightarrow A}$

[^{35}S]GTPγS experiments were performed at the mutant receptor applying increasing concentrations of the endogenous agonist ACh, the superagonist iperoxo and the two full agonists

isox and OOM. The aim of these experiments was to analyze the differences with the functional data reported at the wild type M_2. As shown in Fig. 3.37, the potency of ACh and iperoxo is decreased when tested in the inactive (Tris NaCl) compared to the active system (Tris). Additionaly, iperoxo tends to have an efficacy that surpasses that of ACh in both buffers, even though not significantly. The full agonists isox and OOM did not show significant differences in potency when they were tested in the quiescent or the spontaneously active system. Unexpectedly, the efficacy of isox resulted significantly decreased in Tris NaCl compared to Tris buffer.

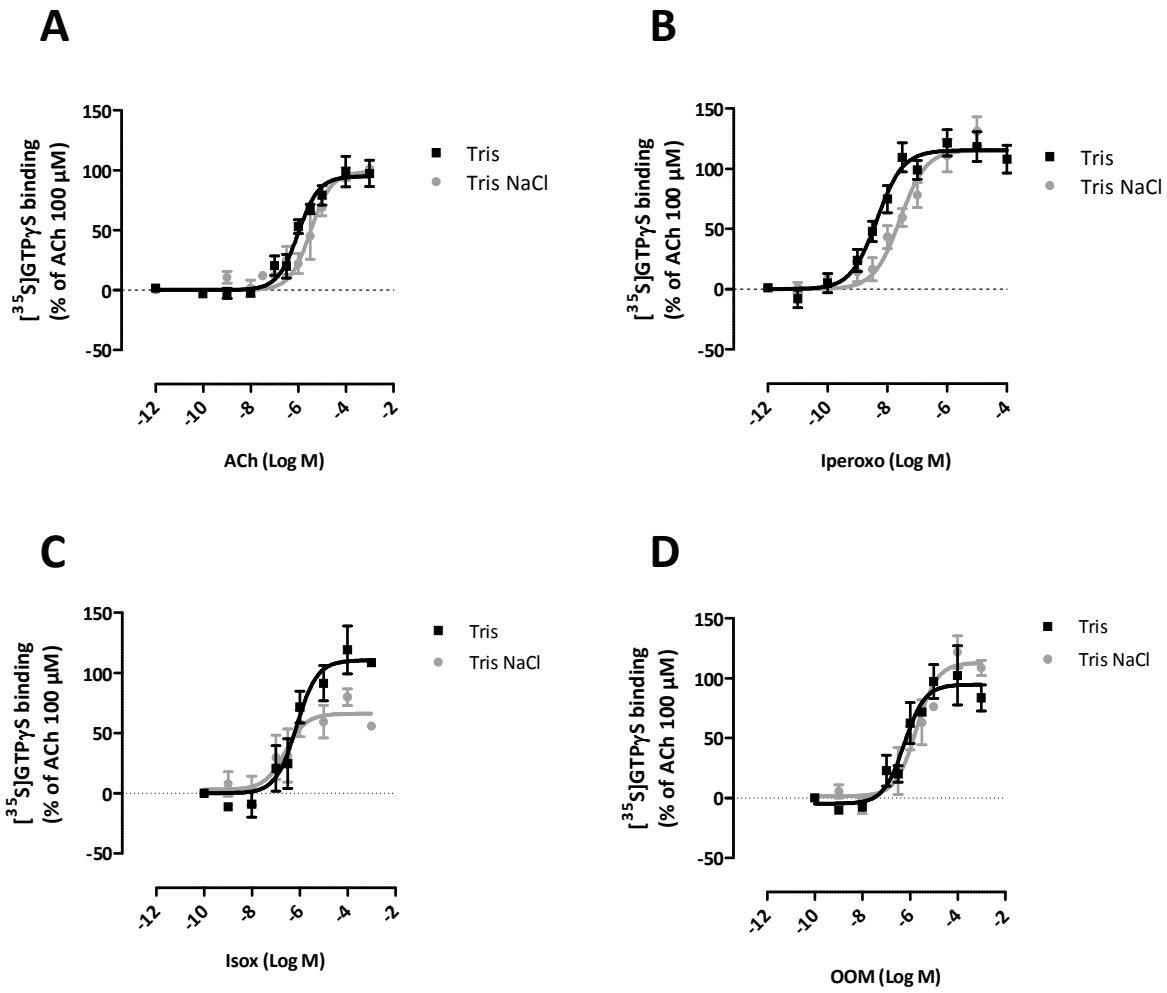

Figure 3.37: Test compound-induced [^{35}S]GTPγS binding to membrane suspensions from FlpIn CHO-$M_2^{422W\rightarrow A}$ cells in the indicated buffers. Ordinate: percentage of [^{35}S]GTPγS binding, normalized on the maximum effect of 100 µM ACh which was set to 100%. 0% corresponds to the lower plateau (basal [^{35}S]GTPγS binding). Abscissa: logarithm of the concentrations of the compounds. The assay was performed with an incubation time of 60 minutes at 24°C. The graph shows the mean values ± SEM of 3-5 experiments performed in triplicate. Curve fitting: "Four-parameter logistic equation" (Eq. 8).

The statistical parameters derived from these experiments are listed in table 3.24.

Compound	*Buffer*	*pEC_{50}*	*E_{max} (%)*	*n*
ACh	Tris	5.95 ± 0.06	100 ± 1	3
	Tris NaCl	5.29 ± 0.18*	100 ± 2	3
Iperoxo	Tris	8.29 ± 0.10	121 ± 9	5
	Tris NaCl	7.53 ± 0.20**	114 ± 10	5
Isox	Tris	6.23 ± 0.42	116 ± 13	3
	Tris NaCl	6.62 ± 0.51	68 ± 3$^{*/aa}$	3
OOM	Tris	6.19 ± 0.10	96 ± 11	3
	Tris NaCl	5.82 ± 0.36	116 ± 11	3

Table 3.24: Parameter values derived from Figure 3.37; pEC_{50}: negative common logarithm of the concentration of test compound causing a half maximum effect; E_{max}: maximum level of [^{35}S]GTPγS binding in percent normalized on 100 µM ACh which was set to 100%; n: number of performed experiments. The table shows mean values ± SEM of 3-5 independent experiments carried out in triplicate with FlpIn CHO-$M_2^{422W\rightarrow A}$ cells. *,**,***: ($p<0.05$, 0.01, 0.001), significantly different from the value reported in Tris buffer. ^{a},^{aa},^{aaa}: ($p<0.05$, 0.01, 0.001), significantly different from the value reported for ACh.

3.10 Influence of NaCl and spontaneous activity on dualsteric signaling at $M_2^{422W\rightarrow A}$

G_i-signaling induced by the dualsteric ligands at the single mutant $M_2^{422W\rightarrow A}$ was investigated in Tris and Tris NaCl buffer to better elucidate the influence of a functional allosteric vestibule for protean agonism at M_2. As shown in Fig. 3.38, all the tested compounds were partial agonists at the mutant receptor, including isox-6-naph, iper-0-naph and OOM-6-naph, which were protean agonists at the wild type M_2AChR.

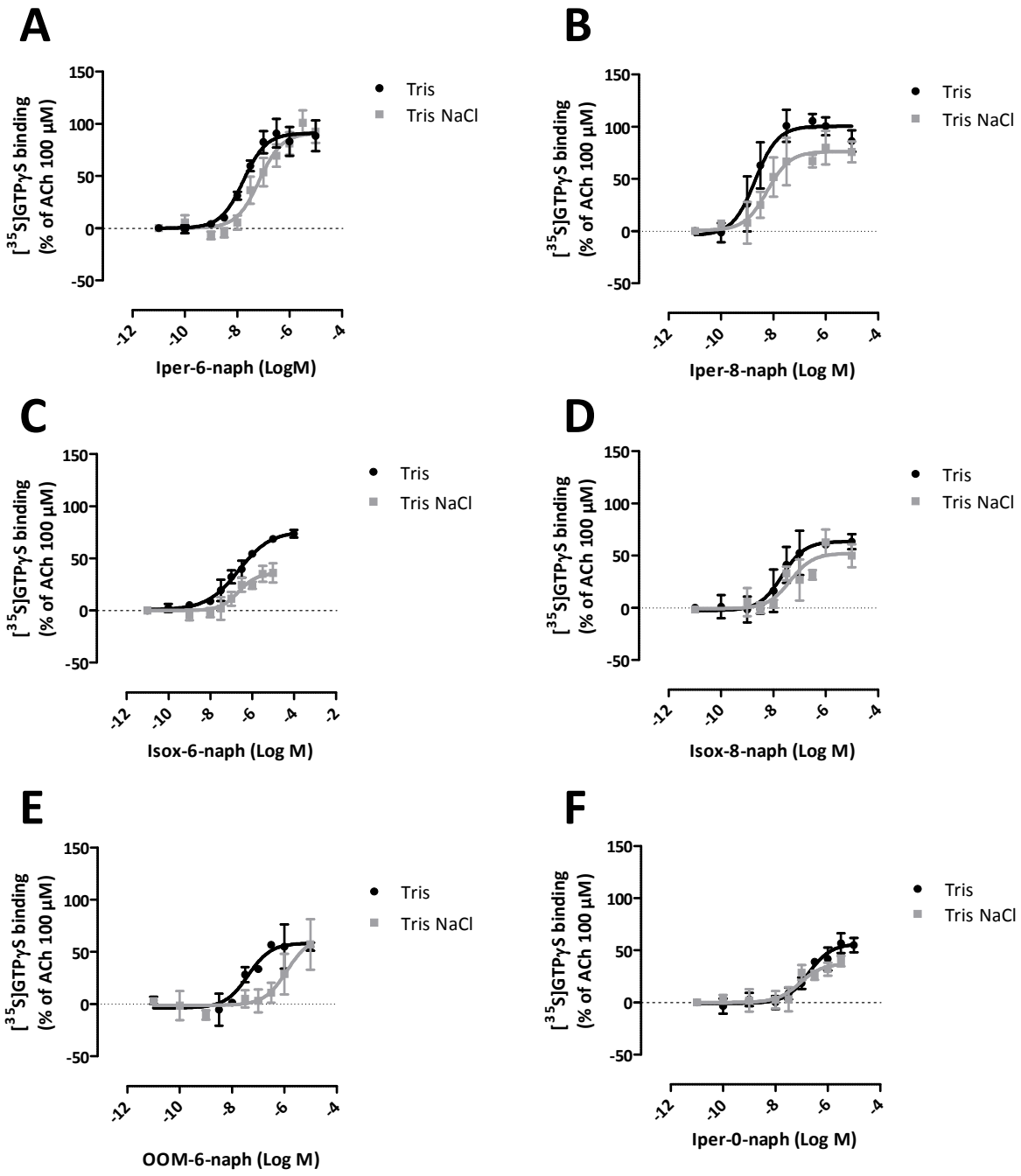

Figure 3.38: Test compound-induced [^{35}S]GTPγS binding to membrane suspensions from FlpIn CHO-$M_2^{422W\rightarrow A}$ cells in the indicated buffers. Ordinate: percentage of [^{35}S]GTPγS binding, normalized on the maximum effect of 100 µM ACh which was set to 100%. 0% corresponds to the lower plateau (basal [^{35}S]GTPγS binding). Abscissa: logarithm of the concentrations of the compounds. The assay was performed with an incubation time of 60 minutes at 24°C. The graph shows the mean values ± SEM of 3-6 experiments performed in triplicate. Curve fitting: "Four-parameter logistic equation" (Eq. 8).

The parameter values derived from these experiments are summarized in table 3.25.

Compound	*Buffer*	*pEC_{50}*	*E_{max} (%)*	*n*
Iper-6-naph	Tris	7.79 ± 0.08	94 ± 15	6
	Tris NaCl	7.16 ± 0.21*	97 ± 9	6
Iper-8-naph	Tris	8.65 ± 0.31	104 ± 3	4
	Tris NaCl	8.26 ± 0.42	82 ± 8*	4
Isox-6-naph	Tris	6.82 ± 0.27	68 ± 2	3
	Tris NaCl	6.84 ± 0.26	36 ± 6**	4
Isox-8-naph	Tris	7.52 ± 0.47	71 ± 4	3
	Tris NaCl	7.09 ± 0.38	55 ± 10	4
OOM-6-naph	Tris	7.28 ± 0.11	62 ± 9	3
	Tris NaCl	n.d.	n.d.	4
Iper-0-naph	Tris	6.73 ± 0.10	57 ± 7	3
	Tris NaCl	7.31 ± 0.53	37 ± 7	3

Table 3.25: Parameter values derived from Figure 3.38; pEC_{50}: negative common logarithm of the concentration of test compound causing a half maximum effect; E_{max}: maximum level of [^{35}S]GTPγS binding in percent normalized on 100 µM ACh which was set to 100%; n: number of performed experiments. The table shows mean values ± SEM of 3-6 independent experiments carried out in triplicate with FlpIn CHO-$M_2^{422W\rightarrow A}$ cells. *,**,***: ($p<0.05$, 0.01, 0.001), significantly different from the value reported in Tris buffer; n.d.: not determined.

In conclusion, these data show that the single mutation of a residue involved in allosteric modulator's binding causes a dramatic change in signaling of the dualsteric protean ligands, confirming the importance of a functional allosteric site in evoking protean agonism.

4 DISCUSSION

4.1 The spontaneous activity of the M_2 receptor can be fine-tuned by buffer osmolarity

Protean ligands induce opposing effects (E_{max}) depending on the level of spontaneous activity of a G protein-coupled receptor. This phenomenon was first reported in 1995 (Kenakin, 1995a) and is based on the assumption that ligand–bound GPCRs may adopt not only one (fully) active and one inactive conformation, but also intermediate conformations engendering intermediate intrinsic efficacies for activation of intracellular signaling pathways. In this regard, receptor species with a lower efficacy than the spontaneously active one yield *positive* signaling in the presence of quiescent receptors and *negative* signaling when the majority of receptors is constitutively active (Kenakin, 1997, 2001; Chidiac, 2002).

Experimentally, the discovery of protean ligands remains challenging for two reasons, i.e. the lack of (i) stable and reliable spontaneously active systems for several GPCRs and (ii) strategies for the rational design of this class of agonists. Furthermore, studies which identified protean agonists by comparison of agonist-induced signaling in two different functional assay systems may be compromised by biased signaling (Jansson et al., 1998; Gbahou et al., 2003). Therefore, two experimental systems which differ only in the amount of spontaneous activity are essential for the identification of protean agonists. To this end, several strategies have been employed to study agonism in the presence and absence of spontaneously active receptors. For instance, constitutively activating receptor mutations (Ganguli et al., 1998; Fathy et al., 1999; Pauwels et al., 2002), an increased expression of receptor/G protein (Jakubík et al., 1998), or a change in buffer composition (Newman-Tancredi et al., 2003), have been applied.

Here, we choose to alter M_2 wild type receptor activity by a variation of the buffer ingredients. At first, sodium ions, which previous studies demonstrated responsible for keeping class A GPCRs in an inactive conformation (Liu et al., 2012; Katritch et al., 2014), were either substituted with potassium ions or removed in HEPES buffer (see 3.1.1 and 3.1.2). Since none of these tested conditions led to a spontaneously active receptor system, a Tris buffer with varying concentrations of GDP was tested at different incubation times and temperatures and at variable membrane

protein and BSA concentrations. At the end of this part of the study, we recognized that [^{35}S]GTPγS experiments performed in Tris buffer with 1 µM GDP, 40 µg/ml membrane proteins and 0.5% BSA incubated for 60 minutes at 24°C assured a stable level of spontaneous activity (see 3.1.2). Since a quiescent AChM$_2$R system was another requirement for investigating protean agonism, high concentrations of NaCl were applied and found to abolish spontaneous activity of the receptor, as expected. Accordingly, a high concentration of NaBr also diminished constitutive activity. Surprisingly, also high concentrations of KCl and NMDGCl were able to reduce spontaneous receptor activity, even though both of them do not contain Na^+. Thus, the obtained results indicate that inactivation of the M$_2$AChR by a high concentration of sodium ions depends on high buffer osmolarity rather than on the salt composition.

4.2 Dualsteric compounds with specific molecular features act as protean agonists at M$_2$

In the previous chapter, it was shown that spontaneous activity of the muscarinic M$_2$ receptor can reliably be titrated by changing the osmolarity of the buffer in CHO-M$_2$ [^{35}S]GTPγS binding assays.
To test whether dualsteric ligands could promote protean agonism at this receptor, a set of 14 hybrid compounds, combining three orthosteric moieties and five allosteric fragments connected via different linker length spacers, were chosen for testing in spontaneously active and quiescent M$_2$ receptor systems. Three dualsteric ligands, namely iper-0-naph, isox-6-naph, and OOM-6-naph (see 2.7.5), were found to be protean agonists, since they acted as inverse agonists in the presence of spontaneous activity (Tris buffer) and as partial agonists at the quiescent receptor (Tris NaCl buffer).

4.2.1 Reasons for exclusion of iper-0-naph from structure-activity relationship analysis of M$_2$ dualsteric protean agonists

In order to understand the structure-activity relationships that make a dualsteric compound a protean agonist, the common molecular features of the protean ligands were analyzed. At first, we decided to exclude iper-0-naph from this analysis, because this compound presents no linker, and it is thus too short to bind simultaneously to the allosteric and orthosteric sites of the receptor, that according to crystallographic studies are at about 15 Å of distance (Dror et al.,

2013). Most likely, iper-0-naph binds either to the orthosteric site or to the allosteric site, one at a time, but cannot adopt the two binding poses that are required for assuring dynamic ligand binding, which we hypothesized as the possible mechanism eliciting dualsteric protean agonism (see 1.7). The compounds comprising a hexamethylene linker of about 9 Å, such as isox-6-naph and OOM-6-naph, on the other hand, are able to engage both sites on the receptor, as recently confirmed by molecular docking simulations with C6-linker ligands (Bock et al., 2016). The molecular structures that are shared by both OOM-6-naph and isox-6-naph are a linker of six carbons atoms and a naphmethonium-derived allosteric moiety (Fig. 4.1).

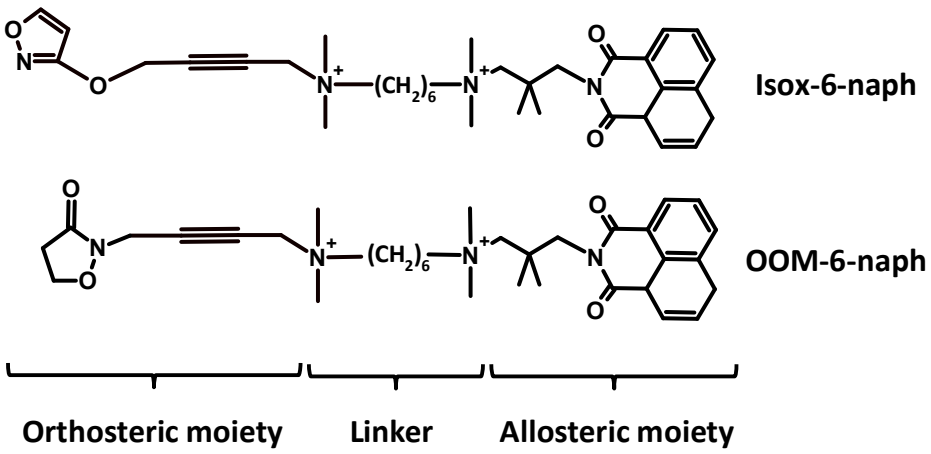

Figure 4.1: Comparison of the chemical structures of the two protean agonists isox-6-naph and OOM-6-naph.

4.2.2 Relevance of the orthosteric moiety's affinity and efficacy for protean agonism

The two protean agonists OOM-6-naph and isox-6-naph differ from the partial agonist iper-6-naph only for their orthosteric moiety. Interestingly, when we compare the partial agonist iper-6-naph with the protean agonist isox-6-naph, it is notable that the removal of only a double bond in the heterocycle causes a switch from partial to protean activity (Fig. 4.2).

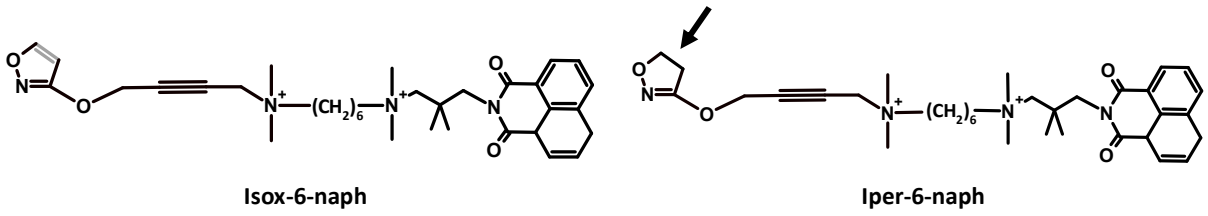

Figure 4.2: Comparison of the chemical structures of the partial agonist iper-6-naph and the protean agonist isox-6-naph.

Since we were interested in the molecular explanation for this result, pharmacological characterization of the three orthosteric fragments iperoxo, isox and OOM was performed in Tris and Tris NaCl buffer. All the orthosteric ligands were full agonists in both buffers (see 3.2.1), with a maximum effect that did not significantly differ from the one measured with the endogenous agonist ACh. Notably, iperoxo, which is classified as an M_2 superagonist (Schrage et al., 2013), had a potency (pEC_{50}) that was up to 390-times higher in Tris and up to 19-times higher in Tris NaCl in comparison to the pEC_{50} values of isox and OOM. Additionally, in equilibrium binding studies, the superagonist had an affinity up to 180-times higher in Tris and 120-times higher in Tris NaCl when compared to isox and OOM (Fig. 4.3).

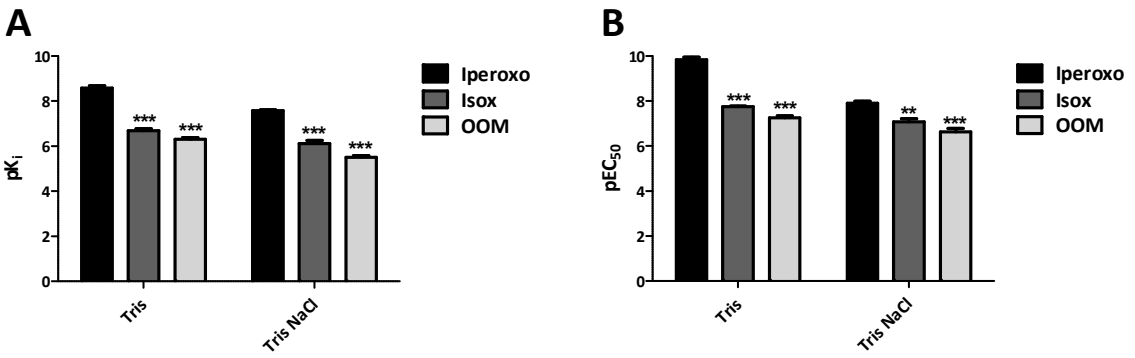

Figure 4.3: Comparison of pK_i and pEC_{50} of the test compounds in Tris and Tris NaCl. pK_i: negative common logarithm of the dissociation binding constant of the test compounds; pEC_{50}: potency of the compounds in [^{35}S]GTPγS assays. The bar diagrams show mean value + SEM of 3-7 independent experiments carried out in triplicate. **,***: ($p<0.01$, 0.001), significantly different from the value reported for iperoxo according to one-way ANOVA with Bonferroni post-test.

Taken together, the affinity and potency of the orthosteric moiety of the dualsteric compounds are determinant in eliciting protean agonism. Specifically, these data suggest that a dualsteric protean agonist should comprise an orthosteric fragment with full agonist, but not superagonist, activity at the AChM$_2$R.

4.2.3 Relevance of the allosteric moiety's steric hindrance for protean agonism

Dualsteric ligands evaluated in this thesis are composed of three main blocks, i.e. an orthosteric moiety with agonistic properties, an allosteric fragment able to inactivate the receptor (Fig. 3.21), and a linker of different length. Once we established the characteristics required to the orthosteric moiety for engineering dualsteric protean agonists, we wanted to determine the structural

elements required by the allosteric fragment for being embedded in a dualsteric protean ligand. OOM-6-naph and isox-6-naph share the same allosteric fragment, which is derived from the allosteric modulator naphmethonium. Interestingly, the corresponding dualsteric compounds formed by a W84-derived allosteric moiety (OOM-6-phth and isox-6-phth), although stimulating a comparable amount of [^{35}S]GTPyS binding in Tris NaCl, did not act as inverse agonists in the spontaneously active system (Fig. 4.4), thus they do not behave as protean ligands.

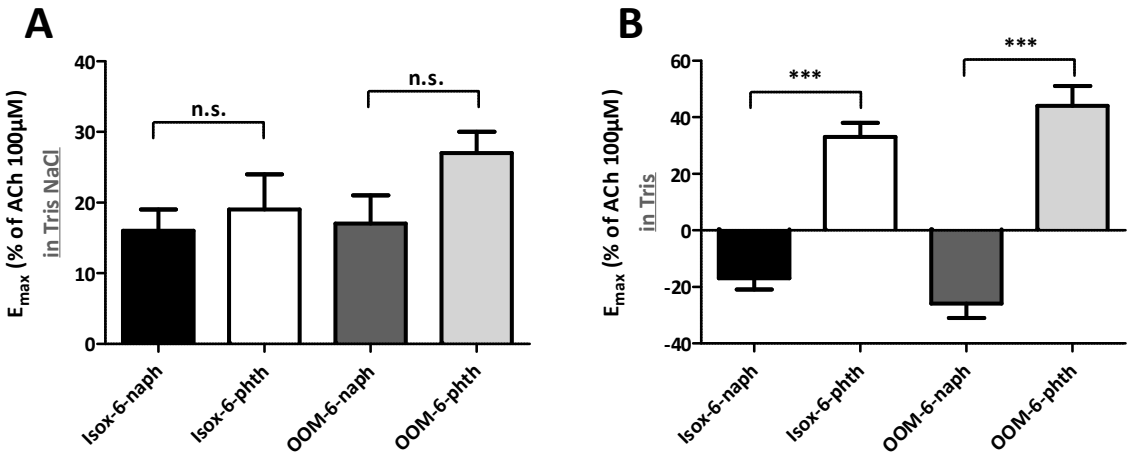

Figure 4.4: Comparison between the E_{max} of the protean agonists isox-6-naph and OOM-6-naph with the dualsteric ligands embedding a less voluminous allosteric moiety, i.e. isox-6-phth and OOM-6-phth, in Tris and Tris NaCl. The bar diagrams show means ± SEM of 4-7 independent experiments performed in triplicate. n.s.: not significant. ***: ($p<0.001$), significantly different according to one-way ANOVA with Bonferroni's post-test.

This result indicates that a bulky residue, i.e. the sterically demanding 1,8-naphthalimide moiety, is superior to the less voluminous phthalimide analog in stimulating protean agonism of the derivative compounds. Unfortunately, even though it would be interesting to make considerations also regarding the affinity of the allosteric fragments in the two buffer systems, this is not feasible, due to the contradictory results obtained with the allosteric modulator 6-naph in equilibrium binding studies (see 3.5.3). Indeed, the allosteric modulator 6-naph, as well as 8-naph, either increased or decreased [^{3}H]NMS binding in the same assay system, hampering an univocal conclusion regarding cooperativity and affinity of these modulators. Accordingly, previous work also reported conflicting results regarding 6-naph, which was described either as positive cooperative with [^{3}H]NMS (Bock et al., 2014) or negative cooperative with the same radioligand (Vogel, Dissertation, 2015).

4.2.4 Importance of a hexamethylene linker for engineering protean agonism at M_2

The linker between orthosteric and allosteric moiety of muscarinic dualsteric ligands was the last variable analyzed in order to clarify the structure-activity relationships that allow a dualsteric ligand to be a protean agonist. The importance of linker length in eliciting a peculiar signaling profile was already demonstrated by a paper from Bock et al. (2012), where it was shown that compounds presenting a hexamethylene linker were able to stimulate G_i-biased signaling at the M_2 receptor, while one ligand with an octamethylene linker did not show any bias. As expected, different linker lengths led to different signaling profiles within the set of dualsteric ligands examined. Only a C6 chain, of about 9 Å, resulted in compounds eliciting protean agonism, while a slightly shorter linker (C4,~6.5 Å) and a longer one (C8,~11.5 Å) resulted in ligands that were only partial agonists in both buffers (see 3.6.2 and 3.6.3). One explanation for this result may be that dualsteric compounds with a C6 linker lead to stronger restriction in the flexibility of the allosteric binding site of the receptor protein than a C8 linker chain (Bock et al., 2012). Moreover, it has been shown that the purely allosteric binding pose of C8 ligands is less stable than that of the C6 ligands (Bock et al., 2016). Regarding the C4 linkers, molecular docking studies would be needed to confirm whether they are able to bind simultaneously to the two binding sites or whether their linker is too short to adopt a dualsteric pose.

In conclusion, only slight alterations of the three chemical moieties were sufficient to shift the profile of two dualsteric compounds from protean agonism to “classical” partial agonism. The molecular features required for protean agonism at the muscarinic M_2 receptor were elucidated and they are: an orthosteric moiety endowed with an acetylcholine-like efficacy, a bulky allosteric moiety to impair the flexibility of the extracellular loop area, and a flexible linker chain of 6 carbon atoms (Fig. 4.1).

4.3 Dualsteric ligands uncover a new molecular mechanism eliciting protean agonism

Up until now, protean agonism was thought to reside in the intrinsic efficacy of a ligand (Kenakin, 1997). Our results point to an additional mechanism that may underlie this phenomenon at GPCRs

in case a ligand can simultaneously occupy both the binding site for the endogenous messenger and an allosteric binding site of the receptor protein. These dualsteric compounds may bind to a receptor protein in two distinct binding modes (Bock et al., 2014; Bock et al., 2016): a purely allosteric and a dualsteric mode (Fig. 1.4) and may thus have two distinct efficacies for receptor activation. The findings presented here go in line with the idea that the two protean agonists isox-6-naph and OOM-6-naph prefer binding in the purely allosteric binding pose, as has already been demonstrated for isox-6-naph in a previous study (Bock et al., 2014). Both compounds display functional inverse agonism under conditions in which the M_2 receptor displays a substantial amount of spontaneous activity (Fig. 3.28 and 3.30). However, at least under conditions in which the receptor does not display any spontaneous activity, a significant fraction of receptors must be bound in a dualsteric binding pose, as we observed functional agonism in the quiescent M_2 system. This indicates dynamic ligand binding as the molecular mechanism of protean agonism of isox-6-naph and OOM-6-naph. At this point, the question was whether the compounds swapped their binding poses in the different buffers. To better clarify this issue, radioligand binding experiments were performed and the allosteric binding affinity of several dualsteric ligands was investigated. The allosteric affinity of isox-6-naph was 20-times higher in Tris than in Tris NaCl buffer, whereas the orthosteric building block isox gained only 3.5-fold in affinity under these conditions (Fig. 3.32 and 3.19). We assume that the affinities of the allosteric and of the orthosteric moiety determine the fraction of ligand bound in one or the other pose, according to the model published by Bock et al. (2014). Based on this model, the dualsteric ligand distributes over the receptor population with the fraction of the respective subpopulation determined by the affinity ratio between the active signaling-competent (dualsteric) and the inactive (allosteric) pose. Thus, this result supports the idea that isox-6-naph increases in allosteric binding pose in the low osmolarity buffer. Yet, OOM-6-naph displayed only a slight increase in allosteric binding affinity in Tris *vs.* Tris NaCl buffer (Fig. 3.32). This effect was comparable to the increase in orthosteric affinity of the orthosteric building block OOM (Fig. 3.19). Even if these data indicate that OOM-6-naph does not display increased allosteric binding in Tris buffer, the dominant binding pose under these conditions is the allosteric one, as indicated by the inverse agonism seen at the spontaneously active M_2AChR (Fig. 3.30).

One might argue that protean agonism of isox-6-naph and OOM-6-naph resides in the rather low efficacy of the two ligands and is not necessarily due to dynamic ligand binding. However,

dualsteric ligands such as isox-6-phth and OOM-6-phth did not display any protean agonism although the efficacy of these compounds did not differ significantly from the efficacy of the two protean agonists at the quiescent M_2AChR (Fig. 4.4). In sum, these data indicate that dynamic ligand binding (Bock et al., 2014) is the underlying molecular mechanism for protean agonism of isox-6-naph and OOM-6-naph at M_2AChR.

Of note, we also observed an increase in allosteric binding for iper-6-naph, iper-8-naph, ALB3 and ALB4 to the M_2 receptor in Tris compared to Tris NaCl (Fig. 3.32) although these four compounds clearly did not display any protean agonism. For iper-6-naph and iper-8-naph this might be explained by the higher intrinsic efficacy for receptor activation of the orthosteric moiety iper in comparison to isox and OOM. In consequence, the beneficial effect of the spontaneously active M_2 receptor on the orthosteric superagonist iperoxo (increase in binding affinity 10-fold in Tris *vs.* Tris NaCl) surpassed the increase in allosteric binding (increase in allosteric binding affinity 3.5-fold and 7-fold for iper-6-naph and iper-8-naph, respectively) and this precluded protean agonism. Regarding ALB3 and ALB4, even though the increase in allosteric binding in Tris was 12-times and 8-times, respectively, their allosteric affinity was presumably too low to adopt a prevailing purely allosteric pose. Indeed, ALB3 and ALB4 are composed of an allosteric moiety that presents an additional ring in its chemical structure that impairs the allosteric affinity (Fig. 3.24), as already reported in previous work (De Min, Master Thesis, 2012).

4.3.1 Equilibrium binding experiments further strengthen the proposed mechanism for dualsteric protean agonism

Equilibrium binding studies performed in Tris and Tris NaCl buffer further confirmed that the prevailing binding pose of the protean agonists isox-6-naph and OOM-6-naph is the pure allosteric pose. Indeed, these two ligands showed either positive or neutral cooperativity with [^{3}H]NMS, that is indicative of allosteric binding (Fig. 3.35). Regarding isox-6-naph, the compound increases radioligand binding both in Tris and Tris NaCl buffer; this result suggests that the allosteric binding pose is preferred in both buffers. On the other hand, OOM-6-naph was neutrally cooperative with the radioligand in Tris buffer and slightly negative cooperative in Tris NaCl buffer. Thus, the data steer to an increase in dualsteric binding of the OOM-derived hybrid in the high osmolarity buffer, i.e. under conditions similar to those applied in the functional assays where partial agonism is reported for this compound.

One might claim that a model estimating the fraction of compound bound in one or the other pose was recently published for dualsteric hybrids binding the M_2 receptor (Bock et al., 2014) and could be the final corroboration of our hypothesized mechanism. Unfortunately, the model could not be applied here, since it does not account for the inverse agonism induced by the ligands in Tris buffer. Thus, a more extended mathematical model would be required to fit the data presented in this thesis.

4.4 A functional allosteric site is critical for stimulating protean agonism at M_2

The functional and binding data collected for the dualsteric hybrids at the wild type M_2 receptor pointed to *dynamic ligand binding* as the underlying mechanism for protean agonism. Thus, the adoption of a purely allosteric binding pose is of fundamental importance for this hypothesized mechanism. The next question was whether a mutation in this binding site would abolish protean agonism of isox-6-naph and OOM-6-naph. We chose to mutate the residue W422 to alanine, since this tryptophan is known to be part of a series of amino acids lining the core region of the allosteric site and to be critical for allosteric ligand binding (Prilla et al., 2006; Haga et al., 2012). Since the spontaneous activity reported at the wild type M_2 was present also at the mutant receptor when assayed in Tris buffer, and abolished in the presence of 200 mM NaCl (Fig. 3.36), we were convinced that the conditions necessary for identifying protean agonists were present also at the mutant receptor. Furthermore, the tested orthosteric agonists were still able to induce a positive response (Fig. 3.37), a result that is indicative of a functional orthosteric site. Thus, a group of dualsteric ligands was investigated in Tris and Tris NaCl buffers for G_i-signaling stimulation at the $M_2^{422W\rightarrow A}$ and it was found that the protean activity of isox-6-naph and OOM-6-naph was absent at this allosteric loss-of-affinity mutant. Moreover, all compounds had an increased E_{max} in Tris and/or Tris NaCl buffer in comparison to the E_{max} reported at the wild type M_2 receptor (Fig. 4.5).

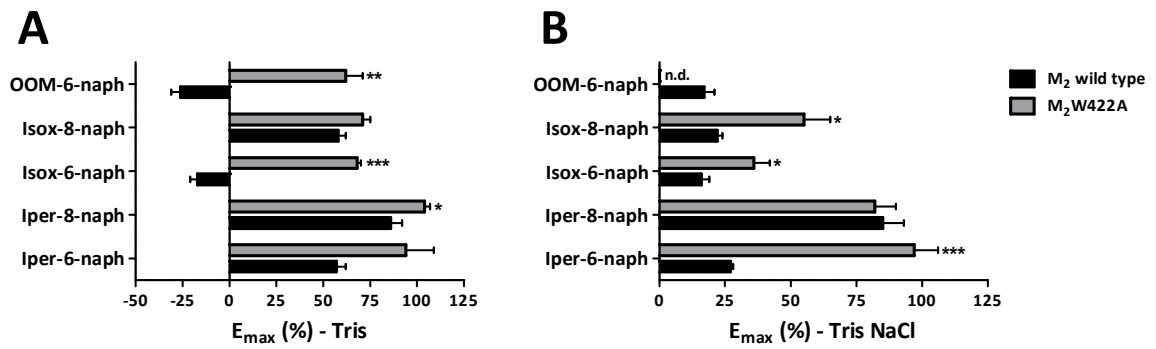

Figure 4.5: Comparison between the E_{max} of dualsteric ligands at the wild type M_2 and the mutant $M_2^{422W\rightarrow A}$ in Tris and Tris NaCl. n.d.: not determined. The bar diagrams show means ± SEM of 3-6 independent experiments performed in triplicate. *,**,***: ($p<0.05$, 0.01, 0.001), significantly different from the value reported at the wild type receptor according to a two-tailed t-test.

This is consistent with previous findings by Bock et al. (2012), who found an increased efficacy of the dualsteric ligands tested in the study when investigated at the mutant $M_2^{422W\rightarrow A}$ in comparison to the wild type receptor. This result might be explained considering that the allosteric loss-of-affinity mutant is expected to have an impaired allosteric site. As a consequence, the (antagonistic) allosteric moieties embedded in the dualsteric ligands may be unable to properly bind to this site, resulting in both decreased antagonistic effects (and thus an increased E_{max} of the dualsteric compounds) and a reduction in pure allosteric binding pose of the tested ligands.
Taken together, a fully functional allosteric binding site is of major importance for inducing dualsteric protean agonism, as allosteric binding of the antagonistic moieties of the ligands is necessary for guarantying a prevailing purely allosteric pose of the dualsteric protean agonists.

4.5 The level of spontaneous activity influences the apparent efficacy of both orthosteric and dualsteric agonists

One of the main findings of this thesis is that the spontaneous activity of the M_2 receptor can be titrated by buffer osmolarity and that this enables the recognition of protean agonists at this receptor subtype, and virtually at other GPCRs. Interestingly, a receptor system with a sustained level of constitutive activity and another with low levels of spontaneous activity also allowed us to determine whether there were differences in apparent efficacy not only of the two identified protean agonists, but also of the full and partial agonists tested.

In the low osmolarity Tris buffer (*Tris*), both basal and also agonist-induced [^{35}S]GTPγS binding were increased in CHO-M_2 membranes in comparison with a buffer system with high concentrations of sodium (*Tris NaCl*) or potassium ions (*Tris KCl*) (Fig. 3.13). This is in line with previous findings (Tian et al., 1994) for the adrenergic α_2-AR and reflects a stronger stimulus-response-coupling and ternary complex formation of agonist, receptor and G protein of the spontaneously active M_2 receptor compared to quiescent M_2.

Accordingly, almost all dualsteric compounds which did not display protean agonism showed increased E_{max} values and all orthosteric agonists gained binding affinity and potency in Tris compared to Tris NaCl buffer, indicating that agonists prefer binding to an active rather than an inactive receptor, as already confirmed in previous work (De Lean et al., 1980). The classical muscarinic partial agonist pilocarpine was an exception to this behavior as the compound changed neither in potency nor in efficacy depending on the buffer composition. Correspondingly, a previous report (Tota and Schimerlik, 1990) described that pilocarpine does not distinguish between active and inactive receptors.

Taken together, the two M_2 receptor systems, i.e. a constitutively active and an inactive system, conveyed a means to identify the different apparent efficacies of muscarinic ligands upon binding at a spontaneous or quiescent receptor. The data indicated that (i) orthosteric full agonists prefer to bind to spontaneously active receptors, as demonstrated by the increase in potency/affinity of these ligands and that (ii) for dualsteric ligands their binding preference is structure-dependent.

5 SUMMARY

Protean agonists are of great pharmacological interest as their apparent efficacy may change in magnitude and direction depending on the constitutive activity of a receptor. Yet, this intriguing phenomenon has been poorly described and understood, due to the lack of stable experimental systems and design strategies. In this thesis, the main aim was to investigate whether a dualsteric design principle, i.e. molecular probes carrying two pharmacophores to simultaneously adopt orthosteric and allosteric topography within a G protein-coupled receptor, may represent a novel approach to generate protean agonism at the M_2 receptor. First, we overcame the methodological limitations: we established two experimental systems, which have either a high level of spontaneous activity (Tris buffer) or a low amount of constitutive activity (Tris NaCl buffer), and we demonstrated that a high buffer osmolarity rather than a high concentration of sodium ions is responsible for receptor inactivation. Then, we identified two new dualsteric protean agonists at the M_2 muscarinic acetylcholine receptors, namely isox-6-naph and OOM-6-naph and we pinpointed three molecular requirements within dualsteric compounds that elicit protean agonism at this receptor subtype: (i) an orthosteric part endowed with an acetylcholine-like efficacy, (ii) a bulky allosteric part to impair the flexibility of the extracellular loop area, and (iii) a flexible linker chain of 6 carbon atoms.

Using radioligand binding and functional assays we posit that dynamic ligand binding may be the mechanism underlying protean agonism of dualsteric ligands. Therefore, given that protean agonism was thought to reside in the intrinsic efficacy of a ligand, these results introduce an unprecedented molecular mechanism to elicit protean agonism.

Finally, assays performed with an allosteric loss-of-affinity mutant confirmed that a functional allosteric site is critical for eliciting protean agonism at the M_2 receptor. Indeed, a single mutation in this binding site converted the behaviour of isox-6-naph and OOM-6-naph from protean to partial agonism.

In conclusion, the findings of this thesis provide new mechanistic insights into the still enigmatic phenomenon of protean agonism and form a rationale for the design of such compounds for a G protein-coupled receptor.

Thus, in addition to the great potential of biased GPCR signaling, improved understanding of protean agonism may provide another level towards a targeted exploitation of the GPCR signaling machinery, which could be relevant to the knowledge-based design of innovative drug candidates.

6 ABBREVIATION LIST

[^{35}S]GTPγS	Guanosine 5'-O-(gamma-[^{35}S]thio)triphosphate)
[^{3}H]NMS	[^{3}H]*N*-methylscopolamine
°C	Degrees Celsius
5-HT_{1B}R	Serotonin receptor 1B
7TMs	Seven transmembrane helices
A	Alanine
ACh	Acetylcholine
ANOVA	Analysis of variance
ATCM	Allosteric ternary complex model
Atr	Atropine
ATSM	Allosteric two-state model
B_2R	Bradykinin receptor 2
BSA	Bovine serum albumine
cAMP	*Cyclic* adenosine monophosphate
CB_2R	Cannabinoid receptor 2
CHO	Chinese hamster ovary
CHO-hM_2	CHO stably expressing the human muscarinic acetylcholine M_2 receptor
CNS	Central nervous system
DTT	DL-dithiothreitol
FCS	Fetal calf serum
G proteins	Guanine nucleotide-binding proteins
GDP	Guanosine diphosphate
GIRKs	G protein-coupled inwardly-rectifying potassium channels
GPCR	G protein-coupled receptors
GRKs	G protein-coupled receptor kinases
GTP	Guanosine triphosphate
H_3R	Histamine receptor 3
Ham's F-12	Ham's nutrient mixture F-12
HEPES	4-(2-Hydroxyethyl)-1-piperazineethane sulfonic acid
HSA	Human Serum Albumin
I_{KACh}	Acetylcholine-activated potassium channel
iper	Iperoxo
M_2AChR	Muscarinic acetylcholine receptor 2
mAChRs	Muscarinic acetylcholine receptors
min	Minutes
MWC model	Monod, Wyman and Changeux model

nAChRs	Nicotinic acetylcholine receptors
NMDG	*N*-methyl-D-glucamine
NMS	N-methylscopolamine
NMS	N-methylscopolamine
OOM	Oxo-oxotremorine M
PBS	Phosphate buffered saline
PKA	Protein kinase A
PKC	Protein kinase C
PLCβ	Phospholipase C beta
PNS	Peripheral nervous system
RGS	Regulators of G-protein signalling
SEM	Standard error of mean
Thr	Threonine
Tris	*Tris*(*hydroxymethyl*)*aminomethane*
Trp	Tryptophan
Tyr	Tyrosine
W	Tryptophan
wt	Wild type
α_{2A}AR	Alpha-2A adrenergic receptor
β_2AR	Beta-2 adrenergic receptor

7 REFERENCES

Ashkenazi A, Winslow JW, Peralta EG, Peterson GL, Schimerlik MI, Capon DJ, and Ramachandran J (1987) An M2 muscarinic receptor subtype coupled to both adenylyl cyclase and phosphoinositide turnover. *Science* **238:**672–675.

Barann M, Schmidt K, Göthert M, Urban BW, and Bönisch H (2004) Influence of sodium substitutes on 5-HT-mediated effects at mouse 5-HT3 receptors. *Br. J. Pharmacol.* **142:**501–508.

Bennett KA, Langmead CJ, Wise A, and Milligan G (2009) Growth hormone secretagogues and growth hormone releasing peptides act as orthosteric super-agonists but not allosteric regulators for activation of the G protein Galpha(o1) by the Ghrelin receptor. *Mol. Pharmacol.* **76:**802–811.

Benovic JL, Kühn H, Weyand I, Codina J, Caron MG, and Lefkowitz RJ (1987) Functional desensitization of the isolated beta-adrenergic receptor by the beta-adrenergic receptor kinase: potential role of an analog of the retinal protein arrestin (48-kDa protein). *Proc. Natl. Acad. Sci. U.S.A.* **84:**8879–8882.

Billups D, Billups B, Challiss RAJ, and Nahorski SR (2006) Modulation of Gq-protein-coupled inositol trisphosphate and Ca2+ signaling by the membrane potential. *J. Neurosci.* **26:**9983–9995.

Bock A, Bermudez M, Krebs F, Matera C, Chirinda B, Sydow D, Dallanoce C, Holzgrabe U, Amici M de, Lohse MJ, Wolber G, and Mohr K (2016) Ligand Binding Ensembles Determine Graded Agonist Efficacies at a G Protein-Coupled Receptor. *J. Biol. Chem.*

Bock A, Chirinda B, Krebs F, Messerer R, Bätz J, Muth M, Dallanoce C, Klingenthal D, Tränkle C, Hoffmann C, De Amici M, Holzgrabe U, Kostenis E, and Mohr K (2014) Dynamic ligand binding dictates partial agonism at a G protein-coupled receptor. *Nat. Chem. Biol.* **10:**18–20.

Bock A, Merten N, Schrage R, Dallanoce C, Bätz J, Klöckner J, Schmitz J, Matera C, Simon K, Kebig A, Peters L, Müller A, Schrobang-Ley J, Tränkle C, Hoffmann C, De Amici M, Holzgrabe U, Kostenis E, and Mohr K (2012) The allosteric vestibule of a seven transmembrane helical receptor controls G-protein coupling. *Nat. Commun.* **3:**1044.

Bolognini D, Cascio MG, Parolaro D, and Pertwee RG (2012) AM630 behaves as a protean ligand at the human cannabinoid CB2 receptor. *Br. J. Pharmacol.* **165:**2561–2574.

Bonner TI, Buckley NJ, Young AC, and Brann MR (1987) Identification of a family of muscarinic acetylcholine receptor genes. *Science* **237:**527–532.

Bonner TI, Young AC, Brann MR, and Buckley NJ (1988) Cloning and expression of the human and rat m5 muscarinic acetylcholine receptor genes. *Neuron* **1:**403–410.

Brown BR and Crout JR (1970) The sympathomimetic effect of gallamine on the heart. *J. Pharmacol. Exp. Ther.* **172:**266–273.

Buller S, Zlotos DP, Mohr K, and Ellis J (2002) Allosteric site on muscarinic acetylcholine receptors: a single amino acid in transmembrane region 7 is critical to the subtype selectivities of caracurine V derivatives and alkane-bisammonium ligands. *Mol. Pharmacol.* **61:**160–168.

Bünemann M, Frank M, and Lohse MJ (2003) Gi protein activation in intact cells involves subunit rearrangement rather than dissociation. *Proc. Natl. Acad. Sci. U.S.A.* **100:**16077–16082.

Chan WY, McKinzie DL, Bose S, Mitchell SN, Witkin JM, Thompson RC, Christopoulos A, Lazareno S, Birdsall NJ, Bymaster FP, and Felder CC (2008) Allosteric modulation of the muscarinic M4 receptor as an approach to treating schizophrenia. *Proc. Natl. Acad. Sci. U.S.A.* **105:**10978–10983.

Chang RS L. and Snyder SH (1980) Histamine H 1 -Receptor Binding Sites in Guinea Pig Brain Membranes: Regulation of Agonist Interactions by Guanine Nucleotides and Cations. *J. Neurochem.* **34:**916–922.

Cheng Y and Prusoff WH (1973) Relationship between the inhibition constant (K1) and the concentration of inhibitor which causes 50 per cent inhibition (I50) of an enzymatic reaction. *Biochem. Pharmacol.* **22:**3099–3108.

Chidiac P (2002) Considerations in the evaluation of inverse agonism and protean agonism at G protein-coupled receptors. *Meth. Enzymol.* **343:**3–16.

Chidiac P, Hebert TE, Valiquette M, Dennis M, and Bouvier M (1994) Inverse agonist activity of beta-adrenergic antagonists. *Mol. Pharmacol.* **45:**490–499.

Chidiac P, Nouet S, and Bouvier M (1996) Agonist-induced modulation of inverse agonist efficacy at the beta 2-adrenergic receptor. *Mol. Pharmacol.* **50:**662–669.

Christopoulos A (2002) Allosteric binding sites on cell-surface receptors: novel targets for drug discovery. *Nat. Rev. Drug Discov.* **1:**198–210.

Conn PJ, Christopoulos A, and Lindsley CW (2009) Allosteric modulators of GPCRs: a novel approach for the treatment of CNS disorders. *Nat. Rev. Drug Discov.* **8:**41–54.

Costa T and Herz A (1989) Antagonists with negative intrinsic activity at delta opioid receptors coupled to GTP-binding proteins. *Proc. Natl. Acad. Sci. U.S.A.:*7321–7325.

De Lean A, Stadel JM, and Lefkowitz RJ (1980) A ternary complex model explains the agonist-specific binding properties of the adenylate cyclase-coupled beta-adrenergic receptor. *J. Biol. Chem.* **255:**7108–7117.

DeBlasi A, O'Reilly K, and Motulsky HJ (1989) Calculating receptor number from binding experiments using same compound as radioligand and competitor. *Trends Pharmacol. Sci.* **10:**227–229.

Della Bella D, Rognoni F, and Gopal K (1961) Curare-like drugs and cardiovagal synapses: comparative study in vitro on isolated guinea-pig vagus-heart preparation. *Journal of Pharmacy and Pharmacology* **13:**93–97.

De Min A (2012). Binding topography and signaling profile of two novel dualsteric ligands at the muscarinic M_2 receptor. Master thesis, Bonn.

Dhein S, van Koppen, C J, and Brodde OE (2001) Muscarinic receptors in the mammalian heart. *Pharmacol. Res.* **44:**161–182.

Disingrini T, Muth M, Dallanoce C, Barocelli E, Bertoni S, Kellershohn K, Mohr K, De Amici M, and Holzgrabe U (2006) Design, synthesis, and action of oxotremorine-related hybrid-type allosteric modulators of muscarinic acetylcholine receptors. *J. Med. Chem.* **49:**366–372.

Doughty AG and Wylie W (1951) An Assessment of Flaxedil (Galiamine Triethiodide, B.P.). *Proceedings of the Royal Society of Medicine* **1951:**375–388.

Dror RO, Green HF, Valant C, Borhani DW, Valcourt JR, Pan AC, Arlow DH, Canals M, Lane JR, Rahmani R, Baell JB, Sexton PM, Christopoulos A, and Shaw DE (2013) Structural basis for modulation of a G-protein-coupled receptor by allosteric drugs. *Nature* **503:**295–299.

Ehlert FJ (1988) Estimation of the affinities of allosteric ligands using radioligand binding and pharmacological null methods. *Mol. Pharmacol.* **33:**187–194.

Ellis J, Huyler J, and Brann MR (1991) Allosteric regulation of cloned m1-m5 muscarinic receptor subtypes. *Biochem. Pharmacol.* **42:**1927–1932.

Ellis J, Seidenberg M, and Brann MR (1993) Use of chimeric muscarinic receptors to investigate epitopes involved in allosteric interactions. *Mol. Pharmacol.* **44:**583–588.

Engström M, Tomperi J, El-Darwish K, Ahman M, Savola J, and Wurster S (2005) Superagonism at the human somatostatin receptor subtype 4. *J. Pharmacol. Exp. Ther.* **312:**332–338.

Fathy DB, Leeb T, Mathis SA, and Leeb-Lundberg LM (1999) Spontaneous human B2 bradykinin receptor activity determines the action of partial agonists as agonists or inverse agonists. Effect of basal desensitization. *J. Biol. Chem.* **274:**29603–29606.

Fenalti G, Giguere PM, Katritch V, Huang X, Thompson AA, Cherezov V, Roth BL, and Stevens RC (2014) Molecular control of δ-opioid receptor signalling. *Nature* **506:**191–196.

Frank M, Thümer L, Lohse MJ, and Bünemann M (2005) G Protein activation without subunit dissociation depends on a G{alpha}(i)-specific region. *J. Biol. Chem.* **280:**24584–24590.

Fredriksson R, Lagerström MC, Lundin L, and Schiöth HB (2003) The G-protein-coupled receptors in the human genome form five main families. Phylogenetic analysis, paralogon groups, and fingerprints. *Mol. Pharmacol.* **63:**1256–1272.

Ganguli SC, Park C, Holtmann MH, Hadac EM, Kenakin TP, and Miller LJ (1998) Protean effects of a natural peptide agonist of the G protein-coupled secretin receptor demonstrated by receptor mutagenesis. *J. Pharmacol. Exp. Ther.:*593–598.

Gbahou F, Rouleau A, Morisset S, Parmentier R, Crochet S, Lin J, Ligneau X, Tardivel-Lacombe J, Stark H, Schunack W, Ganellin CR, Schwartz J, and Arrang J (2003) Protean agonism at histamine H3 receptors in vitro and in vivo. *Proc. Natl. Acad. Sci. U.S.A.* **100:**11086–11091.

Gnagey A and Ellis J (1996) Allosteric regulation of the binding of [3H]acetylcholine to m2 muscarinic receptors. *Biochem. Pharmacol.* **52:**1767–1775.

Haga K, Kruse AC, Asada H, Yurugi-Kobayashi T, Shiroishi M, Zhang C, Weis WI, Okada T, Kobilka BK, Haga T, and Kobayashi T (2012) Structure of the human M2 muscarinic acetylcholine receptor bound to an antagonist. *Nature* **482:**547–551.

Hall DA (2000) Modeling the functional effects of allosteric modulators at pharmacological receptors: an extension of the two-state model of receptor activation. *Mol. Pharmacol.* **58:**1412–1423.

Harrison C and Traynor JR (2003) The [35S]GTPgammaS binding assay: approaches and applications in pharmacology. *Life Sci.* **74:**489–508.

Hilf G and Jakobs KH (1989) Activation of cardiac G-proteins by muscarinic acetylcholine receptors: regulation by Mg2+ and Na+ ions. *European Journal of Pharmacology: Molecular Pharmacology* **172:**155–163.

Holst B, Brandt E, Bach A, Heding A, and Schwartz TW (2005) Nonpeptide and peptide growth hormone secretagogues act both as ghrelin receptor agonist and as positive or negative allosteric modulators of ghrelin signaling. *Mol. Endocrinol.* **19:**2400–2411.

Huang X, Prilla S, Mohr K, and Ellis J (2005) Critical amino acid residues of the common allosteric site on the M2 muscarinic acetylcholine receptor: more similarities than differences between the structurally divergent agents gallamine and bis(ammonio)alkane-type hexamethylene-bis-[dimethyl-(3-phthalimidopropyl)ammonium]dibromide. *Mol. Pharmacol.* **68:**769–778.

Hulme EC, Birdsall NJ, and Buckley NJ (1990) Muscarinic receptor subtypes. *Annu. Rev. Pharmacol. Toxicol.* **30:**633–673.

Jakubík J, Bacáková L, el-Fakahany EE, and Tucek S (1995) Subtype selectivity of the positive allosteric action of alcuronium at cloned M1-M5 muscarinic acetylcholine receptors. *J. Pharmacol. Exp. Ther.* **274:**1077–1083.

Jakubík J, Haga T, and Tucek S (1998) Effects of an agonist, allosteric modulator, and antagonist on guanosine-gamma-[35S]thiotriphosphate binding to liposomes with varying muscarinic receptor/Go protein stoichiometry. *Mol. Pharmacol.* **54:**899–906.

Janetopoulos C, Jin T, and Devreotes P (2001) Receptor-mediated activation of heterotrimeric G-proteins in living cells. *Science* **291:**2408–2411.

Jansson CC, Kukkonen JP, Näsman J, Huifang G, Wurster S, Virtanen R, Savola JM, Cockcroft V, and Akerman KE (1998) Protean agonism at alpha2A-adrenoceptors. *Mol. Pharmacol.* **53:**963–968.

Katritch V, Fenalti G, Abola EE, Roth BL, Cherezov V, and Stevens RC (2014) Allosteric sodium in class A GPCR signaling. *Trends Biochem. Sci.* **39:**233–244.

Kenakin T (1995a) Pharmacological proteus? *Trends Pharmacol. Sci.* **16:**256–258.

Kenakin T (1995b) Agonist-receptor efficacy. II. Agonist trafficking of receptor signals. *Trends Pharmacol. Sci.* **16:**232–238.

Kenakin T (1997) Protean agonists. Keys to receptor active states? *Ann. N. Y. Acad. Sci.* **812:**116–125.

Kenakin T (2001) Inverse, protean, and ligand-selective agonism: matters of receptor conformation. *FASEB J.* **15:**598–611.

Kenakin T (2002) Efficacy at G-protein-coupled receptors. *Nat. Rev. Drug Discov.* **1:**103–110.

Kenakin T (2003) Ligand-selective receptor conformations revisited: the promise and the problem. *Trends Pharmacol. Sci.* **24:**346–354.

Kenakin T (2007) Collateral efficacy in drug discovery: taking advantage of the good (allosteric) nature of 7TM receptors. *Trends Pharmacol. Sci.* **28:**407–415.

Kenakin T (2011) Functional selectivity and biased receptor signaling. *J. Pharmacol. Exp. Ther.* **336:**296–302.

Kjelsberg MA, Cotecchia S, Ostrowski J, Caron MG, and Lefkowitz RJ (1992) Constitutive activation of the alpha 1B-adrenergic receptor by all amino acid substitutions at a single site. Evidence for a region which constrains receptor activation. *J. Biol. Chem.* **267:**1430–1433.

Krejcí A and Tucek S (2002) Quantitation of mRNAs for M1 to M5 subtypes of muscarinic receptors in rat heart and brain cortex. *Mol. Pharmacol.* **61:**1267–1272.

Kruh J (1982) Effects of sodium butyrate, a new pharmacological agent, on cells in culture. *Mol. Cell Biochem.* **42:**65–82.

Kruse AC, Ring AM, Manglik A, Hu J, Hu K, Eitel K, Hübner H, Pardon E, Valant C, Sexton PM, Christopoulos A, Felder CC, Gmeiner P, Steyaert J, Weis WI, Garcia KC, Wess J, and Kobilka BK (2013) Activation and allosteric modulation of a muscarinic acetylcholine receptor. *Nature* **504:**101–106.

Lagerström MC and Schiöth HB (2008) Structural diversity of G protein-coupled receptors and significance for drug discovery. *Nat. Rev. Drug Discov.* **7:**339–357.

Langmead CJ, Watson J, and Reavill C (2008) Muscarinic acetylcholine receptors as CNS drug targets. *Pharmacol. Ther.* **117:**232–243.

Lanzafame AA, Christopoulos A, and Mitchelson F (2003) Cellular signaling mechanisms for muscarinic acetylcholine receptors. *Recept. Channels* **9:**241–260.

Lappano R and Maggiolini M (2011) G protein-coupled receptors: novel targets for drug discovery in cancer. *Nat. Rev. Drug Discov.* **10:**47–60.

Lazareno S and Birdsall NJ (1995) Detection, quantitation, and verification of allosteric interactions of agents with labeled and unlabeled ligands at G protein-coupled receptors: interactions of strychnine and acetylcholine at muscarinic receptors. *Mol. Pharmacol.* **48:**362–378.

Leach K, Loiacono RE, Felder CC, McKinzie DL, Mogg A, Shaw DB, Sexton PM, and Christopoulos A (2010) Molecular mechanisms of action and in vivo validation of an M4 muscarinic acetylcholine receptor allosteric modulator with potential antipsychotic properties. *Neuropsychopharmacology* **35:**855–869.

Leff P (1995) The two-state model of receptor activation. *Trends Pharmacol. Sci.* **16:**89–97.

Lefkowitz RJ (2004) Historical review: a brief history and personal retrospective of seven-transmembrane receptors. *Trends Pharmacol. Sci.* **25:**413–422.

Lefkowitz RJ, Cotecchia S, Samama P, and Costa T (1993) Constitutive activity of receptors coupled to guanine nucleotide regulatory proteins. *Trends Pharmacol. Sci.* **14:**303–307.

Leppik RA, Miller RC, Eck M, and Paquet JL (1994) Role of acidic amino acids in the allosteric modulation by gallamine of antagonist binding at the m2 muscarinic acetylcholine receptor. *Mol. Pharmacol.* **45:**983–990.

Liu W, Chun E, Thompson AA, Chubukov P, Xu F, Katritch V, Han GW, Roth CB, Heitman LH, IJzerman AP, Cherezov V, and Stevens RC (2012) Structural basis for allosteric regulation of GPCRs by sodium ions. *Science* **337:**232–236.

Lohse MJ, Lenschow V, and Schwabe U (1984) Two Affinity States of R1 Adenosine Receptors in Brain Membranes: Analysis of Guanine Nucleotide and Temperature Effects on Radioligand Binding. *Mol. Pharmacol.* **1984:**1–9.

Lowry OH, Rosebrough NJ, FARR AL, and Randall RJ (1951) Protein measurement with the Folin phenol reagent. *J. Biol. Chem.* **193:**265–275.

Lüllmann H, Ohnesorge FK, Schauwecker GC, and Wassermann O (1969) Inhibition of the actions of carbachol and DFP on guinea pig isolated atria by alkane-bis-ammonium compounds. *Eur. J. Pharmacol.* **6:**241–247.

Malmberg A and Mohell N (1995) Characterization of [3H]quinpirole binding to human dopamine D2A and D3 receptors: effects of ions and guanine nucleotides. *J. Pharmacol. Exp. Ther.* **274:**790–797.

Mancini I, Brusa R, Quadrato G, Foglia C, Scandroglio P, Silverman LS, Tulshian D, Reggiani A, and Beltramo M (2009) Constitutive activity of cannabinoid-2 (CB2) receptors plays an essential role in the protean agonism of (+)AM1241 and L768242. *Br. J. Pharmacol.* **158:**382–391.

Marie J, Koch C, Pruneau D, Paquet JL, Groblewski T, Larguier R, Lombard C, Deslauriers B, Maigret B, and Bonnafous JC (1999) Constitutive activation of the human bradykinin B2 receptor induced by mutations in transmembrane helices III and VI. *Mol. Pharmacol.* **55:**92–101.

May LT and Christopoulos A (2003) Allosteric modulators of G-protein-coupled receptors. *Curr. Opin. Pharmacol.* **3:**551–556.

Miller-Gallacher JL, Nehmé R, Warne T, Edwards PC, Schertler, Gebhard F X, Leslie AG W., and Tate CG (2014) The 2.1 Å resolution structure of cyanopindolol-bound β1-adrenoceptor identifies an intramembrane Na+ ion that stabilises the ligand-free receptor. *PLoS ONE* **9:**e92727.

Milligan G (2003) Constitutive activity and inverse agonists of G protein-coupled receptors: a current perspective. *Mol. Pharmacol.* **64:**1271–1276.

Milligan G and Kostenis E (2006) Heterotrimeric G-proteins: a short history. *Br. J. Pharmacol.* **147 Suppl 1:**S46-55.

Monod J, Wyman J, and Changeux JP (1965) On the nature of allosteric transitions: a plausible model. *J. Mol. Biol.* **12:**88–118.

Moore CAC, Milano SK, and Benovic JL (2007) Regulation of receptor trafficking by GRKs and arrestins. *Annu. Rev. Physiol.* **69:**451–482.

Nelson CD, Perry SJ, Regier DS, Prescott SM, Topham MK, and Lefkowitz RJ (2007) Targeting of diacylglycerol degradation to M1 muscarinic receptors by beta-arrestins. *Science* **315:**663–666.

Neve KA (1991) Regulation of dopamine D2 receptors by sodium and pH. *Mol. Pharmacol.* **39:**570–578.

Newman-Tancredi A, Cussac D, Marini L, Touzard M, and Millan MJ (2003) h5-HT(1B) receptor-mediated constitutive Galphai3-protein activation in stably transfected Chinese hamster ovary cells: an antibody capture assay reveals protean efficacy of 5-HT. *Br. J. Pharmacol.* **138:**1077–1084.

Pauwels PJ, Rauly I, Wurch T, and Colpaert FC (2002) Evidence for protean agonism of RX 831003 at alpha 2A-adrenoceptors by co-expression with different G alpha protein subunits. *Neuropharmacology* **42:**855–863.

Perry SJ, Baillie GS, Kohout TA, McPhee I, Magiera MM, Ang KL, Miller WE, McLean AJ, Conti M, Houslay MD, and Lefkowitz RJ (2002) Targeting of cyclic AMP degradation to beta 2-adrenergic receptors by beta-arrestins. *Science* **298:**834–836.

Pert CB and Snyder SH (1973) Properties of opiate-receptor binding in rat brain. *Proc. Natl. Acad. Sci. U.S.A.* **70:**2243–2247.

Pierce KL, Premont RT, and Lefkowitz RJ (2002) Seven-transmembrane receptors. *Nat. Rev. Mol. Cell. Biol.* **3:**639–650.

Pihlavisto M, Sjöholm B, Scheinin M, and Wurster S (1998) Modulation of agonist binding to recombinant human alpha2-adrenoceptors by sodium ions. *Biochim. Biophys. Acta* **1448:**135–146.

Price MR, Baillie GL, Thomas A, Stevenson LA, Easson M, Goodwin R, McLean A, McIntosh L, Goodwin G, Walker G, Westwood P, Marrs J, Thomson F, Cowley P, Christopoulos A, Pertwee RG, and Ross RA (2005) Allosteric modulation of the cannabinoid CB1 receptor. *Mol. Pharmacol.* **68:**1484–1495.

Prilla S, Schrobang J, Ellis J, Höltje H, and Mohr K (2006) Allosteric interactions with muscarinic acetylcholine receptors: complex role of the conserved tryptophan M2422Trp in a critical cluster of amino acids for baseline affinity, subtype selectivity, and cooperativity. *Mol. Pharmacol.* **70:**181–193.

Rathbun FJ and Hamilton JT (1970) Effect of gallamine on cholinergic receptors. *Canad. Anaes. Soc. J.* **17:**574–590.

Reuveny E, Slesinger PA, Inglese J, Morales JM, Iñiguez-Lluhi JA, Lefkowitz RJ, Bourne HR, Jan YN, and Jan LY (1994) Activation of the cloned muscarinic potassium channel by G protein beta gamma subunits. *Nature* **370:**143–146.

Rosenberger LB, Yamamura HI, and Roeske WR (1980) Cardiac muscarinic cholinergic receptor binding is regulated by Na+ and guanyl nucleotides. *J. Biol. Chem.* **255:**820–823.

Samama P, Cotecchia S, Costa T, and Lefkowitz RJ (1993) A mutation-induced activated state of the beta 2-adrenergic receptor. Extending the ternary complex model. *J. Biol. Chem.* **268:**4625–4636.

Schrage R, De Min A, Hochheiser K, Kostenis E, and Mohr K (2015) Superagonism at G protein-coupled receptors and beyond. *Br. J. Pharmacol.*

Schrage R, Seemann WK, Klöckner J, Dallanoce C, Racké K, Kostenis E, De Amici M, Holzgrabe U, and Mohr K (2013) Agonists with supraphysiological efficacy at the muscarinic M2 ACh receptor. *Br. J. Pharmacol.* **169:**357–370.

Schröter A, Tränkle C, and Mohr K (2000) Modes of allosteric interactions with free and [3H]N-methylscopolamine-occupied muscarinic M2 receptors as deduced from buffer-dependent potency shifts. *Naunyn Schmiedebergs Arch. Pharmacol.* **362:**512–519.

Selley DE, Cao CC, Liu Q, and Childers SR (2000) Effects of sodium on agonist efficacy for G-protein activation in mu-opioid receptor-transfected CHO cells and rat thalamus. *Br. J. Pharmacol.* **130:**987–996.

Shenoy SK and Lefkowitz RJ (2011) β-Arrestin-mediated receptor trafficking and signal transduction. *Trends Pharmacol. Sci.* **32:**521–533.

Shonberg J, Lopez L, Scammells PJ, Christopoulos A, Capuano B, and Lane JR (2014) Biased agonism at G protein-coupled receptors: the promise and the challenges--a medicinal chemistry perspective. *Med. Res. Rev.* **34:**1286–1330.

Simon MI, Strathmann MP, and Gautam N (1991) Diversity of G proteins in signal transduction. *Science* **252:**802–808.

Stiles GL (1988) A1 Adenosine Receptor-G Protein Coupling in Bovine Brain Membranes: Effects of Guanine Nucleotides, Salt, and Solubilization. *J. Neurochem.* **51:**1592–1598.

Stockton JM, Birdsall NJ, Burgen AS, and Hulme EC (1983) Modification of the binding properties of muscarinic receptors by gallamine. *Mol. Pharmacol.* **23:**551–557.

Teague SJ (2003) Implications of protein flexibility for drug discovery. *Nat. Rev. Drug Discov.* **2:**527–541.

Tian WN, Duzic E, Lanier SM, and Deth RC (1994) Determinants of alpha2-adrenergic receptor activation of G proteins: evidence for a precoupled receptor/G protein state. *Mol. Pharmacol.* **45:**524–531.

Tota MR and Schimerlik MI (1990) Partial agonist effects on the interaction between the atrial muscarinic receptor and the inhibitory guanine nucleotide-binding protein in a reconstituted system. *Mol. Pharmacol.* **37:**996–1004.

Tränkle C, Kostenis E, Burgmer U, and Mohr K (1996) Search for lead structures to develop new allosteric modulators of muscarinic receptors. *J. Pharmacol. Exp. Ther.* **279:**926–933.

U'Prichard DC and Snyder SH (1978) Guanyl nucleotide influences on 3H-ligand binding to alpha-noradrenergic receptors in calf brain membranes. *J. Biol. Chem.* **253:**3444–3452.

Urban JD, Clarke WP, Zastrow M von, Nichols DE, Kobilka BK, Weinstein H, Javitch JA, Roth BL, Christopoulos A, Sexton PM, Miller KJ, Spedding M, and Mailman RB (2007) Functional selectivity and classical concepts of quantitative pharmacology. *J. Pharmacol. Exp. Ther.* **320:**1–13.

Violin JD and Lefkowitz RJ (2007) Beta-arrestin-biased ligands at seven-transmembrane receptors. *Trends Pharmacol. Sci.* **28:**416–422.

Vivo M, Lin H, and Strange PG (2006) Investigation of cooperativity in the binding of ligands to the D(2) dopamine receptor. *Mol. Pharmacol.* **69:**226–235.

Vogel L (2015). Einfluss des orthosterischen / allosterischen Epitops Trp 7.35 auf Ligandbindung, Rezeptoraktivierung und Signalweiterleitung. PhD thesis, Bonn.

Voigtländer U, Jöhren K, Mohr M, Raasch A, Tränkle C, Buller S, Ellis J, Höltje H, and Mohr K (2003) Allosteric site on muscarinic acetylcholine receptors: identification of two amino acids in the muscarinic M2 receptor that account entirely for the M2/M5 subtype selectivities of some structurally diverse allosteric ligands in N-methylscopolamine-occupied receptors. *Mol. Pharmacol.* **64:**21–31.

Watson C, Jenkinson S, Kazmierski W, and Kenakin T (2005) The CCR5 receptor-based mechanism of action of 873140, a potent allosteric noncompetitive HIV entry inhibitor. *Mol. Pharmacol.* **67:**1268–1282.

Wess J (1998) Molecular basis of receptor/G-protein-coupling selectivity. *Pharmacol. Ther.* **80:**231–264.

Wess J (2004) Muscarinic acetylcholine receptor knockout mice: novel phenotypes and clinical implications. *Annu. Rev. Pharmacol. Toxicol.* **44:**423–450.

Wess J, Eglen RM, and Gautam D (2007) Muscarinic acetylcholine receptors: mutant mice provide new insights for drug development. *Nat. Rev. Drug. Discov.* **6:**721–733.

Wu H, Wacker D, Mileni M, Katritch V, Han GW, Vardy E, Liu W, Thompson AA, Huang X, Carroll FI, Mascarella SW, Westkaemper RB, Mosier PD, Roth BL, Cherezov V, and Stevens RC (2012) Structure of the human κ-opioid receptor in complex with JDTic. *Nature* **485:**327–332.

Xu JJ, Diaz P, Astruc-Diaz F, Craig S, Munoz E, and Naguib M (2010) Pharmacological characterization of a novel cannabinoid ligand, MDA19, for treatment of neuropathic pain. *Anesth. Analg.* **111:**99–109.

Yao BB, Mukherjee S, Fan Y, Garrison TR, Daza AV, Grayson GK, Hooker BA, Dart MJ, Sullivan JP, and Meyer MD (2006) In vitro pharmacological characterization of AM1241: a protean agonist at the cannabinoid CB2 receptor? *Br. J. Pharmacol.* **149:**145–154.

Zhang C, Srinivasan Y, Arlow DH, Fung JJ, Palmer D, Zheng Y, Green HF, Pandey A, Dror RO, Shaw DE, Weis WI, Coughlin SR, and Kobilka BK (2012) High-resolution crystal structure of human protease-activated receptor 1. *Nature* **492:**387–392.

8 PUBLICATIONS

Articles

- De Min A., Matera C., Bock A., Holze J., Kloeckner J., De Amici M., Muth M., Kenakin T., Holzgrabe U., Dallanoce C., Kostenis E., Schrage R., Mohr K. A new molecular mechanism to engineer protean agonism at a G protein-coupled receptor. *Submitted*.

- Schrage R., De Min A., Hochheiser K., Kostenis E., Mohr K. Superagonism at G protein-coupled receptors and beyond. *Br J Pharmacol*. 2015 Aug 15

Conference abstracts

- De Min A., Matera C., Dallanoce C., Holzgrabe U., De Amici M., Mohr K. Muscarinic dualsteric ligands behave as partial or protean agonists depending on the affinity of their orthosteric moiety. Conference: GPCRs: Beyond structure towards therapy, 2015.

- De Min A., Matera C., Messerer R., Dallanoce C., Holzgrabe U., Mohr K. Protean agonism at the muscarinic M_2 receptor*. Naunyn Schmiedebergs Arch Pharmacol. 2015 Feb (Suppl 1).*

- De Min, A., Mohr, K. Monovalent cations influence muscarinic M_2 receptor spontaneous activity and agonist-dependent signaling. Conference: DphG Jahrestagung, 2014.

9 CURRICULUM VITAE

10 ACKNOWLEDGMENTS

I would like to express my sincere gratitude to Prof. Dr. K. Mohr for giving me the opportunity to carry out my PhD studies in his group. I thank him very much for the supervision that he provided me during my period in his department and for his help in my scientific development.

I would also like to thank Prof. Dr. I. von Kügelgen for being the second member of the examining committee for my thesis.

I would like to express my profound appreciation to Prof. Dr. E. Kostenis for being my co-supervisor in the Research Training Group 1873, for her great support and contribution during the final period of my PhD and also for being the third member of the examining committee for my thesis.

I would also like to thank Prof. Dr. D. Bartels for her participation as the fourth member of the examining committee evaluating this thesis.

I would like to acknowledge the Research Training Group "Pharmacology of 7TM-receptors and downstream signaling pathways" for funding my PhD project and all its members for their support and ideas regarding my research.

I also thank all my coworkers of the Pharmacology and Toxicology department for their help and support and for being able to put up with me. I really enjoyed the friendly atmosphere that you contributed to create in the lab and in the offices.

I would like to thank the group of Prof. Holzgrabe and Prof. De Amici for synthesis (and several re-synthesis) of the compounds tested in this study. A special thank goes to Carlo, Clelia and Marco that were always available for requests/questions.

I genuinely thank all my friends for making my stay away from home easier and enjoyable.

Finally, I would like to thank my parents, my sister and my entire family for the immense support that they gave me during these years abroad. This wouldn't have been possible without your love and encouragement.